PTB bericht
Wissenschaftliche Veröffentlichungen

Diss-32
Mai 2026

Dissertation

Yan Yan Beer

Development of a reference method for quantifying viral load

ISSN 2941-1297
ISBN 978-3-944659-64-0

DOI 10.7795/110.20260518

Yan Yan Beer

Development of a reference method for quantifying viral load

Dissertation
PTB-Diss- 32

Braunschweig, Mai 2026

ISSN 2751-6598
ISBN 978-3-944659-64-0

DOI 10.7795/110.20260518

Empfohlene Zitierweise/recommended citation

Beer, Y.Y., 2026. *Development of a reference method for quantifying viral load*. Dissertation an der Technischen Universität Braunschweig, Fakultät für Lebenswissenschaften. Braunschweig: Physikalisch-Technische Bundesanstalt. PTB-Bericht Diss-32. ISBN 978-3-944659-64-0. Verfügbar unter: https://doi.org/10.7795/110.20260518

Herausgeber:
Physikalisch-Technische Bundesanstalt
ISNI: 0000 0001 2186 1887

Presse und Öffentlichkeitsarbeit

Bundesallee 100
38116 Braunschweig

Telefon: (05 31) 592-93 21
Telefax: (05 31) 592-92 92
www.ptb.de

Development of a reference method for quantifying viral load

Von der Fakultät für Lebenswissenschaften

der Technischen Universität Braunschweig

zur Erlangung des Grades

einer Doktorin der Naturwissenschaften

(Dr. rer. nat.)

genehmigte

D i s s e r t a t i o n

von Yan Yan Beer
aus Goslar, Germany

1. Referent: Prof. Dr. Gavin O'Connor
2. Referentin: Prof. Dr. Melanie M. Brinkmann
eingereicht am: 16.01.2026
mündliche Prüfung (Disputation) am: 22.04.2026

Druckjahr 2026

https://doi.org/10.7795/110.20260518

https://doi.org/10.7795/110.20260518

Vorveröffentlichungen der Dissertation

Teilergebnisse aus dieser Arbeit wurden mit Genehmigung der Fakultät für Lebenswissenschaften, vertreten durch den Mentor der Arbeit, in folgenden Beiträgen vorab veröffentlicht:

Tagungsbeiträge (Vorträge)

Beer YY., Henrion A., Brinkmann MM, O'Connor G.: Development of a reference method to quantify viral proteins using mass spectrometry, B-IGSM, online (2021)

Beer YY: Measuring viral load in CT values is like measuring bodyweight in pumpkin numbers, B-IGSM, Sciens Slam, online (2022)

Beer YY: How can we improve viral load measurements? – Metrology's role in achieving accurate and reliable results through SI-traceable protein and DNA measurements, Meet the BRICS, TU-BS, Braunschweig, Germany (2023)

Beer YY., Arsene C., Brinkmann MM, O'Connor G.: Accurate protein quantification to support comparable viral load calculations, B-IGSM, Braunschweig, Germany (2024)

Beer YY., Arsene C., Brinkmann MM, O'Connor G.: Boosting accuracy in viral load measurements with a powerful duo – IDMS and ddPCR, 34th Mass Spec Forum Vienna, Vienna, Austria (2024)

Beer YY: Herausforderungen der Viruslastbestimmung – Akkurate Protein- und Nukleinsäuremessungen, PTB Kuratorium, Braunschweig, Germany (2024)

Beer YY., Arsene C., Brinkmann MM, O'Connor G.: Improving viral load measurements through complementary peptide-based protein quantification and digital droplet PCR, CCQM workshop, Towards standardized pathogen measurements, Berlin, Germany (2024)

Posterbeiträge

Beer YY., Henrion A., Brinkmann MM, O'Connor G.: Development of a reference method to quantifiy viral load, PhD symposium, GS Fire, online (2021)

Beer YY., Henrion A., Brinkmann MM, O'Connor G.: How accurate can viral load measurements be?, 1st joint international symposium of FOR2830 (DEEP-DV) and FOR5200, Immune control and its evasion by CMV and other DNA viruses, Dubrovnik, Croatia (2022)

Beer YY., Henrion A., Brinkmann MM, O'Connor G.: Viral protein measurements using mass spectrometry, B-IGSM, International Summer School, Drübeck, Germany (2022)

Beer YY, Brinkmann MM, O'Connor G: Accurate protein quantification to support comparable viral load calculations, DGMS, Dortmund, Germany (2023)

Beer YY., Arsene C., Brinkmann MM, O'Connor G.: A powerful duo for improved viral load determination, #RSCPoster, LinkedIn (2025)

https://doi.org/10.7795/110.20260518

Acknowledgements

This thesis would not have been possible without the support, guidance and contributions of numerous individuals and institutions. I would like to express my sincere gratitude to all of them.

Firstly, I would like to thank my supervisors, Prof. Dr. Gavin O'Connor and Prof. Dr. Melanie M. Brinkmann, for their dedicated supervision, scientific guidance and constant support throughout this work. Their expertise, constructive feedback and encouragement were essential to the successful completion of this thesis.

I would also like to thank Prof. Dr. Martin Korte for chairing the dissertation committee.

My thanks also go to the members of the FB 3.2 and VIMM laboratories for providing a collegial working atmosphere, engaging in stimulating scientific discussions, and supporting me in my daily laboratory work.

I am particularly indebted to Dr Esmeralda Valiente for her training in the ddPCR technique, and for generously sharing her expertise and practical guidance, both of which contributed significantly to this work.

Thanks also go to Bodo Plachter and Nicole Büscher for training me in gradient purification and for their valuable practical guidance.

I am also grateful to the B-IGSM Graduate School and GradTU-BS for the valuable training opportunities they provided throughout my PhD studies.

Finally, I would like to express my deepest gratitude to my husband for his unwavering support, patience and understanding throughout my doctoral journey. His encouragement and belief in me were invaluable during both challenging and rewarding times.

https://doi.org/10.7795/110.20260518

Summary

Accurate, comparable viral load determination is essential for clinical diagnostics and treatment monitoring. However, there is no direct primary method to count viral particles. Laboratories typically measure surrogate quantities, such as viral DNA or protein, which prevents direct data comparison and traceability to the International System of Units (SI). As different analytical approaches quantify distinct molecular components rather than the same physical entity, their results inherently reflect different measurands and therefore cannot be directly compared.

To address this, this thesis proposes a method traceable to the International System of Units (SI) to estimate viral load, using Human Cytomegalovirus (HCMV) as a model. It combines two primary reference measurement procedures: droplet digital PCR (ddPCR), a technique for the absolute counting of viral DNA molecules, and isotope dilution mass spectrometry (IDMS), a method for precise measurement of specific proteins. Together, these methods enable metrologically accurate estimation of viral particle numbers by linking measurements of viral genetic material and proteins through the fixed ratio (stoichiometry) of components in the viral capsid (the protein shell enclosing the genetic material).

Building on this approach, human cytomegalovirus (HCMV) was produced in a cell culture, and viral particles were purified by density gradient ultracentrifugation, a technique that separates components based on their density. Proteomics analysis, an assessment of all proteins within a sample, then identified the major capsid protein (MCP) and triplex subunits Tri1 and Tri2 which were present in a fixed stoichiometry enabling the quantification of the viral particle targets. Signature peptides (unique short protein fragments) from these proteins were selected and obtained commercially. Amino acid analysis with isotope dilution mass spectrometry, a precise method for measuring molecules using labelled standards, provided SI-traceable value assignment. A robust LC–MS/MS (liquid chromatography–tandem mass spectrometry) method in multiple-reaction-monitoring mode was developed for quantifying MCP, Tri1, and Tri2. In parallel, ddPCR (droplet digital polymerase chain reaction) assays targeting the UL54 gene determined absolute genome copy numbers without the need for calibration curves. Multiple extractions showed good reproducibility, with extraction efficiency as the main source of uncertainty.

To support standardisation, a plasmid-based laboratory standard (pYB01) containing the conserved human cytomegalovirus (HCMV) UL54 gene was generated, sequence-verified, and given a quantitative value using droplet digital PCR (ddPCR). This calibrator for quantitative PCR (qPCR) assays is accessible, reproducible, and traceable, enabling standardized viral genome quantification in routine laboratories.

IDMS-based quantification provided independent capsid protein results, complementing molecular measurements. These were converted into capsid numbers using established cryo-electron microscopy stoichiometries. Integrating the ddPCR- and IDMS-derived data yielded an estimated

https://doi.org/10.7795/110.20260518

concentration of ~6 x 10^7 virions per milligram. The uncertainty budgets of both methods overlapped, confirming the reliability of these independent primary approaches.

A detailed uncertainty analysis following the Guide to the Expression of Uncertainty in Measurement (GUM) identified DNA extraction efficiency and the protein-to-capsid conversion factor as the main sources of uncertainty.

Combining ddPCR and IDMS enables SI-traceable viral load measurement. This approach bridges metrology and virology, improving accuracy, reproducibility, and comparability across laboratories. It also supports certified reference materials and standard procedures, strengthening diagnostics and monitoring.

https://doi.org/10.7795/110.20260518

Zusammenfassung

Für die klinische Diagnostik, die Überwachung der Behandlung und die epidemiologische Überwachung ist eine präzise und vergleichbare Messung der Viruslast von entscheidender Bedeutung. Es existiert jedoch keine direkte Primärmethode zur Messung der Anzahl vollständiger Viruspartikel. Stattdessen werden in der Regel Ersatzgrößen wie der Gehalt an viraler DNA oder Proteinen gemessen. Dies führt zu Daten, die nicht direkt zwischen Laboren vergleichbar sind und keine Rückverfolgbarkeit zum Internationalen Einheitensystem (SI) aufweisen.

Die vorliegende Arbeit widmet sich dieser Problematik, indem sie einen Ansatz zur Schätzung der Viruslast vorschlägt, der auf das SI rückführbar ist und das humane Cytomegalievirus (HCMV) als Modellsystem verwendet. Zu diesem Zweck wurden zwei unabhängige primäre Referenzmessverfahren kombiniert: die digitale Tröpfchen-PCR (ddPCR) zur absoluten Quantifizierung der viralen Genomkopien und die Isotopenverdünnungs-Massenspektrometrie (IDMS) zur peptidbasierten Proteinquantifizierung. Die kombinierten Methoden erlauben eine präzise Messung der Viruspartikelzahlen, indem sie die Messungen von Nukleinsäure und Protein anhand der bekannten Stöchiometrie der viralen Kapsidkomponenten miteinander verknüpfen.

Zur Etablierung der Referenzmethode wurde HCMV unter kontrollierten Laborbedingungen hergestellt und mittels Dichtegradienten-Ultrazentrifugation gereinigt. Die proteomische Charakterisierung identifizierte das Major-Kapsidprotein (MCP) sowie die Triplex-Untereinheiten Tri1 und Tri2 als geeignete Proteine für die Quantifizierung. Für die Analyse wurden Signaturpeptide der jeweiligen Proteine ausgewählt und kommerziell beschafft. Die Si-Rückführung erfolgte mittels Aminosäureanalyse mittels exakter Isotopenverdünnungs-Massenspektrometrie. Für die quantitative Analyse von Kapsidproteinen über Signaturpeptide wurde eine LC-MS/MS-Methode entwickelt. Parallel dazu ermöglicht ein ddPCR-Assay aus das virale UL54 Gen, die direkte Bestimmung der absoluten Genomkopienanzahlen.

IDMS-basierte Messungen ermöglichten eine unabhängige Quantifizierung der Kapsidproteine, die unter Verwendung etablierter Kryo-Elektronenmikroskopie-Stöchiometrien in Kapsidzahlen umgewandelt wurden. Die Integration der aus ddPCR und IDMS erhaltenen Messergebnisse resultierte in einer geschätzten Viruspartikelkonzentration von ca. 6 x 10^7 Virionen pro Milligramm Probe. Die Unsicherheitsbudgets beider Methoden wiesen eine Überschneidung auf, was die Zuverlässigkeit dieser beiden unabhängigen primären Ansätze bestätigte.

Eine umfassende Unsicherheitsanalyse gemäß dem „Guide to the Expression of Uncertainty in Measurement“ (GUM) identifizierte die DNA-Extraktionseffizienz und den biologischen Umrechnungsfaktor von Protein zu Kapsidanzahl als Hauptfaktoren für die Gesamtunsicherheit der Messung.

Darüber hinaus wurde ein plasmidbasierter Laborstandard (pYB01) entwickelt, welcher ein HCMV-UL54-Genfragment beinhaltet, durch Sequenzierung verifiziert und mittels ddPCR evaluiert wurde.

https://doi.org/10.7795/110.20260518

Dieses Material fungiert als Kalibrator für quantitative PCR-Assays (qPCR). Es ist SI- rückführbar und ermöglicht eine standardisierte Quantifizierung des Virusgenoms in der Forschung und in der Diagnostik.

Die vorliegende Arbeit demonstriert, dass die Kombination von ddPCR und IDMS die Entwicklung einer SI-rückverfolgbaren Methode zur Bestimmung der Viruslast ermöglicht. Der hier dargestellte Anwendungsansatz vereint die Disziplinen der Metrologie und Virologie und ermöglicht eine verbesserte Präzision, Reproduzierbarkeit und Vergleichbarkeit der Virusquantifizierung der Virenlastbestimmung. Dieser Ansatz bildet die Grundlage für die zukünftige Entwicklung zertifizierter Referenzmaterialien und standardisierter Verfahren in der Virenlastbestimmung. Er trägt zu einer zuverlässigeren Diagnostik, klinischen Überwachung und Reaktion auf Ausbrüche bei.

https://doi.org/10.7795/110.20260518

Table of Contents

https://doi.org/10.7795/110.20260518

https://doi.org/10.7795/110.20260518

https://doi.org/10.7795/110.20260518

https://doi.org/10.7795/110.20260518

1 Introduction

1.1 Metrology and traceability

In order to make direct comparisons between measurements taken at different times and in different places, a shared standard is essential. The need for standardisation dates back to ancient times. In Egypt, for example, building measurements were based on the royal cubit. The cubit was also a traditional unit of length used across Europe and varied from region to region, typically being defined as the length of a person's forearm. It was particularly important in the textile trade and was also used to standardise the size of bread loaves to ensure fair pricing. Early standards were often localised and inconsistent. Such inconsistencies made trade exchanges difficult, even between neighboring cities (1).

Modern metrology is founded on the International System of Units (Système International d'Unités, or SI units), which was established in 1960. The primary goal of this global standardisation effort is to eliminate variations in measurement results for the same sample that arise from differences in measurement methods, geographic location, or timing. To ensure comparability, reference measurement systems are established, enabling traceability to certified reference materials that are directly linked to one of the seven SI base units (kilogram, meter, second, mole, ampere, kelvin, and candela). This traceability is maintained through an unbroken chain of comparisons, each with a documented uncertainty that accounts for all sources of variability (2). This chain typically consists of several calibrators and reference measurement procedures, with the final links being a primary reference material, the material of highest metrological order, and the primary method by which its value was assigned.

Over time, the concept of metrology has expanded beyond the realization of physical constants into chemistry and biology, allowing for the accurate comparison of substance quantities. Within metrology, the amount of material can be expressed in various ways: mass fraction (e.g., mg/g), molar fraction (e.g., nmol/mol), or amount of substance content (e.g., nmol/g) (3).

A primary method is defined as one that aims to determine the "true" value of an unknown quantity with the highest possible accuracy and the lowest possible measurement uncertainty. This is achieved through a complete understanding of the measurement equation. Two types of primary methods were recognised: the primary direct method and the primary ratio method.

A primary direct method, such as gravimetry or coulometry, assigns a value to an unknown directly, referencing either an SI base unit (e.g., the kilogram) or a fundamental physical constant (e.g., Faraday's constant), without relying on another standard material.

https://doi.org/10.7795/110.20260518

In contrast, primary ratio methods are applied to bulk quantities independent of the system's material amount that cannot be measured directly, such as mass fraction or amount of substance content. These methods involve comparing the unknown quantity to a standard of the same quantity to form a ratio. Such methods were extensively used in chemical metrology.

As illustrated Figure 1, this approach provides the highest level of traceability. In this example, a primary reference standard was assigned using a primary ratio method, specifically, isotope dilution mass spectrometry (IDMS) (4, 5).

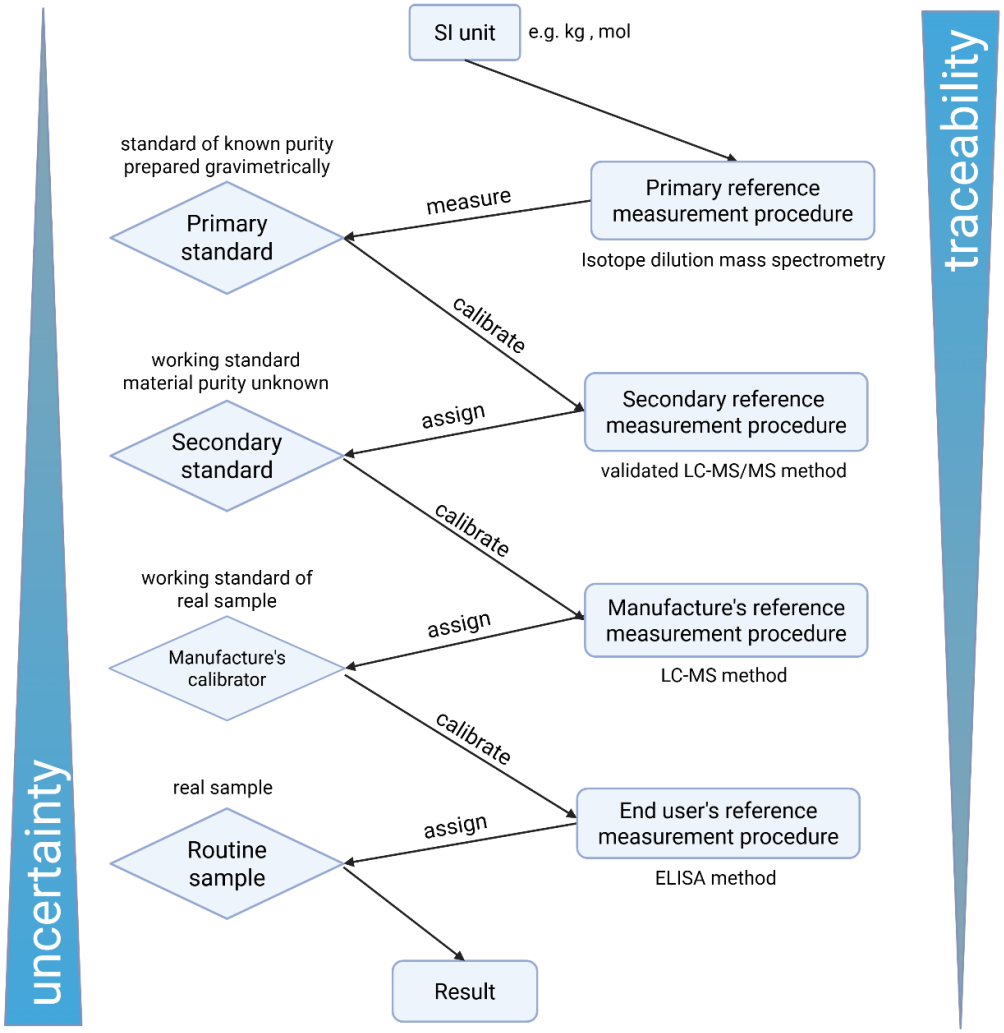

Figure 1: Key components in the metrological traceability chain.
From a routine result to the SI with examples of calibrator and measurement procedures used in chemical metrology at each stage. Adapted from Barwick et al, 2011 (6).

1.1.1 Counting and SI unit “one”

Counting is a basic way of understanding the world. From the earliest human societies, which relied on counting to track animals and crops, to the present day's sophisticated applications in

https://doi.org/10.7795/110.20260518

biotechnology and nanoscience, counting remains a fundamental and direct form of quantification. Despite its ubiquity, counting has traditionally occupied a marginal position within the framework of metrology. For a considerable portion of its existence, the International System of Units has centred on quantifying continuous quantities such as length, mass, and time, articulated through dimensioned units including the metre, kilogram, and second. Conversely, discrete quantities were frequently regarded as "dimensionless" and denoted by the unit symbol These quantities were largely excluded from rigorous metrological analysis (7). This perspective has undergone a notable shift in recent decades. Advancements in the fields of chemistry, biology, information science and environmental monitoring have brought to the attention of the scientific community the critical role of counting in modern measurement science. In these domains, measurements frequently involve counting well-defined but non-identical entities, including DNA copies, viral particles, red blood cells, nanoparticles, and bits of digital information. It is important to recognise that these measurements are not simply a count of items, they require calibration, statistical interpretation, and uncertainty estimation. Consequently, the practice of counting is progressively being acknowledged as a legitimate and verifiable form of measurement, with the unit one emerging as a substantiated SI unit for the expression of the outcomes of such quantifications (8, 9).

The unit “one” is distinguished by its unique status within the SI. It is not derived from any of the seven base quantities (e.g. mass or time) and carries no dimension in the traditional sense. However, this neutrality is precisely what confers its potency, for it facilitates the articulation of both ratio quantities (e.g. mol/mol concentration) and true counting quantities, which in turn reflect the number of discrete entities being measured (8). Ratios frequently involve units of measurement such as mol/mol or kg/kg. In contrast, counted quantities rely solely on the unit "one" and depend heavily on contextual description for clarity. In this context, the counting and utilisation of units are rationalised when specific criteria are met. Firstly, it is necessary to consider the quantity in regard to its composition. In order to facilitate the process of measurement, the quantity must consist of well-defined, discrete entities that can be individually recognised and counted. Secondly, these entities frequently fall outside the domain of the SI base unit for amount of substance, the mole. While the mole is traditionally applied to collections of identical, elementary entities involved in chemical reactions (such as atoms, molecules, or ions), many practical measurements involve non-elementary, heterogeneous, or biologically complex entities. In such cases, the mole is conceptually inappropriate, and counting with unit “one” is more accurate and meaningful (9). For example, consider the field of molecular biology, where the number of DNA copies present in a sample during a quantitative PCR (qPCR) assay is commonly expressed in terms of copies per microlitre. These DNA fragments may vary in length, may not be chemically

https://doi.org/10.7795/110.20260518

identical, and are not typically involved in stoichiometric chemical reactions. The utilisation of moles as a means of expression would result in a misrepresentation of their identity and number. In the domain of clinical diagnostics, red blood cell counts are typically reported in units of 10^6 1/µL. It is crucial to note that these quantities are SI-traceable when validated by standard procedures and reference methods. These values are indicative of the presence of discrete biological entities, rather than quantifiable chemical substances. The utilisation of unit “one” is valid as the entities in question are countable but do not fulfil the criteria for chemical definition in the manner necessary for the mole. As Brown emphasises, it is important to draw a distinction between the amount of substance and the counting of quantities in order to avoid any potential confusion (9). The mole is predicated on the Avogadro constant and presupposes a set of identical elementary particles, such as carbon-12 atoms. Conversely, the term "counting" is more expansive in scope, as it can be applied to a variety of entities, including microbial colonies, blood cells, viral particles and any group of objects that can be defined and distinguished, although not necessarily standardised chemically. This broader application gives rise to a critical question: can counting be traced back to the SI? The response to this question is yes, on the condition that the process of counting is well-defined, the entities are clearly identified, and the measurement is conducted using instruments that have been validated and calibrated. As stated in the SI Brochure (10), the unit “one” is inherently part of the SI and can be utilised to express quantities, provided that the associated measurement method provides traceability. For instance, the measurement of colony-forming units in a microbiological assay is traceable and depends on internationally agreed definitions and protocols. Such definitions and protocols can be found, for example, in ISO 80000-1:2013 for information science and technology (11).

Nevertheless, the expression of counted quantities is often subject to interpretation. For instance, the notation "1/mL" offers minimal insight without the context of the quantity being measured. Consequently, Brown emphasises the pivotal role of verbal description in this context. It is imperative that the quantity is fully described in words; for instance, "number concentration of viable bacterial cells in solution", as opposed to just "1/mL". This approach is adopted to circumvent the potential for confusion and deviation from the established SI conventions that may arise from the utilisation of pseudo-units such as "cells/mL" (7). In conclusion, it is evident that counting is now recognised as a valid and essential part of the SI measurement framework, especially in contexts where the mole is not applicable. The unit one, despite being dimensionless, fulfils a pivotal function in the expression of these quantities, on the condition that the measurement process is adequately defined and traceable. In the fields of chemistry, biology and associated sciences, the necessity to measure discrete entities with precision and consistency has resulted in an expanded conception of what constitutes a measurable

https://doi.org/10.7795/110.20260518

quantity. This expansion has led to the integration of counting within the domain of rigorous metrology.

1.1.2 Traceable protein quantification

The choice between peptide- and protein-based calibrators is critical for ensuring the accuracy and traceability of quantitative proteomics. Although peptides are easier to synthesise and characterise at a high level of purity, several studies have demonstrated that using them as calibrators introduces specific limitations, particularly with regard to digestion efficiency and matrix effects. A recent study by (12) directly compared peptide- and protein-based calibrators for quantifying cardiac troponin I in human serum using isotope dilution LC–MS/MS. Both approaches achieved similar limits of quantification; however, peptide-based calibration introduced systematic quantitative biases in recovery, particularly in complex biological matrices. These findings highlight the importance of exercising caution when using peptide-only calibrators with clinical samples. In another study, Nouri-Nigjeh et al. (13) evaluated various calibration methods, including short peptides, extended peptides and intact proteins, to quantify therapeutic proteins. The study found that, although extended peptides slightly improved accuracy, only protein-based or hybrid calibrations consistently produced results within acceptable uncertainty margins. This was attributed to the fact that full-length proteins better replicate protein digestion kinetics and matrix interactions. Further supporting this, Scott et al., 2015 evaluated internal standard strategies using synthetic peptides and recombinant proteins. Their results clearly showed that full-length protein standards yielded the most accurate and reproducible quantification, primarily because they undergo the same digestion and processing steps as endogenous proteins. It should be noted that synthetic peptides exhibited variable performance unless flanking sequences from the native protein were included, as this helped to approximate natural cleavage patterns more closely (14). These studies highlight that while peptide calibrators offer practical and logistical advantages, they often lack the biochemical context of full-length proteins, leading to potential under- or over-estimation of protein concentrations. Full-length protein standards, although more challenging to produce, provide superior traceability, digestion equivalence, and overall quantitative reliability, especially in clinically relevant or complex sample matrices. Nevertheless, peptide-based calibrators are often preferred due to their ease of synthesis, high purity and cost-effectiveness, especially in targeted LC-MS workflows. They are particularly useful for quantifying multiple proteins or peptides in a single sample because they support multiplexed assays with precise and flexible internal standards. This makes them ideal for high-throughput and routine applications, provided enzymatic digestion is well controlled.

https://doi.org/10.7795/110.20260518

Consequently, traceability in protein quantification must be established indirectly via standards for which purity can be reliably assigned. In the 1990s, an alternative approach was proposed whereby proteins are quantified based on proteotypic peptides released during tryptic digestion (15, 16). In this method, peptides rather than whole proteins are used as standards. While producing pure peptide standards is more feasible than producing pure protein standards, it remains challenging and is best achieved through indirect methods.

Peptide identification and quantification have traditionally been carried out using acid hydrolysis followed by amino acid analysis (17, 18). In this approach, the primary reference standards are the amino acids themselves, small molecules for which purity can be accurately determined using techniques such as liquid chromatography with UV detection (19) or nuclear magnetic resonance (20, 21). The amount-of-substance content is then determined gravimetrically. By tracing the quantification process from amino acids back to the protein, a chain of traceability can be established (16, 22). With the development of traceable pure protein reference materials, it has become feasible to assign values to proteins in complex biological matrices, such as blood or serum (23-26). This further extends the traceability chain from amino acids to complex biological samples. Figure 2 illustrates the traceability chain for proteins, showing how measurement uncertainty increases the further the chain extends from the SI.

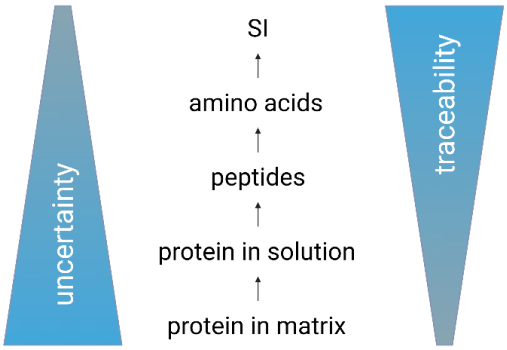

Figure 2: The traceability chain for protein quantification.
The uncertainty increases as the traceability chain becomes longer.

Over the past two decades, the Consultative Committee for the Amount of Substance (CCQM) has played a pivotal role in developing the metrological framework for protein quantification. Initially, efforts focused on amino acid analysis (AAA) as the most reliable means of achieving SI traceability. Through exercises such as CCQM-P55, laboratories around the world showed that combining AAA with isotope dilution mass spectrometry (IDMS) could be used to assign SI-traceable purity values to

https://doi.org/10.7795/110.20260518

peptides (27-29). These exercises identified key gaps in traceability, particularly with regard to peptide purity assignment, digestion variability and comparability across laboratories. This, in turn, limited the robustness of early peptide-based approaches. Subsequent CCQM studies have addressed these issues systematically. For instance, in CCQM-K115 and related comparisons, laboratories were tasked with quantifying clinically relevant proteins using peptide-based IDMS. These studies demonstrated that laboratories could achieve uncertainties well below 10% when using peptide calibrators with SI-traceable purity values (29-32). The results demonstrated that peptide-based strategies, anchored by amino acid analysis (AAA)- characterised calibrators, could deliver reproducible, SI-traceable results across national metrology institutes.

CCQM also provided valuable guidance on closing the remaining traceability gaps, including adopting higher-order purity assessment techniques (e.g. quantitative NMR and mass balance for peptide calibrators), using full-length isotope-labelled proteins as internal standards to minimise digestion-related uncertainty and constructing Guide to the Expression of Uncertainty in Measurement (GUM) compliant uncertainty budgets. This evolution represents a clear maturation of the field, progressing from early methods with limited traceability and high uncertainty to robust, internationally recognised procedures that now underpin Joint Committee for Traceability in Laboratory Medicine (JCTLM)-listed higher-order reference systems. Thus, CCQM's work not only established confidence in peptide-based IDMS as a primary ratio method for protein quantification but also provided a structured approach to closing traceability gaps and reducing measurement uncertainty.

1.1.3 Measurement Uncertainty according to GUM

The result of quantitative measurements is only meaningful when accompanied by a statement of measurement uncertainty, as measurement results are influenced by various sources of error. Accordingly, the result of a measured variable Y should be stated as the measured value or output variable y and an associated measurement uncertainty, which is composed of the measurement uncertainties of the individual input variables xi. The GUM (Guide to the Expression of Uncertainty in Measurement) describes rules for determining the measurement uncertainty of the output quantity y from the measurement uncertainties of the input quantities xi (33). In this work, the measurement uncertainty was determined using the ‘GUM Workbench software (version 2.4.1.392, Metrodata GmbH, Germany), which works according to the rules of the GUM. The principles are briefly explained below.

The first step is to create a model equation that describes the dependence of the output variable y on all input variables xi:

https://doi.org/10.7795/110.20260518

$$y=f\ (x1, x2, x3, \ldots, xi)$$

The second step is to determine the best possible values and associated measurement uncertainties for the input variables xi. A distinction is made between two types of measurement uncertainties, referred to as type A and type B. Type A describes random statistical errors that are determined experimentally from a series of n measurements, the mean value $\bar{x}$ and the standard deviation. This results in the standard deviation of the mean value:

$$u(\bar{x}) = \frac{s}{\sqrt{n}}$$

$u(\bar{x})$: Standard deviation of the mean value

s: Standard deviation

n: Number of measurements

In contrast, Type B uncertainties are not statistical. Information on the values and uncertainties can be taken from certificates or specifications provided by the manufacturer. Furthermore, the various input quantities are classified according to their probability distribution, which is determined by their probability density function. While Type A input quantities are always described by a normal distribution, various distributions can apply to Type B input quantities, e.g. normal distribution, rectangular distribution or triangular distribution.

In addition, a sensitivity coefficient ci is determined, which describes how strongly changes in the respective input variables influence the output variable. The contributions of all input variables to the uncertainty of y are described by a combined measurement uncertainty of y, which is calculated by error propagation of non-correlated input variables as follows:

$$u^2(y) = \sum_{i}^{n} (\frac{\partial y}{\partial xi})^2\ u^2(xi)$$

$u^2(y)$: combined variance of the output variable y

$u^2(xi)$: variance of the various input variables xi

$\partial y/\partial xi$: partial derivative of y with respect to xi

The expanded measurement uncertainty U is calculated by multiplying the combined measurement uncertainty by a so-called expansion factor k. The K-factor is obtained from the two-sided Students's T distribution in consideration of the desired level of confidence (in general 95%).

https://doi.org/10.7795/110.20260518

$$U = k \cdot u(y)$$

U: expanded measurement uncertainty

k: expansion factor

u(y): combined measurement uncertainty of the output variable

The result of the measured variable Y from the output variable y and its expanded measurement uncertainty U is given as follows:

$$Y = y \pm U$$

1.2 Mass spectrometry

Mass spectrometry (MS) is a powerful analytical technique that measures the mass-to-charge ratio *(m/z)* of ions in the gas phase. This enables accurate determination of molecular mass and structural characterisation.

The technique has its origins in the early twentieth century, when J. J. Thomson obtained the first mass spectra of small gaseous ions such as O_2, N_2, CO and CO_2 in 1913 (34). Building on this work, F. W. Aston refined the approach to measure the masses of over 100 stable isotopes (35-37), thereby laying the foundation for modern MS.

A contemporary mass spectrometer consists of three main components: an ion source, a mass analyser and a detector. The ion source generates gaseous ions from neutral molecules, the mass analyser separates these ions according to their mass to charge ratio (*m/z)*, and the detector records a mass spectrum providing information on the *m/z* values and relative abundances of the ions (38-40).

Sample introduction can be performed directly, such as by syringe infusion, or in combination with separation techniques, such as gas chromatography (GC) or high-performance liquid chromatography (HPLC), which can improve analyte resolution prior to ionisation. While a variety of ionisation sources, analysers, and detectors exist, this thesis will focus exclusively on configurations relevant to the experimental work presented herein.

1.2.1 Ionisation

In mass spectrometry, ionisation is the process of converting neutral molecules into charged particles (ions), which can then be manipulated, separated and detected by the instrument. As these ions must travel freely without colliding in a way that could alter their trajectories, mass spectrometry is typically

https://doi.org/10.7795/110.20260518

performed under high vacuum conditions. These vacuum preserves ion integrity and improves transmission efficiency, enabling accurate measurement of the mass-to-charge ratio (*m/z*). The type of ionisation method used determines the types of ions produced, the extent of fragmentation, and the quality of the resulting mass spectrum.

1.2.1.1 Electrospray ionisation

Electrospray ionisation (ESI) is a continuous-flow ionisation technique that facilitates the transfer of analytes from a liquid solution into the gas phase. This makes it ideal for coupling liquid-phase separation methods, such as liquid chromatography, with mass spectrometry. The principle of droplet charging in electrospray was first described by Lord Rayleigh in 1882 (41). In the late 1960s, Dole and his team investigated the electrospray of macromolecules, including polystyrene, to generate intact gas-phase ions from solution without degradation (42). Building on this work, in the 1980s Fenn and his colleagues adapted ESI as a robust interface between LC and MS (43, 44). This development is widely recognised as one of the most significant advances in mass spectrometry in the 20th century. This achievement earned Fenn a share of the Nobel Prize in Chemistry in 2002. The use of ESI has transformed the analysis of large and fragile biomolecules by enabling their ionisation at atmospheric pressure with minimal fragmentation. Today, LC-ESI-MS(/MS) is a leading technique in quantitative bioanalytical research thanks to its high selectivity, sensitivity and compatibility with complex biological matrices (37, 45).

When an LC system is coupled directly to an ESI source, the eluent is delivered through a fine electrospray needle that is held at a high potential in relation to a counter electrode. This electric field generates a spray of positively charged droplets containing both the analyte and the solvent. As these droplets travel towards the counter electrode, the evaporation of the solvent reduces their size, thereby increasing the surface charge density. Once the Rayleigh limit is reached, the point at which the electrostatic repulsion between the surface charges exceeds the surface tension of the droplet, the droplet becomes unstable and undergoes Coulomb fission. This is a process in which the droplet ejects smaller, highly charged particles to reduce its charge density. Through repeated evaporation-fission cycles, this sequence ultimately produces singly and multiply charged analyte ions in the gas phase (41, 46).

https://doi.org/10.7795/110.20260518

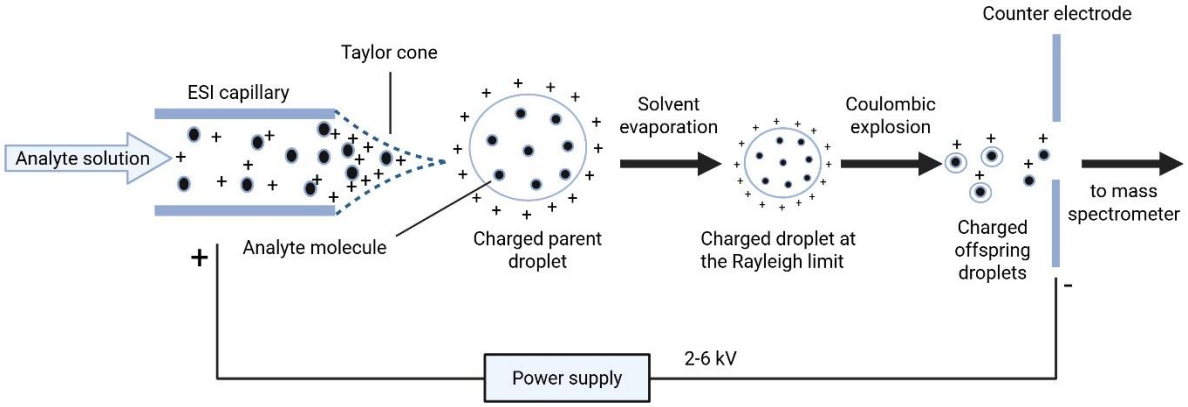

Figure 3: Electrospray ionisation.
Schematic showing the formation of a Taylor cone at the tip of the capillary during electrospray ionisation, as well as the evaporation of the solvent and the formation of gas-phase ions. Generated with Biorender.

1.2.2 Mass analysers

A wide range of mass analysers is available, and the choice of analyser must match the specific requirements of the analytical method. For this thesis work, one of the aims is accurate quantification; therefore, high sensitivity and selectivity are important. Furthermore, the analyser must deliver optimal performance over the required *m/z* range and provide an appropriate dynamic range. It must also ensure efficient ion transmission at each stage to maximise signal intensity.

In a mass spectrometer, ions generated in the ion source are transferred into the evacuated mass analyser, where they are separated according to their mass-to-charge ratio (*m/z*). Based on their operating principles, mass analysers can be broadly classified into two categories. Scanning analysers use dynamic electric or magnetic fields to selectively transmit ions of a specific *m/z* at any given moment (e.g. quadrupole). In contrast, non-scanning analysers detect the full *m/z* range from a single pulse of ions (e.g. Orbitrap). The specific analysers employed in this thesis are described briefly in the following sections

1.2.2.1 Quadrupoles

Quadrupoles are among the most widely used mass analysers due to their versatility. They can transmit a single *m/z* value or scan across an entire *m/z* range by varying the applied electric fields. First developed in the 1950s by Paul and Steinwedel, a quadrupole consists of four parallel metal rods, arranged as two opposing pairs (47). A static direct current (DC) potential is applied to each pair of rods, which is overlaid with an out-of-phase alternating radiofrequency (RF) voltage.

Ions entering the quadrupole experience a combination of DC and RF fields, which determine the stability of their trajectories. Stable ions pass through to the detector, while unstable ions are deflected

https://doi.org/10.7795/110.20260518

into the rods and lost. When the DC and RF values are fixed, only ions with a single *m/z* value can follow a stable path, enabling the quadrupole to act as a mass filter. When these values are scanned, ions of different *m/z* values are transmitted sequentially, producing a mass spectrum. The upper mass range for stable transmission is typically around 4,000 *m/z*.

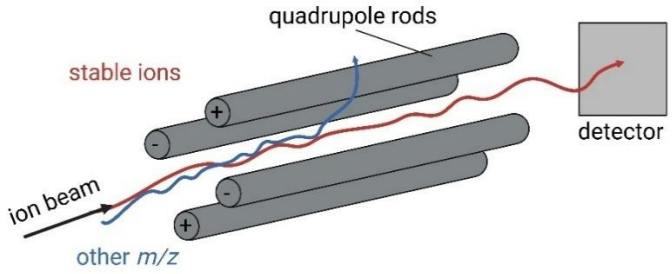

Figure 4: Scheme of a Quadrupole analyser.
Showing that stable ions (red) pass through the quadrupole field and are detected, whereas unstable ions (blue) collide with the quadrupole rods and are lost. Generated with Biorender.

Multiple quadrupoles can be coupled in series to enhance selectivity and specificity. In a triple quadrupole (QqQ) setup, the first quadrupole isolates a selected precursor ion, which is then fragmented in a collision cell via collision-induced dissociation (CID). The third quadrupole then monitors the specific product ions, enabling selected reaction monitoring (SRM) a highly specific transition that is unique to the analyte of interest. This high selectivity is ideal for quantitative analysis, where monitoring a defined transition minimises background noise. Accurate quantification requires well-defined chromatographic peaks, with at least ten data points acquired across each peak. To achieve this, the instrument's scan rate must be faster than the analyte's elution profile. In SRM experiments, transitions are often divided into time windows to minimise the number monitored simultaneously, thereby optimising sensitivity. Overall, QqQs enable the precise and reproducible quantification of predefined peptides across large sample sets (48). Their robustness and wide dynamic range make them particularly well-suited to high-throughput studies and clinical applications, in which reproducible quantification is essential (49). Therefore, a QqQ instrument was used for peptide-based protein quantification.

1.2.2.2 Orbitrap

Quadrupole mass analysers record a full mass spectrum by scanning sequentially across the *m/z* range. In contrast, non-scanning analysers such as the Orbitrap instruments acquire the entire spectrum from a single ion packet by measuring oscillation frequency in the Orbitrap.

The Orbitrap operates on the principle of electrostatic trapping, first described by Kingdon in 1923 (50). Ions are injected tangentially into the gap between a central spindle-shaped electrode and a

https://doi.org/10.7795/110.20260518

surrounding barrel-shaped electrode. The electrostatic field forces them into orbital motion around the central electrode while oscillating along its axis. This axial oscillation frequency is independent of kinetic energy and depends only on the *m/z*. The oscillations induce an image current in detection electrodes, which is recorded over time and processed via Fourier transform into a frequency spectrum, then converted into a high-resolution *m/z* spectrum.

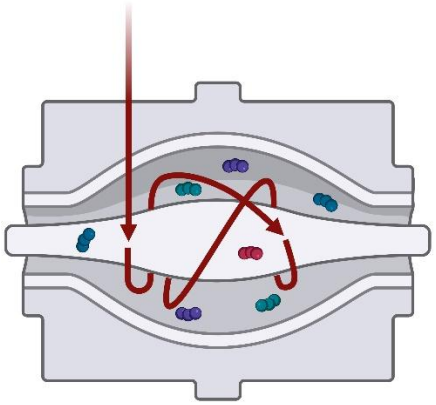

Figure 5: Principle of an Orbitrap analyser.
Ions are injected into the Orbitrap, where they follow stable oscillatory orbits around the central spindle electrode under the influence of an electrostatic field. The frequency of ion oscillation is independent of their initial velocity, depending only on their m/z. This motion is detected and converted into a frequency spectrum, which is then transformed into a mass spectrum.

The commercial LTQ-Orbitrap couples a linear ion trap for ion transmission with an RF-only curved quadrupole (C-trap) for ion storage and rapid injection into the Orbitrap analyser (51). The C-trap is filled with nitrogen bath gas to provide collisional damping, improving ion focusing. To ensure calibration stability and minimize thermal noise, both the analyser and its power supplies must be maintained at a constant temperature. An automatic gain control (AGC) pre-scan in the linear trap determines the optimal ion fill time, preventing space-charge effects. With this configurations, resolving powers exceeding 100,000 (Full Width at Half Maximum, FWHM) can be achieved, and long-term mass accuracy remains better than 5 ppm (51). This high mass resolution is crucial in proteomics, as it allows for the discrimination of near-isobaric peptides and the accurate deconvolution of isotopes. This enables the confident identification of proteins and peptides. However, despite their resolving power, Orbitraps are not ideal for high accuracy quantification. Factors such as space-charge effects, slow scanning speeds and a reduced dynamic range can all compromise the precise measurement of peptide abundances, particularly in complex mixtures (48, 49, 52, 53). Therefore, an LTQ-Orbitrap was used in this thesis for proteomics studies to identify proteins.

1.2.2.3 Collision induced dissociation

Collision cells are a common component of hybrid mass spectrometers and are typically positioned between two quadrupoles. Within the collision cell, preselected and isolated precursor ions collide

https://doi.org/10.7795/110.20260518

with an inert buffer gas, usually argon, nitrogen or helium, converting some of their translational kinetic energy into internal vibrational energy. This collisional activation process increases the internal energy of the ions until specific bonds break, leading to fragmentation.

In low-energy collision-induced dissociation (CID), as employed in triple quadrupole instruments, peptide fragmentation primarily occurs along the backbone, which contains the peptide bond, producing characteristic b- and y-type fragment ions according to the Roepstorff-Fohlman-Biemann nomenclature (54). If the charge is retained on the N-terminal fragment, the ions are designated b, and if it is retained on the C-terminal fragment, they are designated y. Observed mass differences between consecutive ions in these series reveal the identities of the amino acids lost during fragmentation. The extent of energy transfer during CID depends on the kinetic energy of the precursor ion, its mass to charge ratio, and the mass of the collision gas. Ions with a higher m/z require more energy to fragment, while heavier collision gases transfer energy more efficiently. Fragmentation efficiency is also influenced by peptide sequence, charge state and amino acid composition. Fragmentation is charge-directed; basic residues such as arginine (R) and lysine (K) have the highest gas-phase basicity and preferentially sequester protons. Singly charged arginine-containing peptides often require higher energies to mobilise the sequestered proton, and their extent of fragmentation are strongly sequence-dependent.

1.2.3 Isotope dilution mass spectrometry (IDMS) for peptide-based protein quantification

Mass spectrometry combined with isotope dilution (IDMS) is a definitive primary measurement method that can provide accurate, low-uncertainty results for assigning SI-traceable concentrations to primary calibrators (55-57). This technique involves measuring the ratio of isotope fractions in a gravimetrically prepared mixture of the analyte and an isotopically labelled analogue. Successful application requires a stable, isotopically labelled form of the analyte to serve as an internal standard (57).

Ideally, the labelled internal standard would react in a chemical and physical manner identically to that of the target analyte, differing only in mass due to isotopic enrichment with low-abundance atoms such as ^{2}H, ^{13}C, or ^{15}N. Consequently, the labelled and natural forms behave identically during sample preparation yet can be distinguished by their mass in the spectrometer. Quantification is based on the ratio of the measured responses of the two forms, compensating for minor variations in sample complexity or analytical conditions. The only difference between the two forms is the mass shift resulting from isotopic labelling, which ensures identical ionisation efficiency (58). To avoid cross-interference from natural isotopic distribution, the enrichment of the internal standard must be sufficiently high.

https://doi.org/10.7795/110.20260518

To enable accurate recovery correction, the internal standard must be introduced as early as possible in the analytical workflow to allow it to fully equilibrate with the sample. This ensures that both the labelled and natural analytes experience identical conditions. For SI-traceable measurements, primary standards serve as calibrators. The highest-quality metrological standards, standards with the shortest link to the SI, currently available are amino. The National Institute of Standards and Technology (NIST, USA) provides a gravimetrically prepared amino acid mixed solution, quantified by IDMS (59), while the National Metrology Institute of Japan (NMIJ) supplies pure amino acid standards of known purity as characterised by quantitative NMR (21). These primary amino acid standards, together with isotopically labelled amino acids, can be used to assign concentrations to peptide standard solutions. When IDMS is used, peptide quantities can be directly linked to the SI units of mass (kilogram) or amount of substance (mole) (60, 61).

In 1994 exact-matching IDMS (EM-IDMS) was introduced by Henrion (57). In this approach, a calibration blend is prepared gravimetrically to match the ion abundance ratio and molar composition of the natural and labelled peptides in the sample blend. For protein quantification, the calibration blend contains quantified synthetic signature peptides and stable isotopically labelled peptides, while the sample blend contains labelled peptides in known amounts, together with the target protein or peptide. Both blends are enzymatically digested and analysed by LC–MS/MS in selected reaction monitoring (SRM) mode. Quantification is achieved by applying the double exact matching IDMS equation (62).

$$\kappa_x = \kappa_z * \frac{m_z}{m_{yz}} * \frac{m_y}{m_x} * \frac{R_z - R_{bc}}{R_{bc} - R_y} * \frac{R_y - R_b}{R_b - R_x} * P$$

Equation 1: Double exact matching IDMS

κ_x	amount of substance content of sample
κ_z	amount of substance content of reference
m_z	mass of the reference in calibration blend
m_{yz}	mass of spike in calibration blend
m_y	mass of spike in sample blend
m_x	mass of sample in sample blend
R_z	isotope ratio in reference
R_{bc}	isotope ratio in calibration blend
R_y	isotope ratio in the spike
R_b	Isotope ratio in sample blend
R_x	isotope ratio in sample
P	purity of the reference

https://doi.org/10.7795/110.20260518

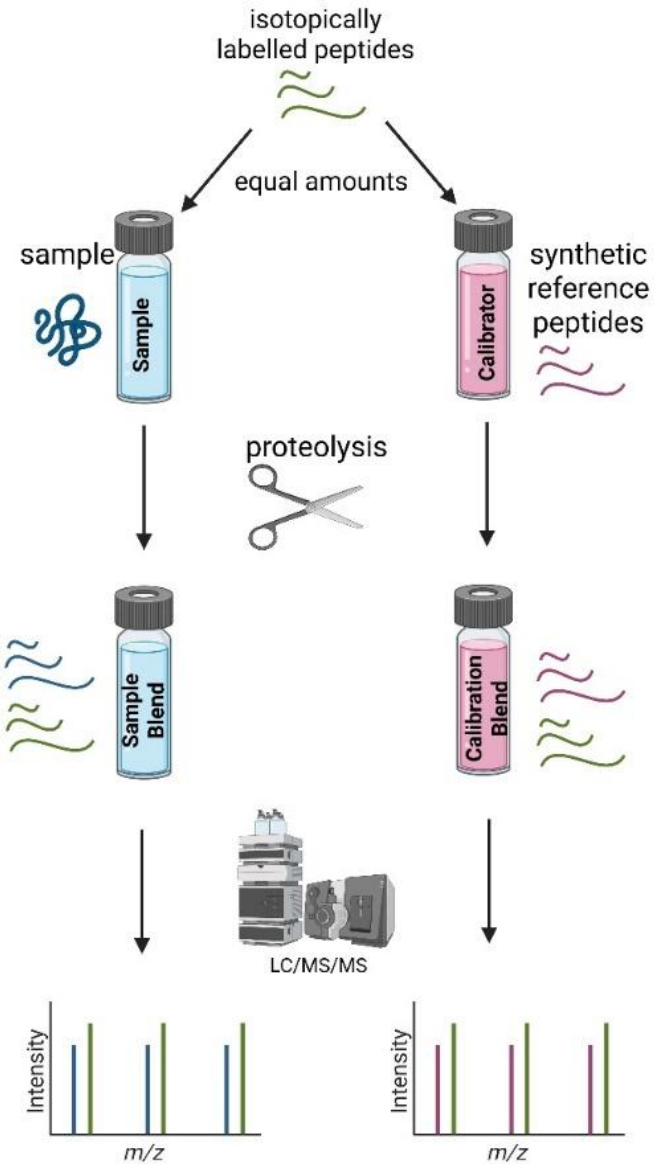

Figure 6: Workflow of exact-matching IDMS.
Equal amounts of isotopically labelled peptides are added to the biological sample and the synthetic peptide calibrator before proteolysis. After digestion, the resulting peptide blends are analysed using LC-MS/MS. Direct comparison of the mass spectrometric signals of the sample and calibration blends enables accurate quantification.

In order for this calibration approach to obtain accurate results the method requires the enzymatic digestion of proteins into unique signature peptides that are liberated in equimolar amounts from the parent protein. These peptides must be free from post-translational modifications and suitable for synthesis in both natural and labelled forms. Furthermore, the peptides must be stable during the digestion protocol. They should also contain at least three amino acids that can be quantified by amino acid analysis (63).

https://doi.org/10.7795/110.20260518

1.3 Polymerase chain reaction (PCR)

The polymerase chain reaction (PCR) is a fundamental molecular biology technique that enables the selective amplification of specific DNA sequences. First developed by Kary B. Mullis in 1983, PCR has revolutionised genetic research and diagnostics by enabling the production of millions to billions of copies of a particular DNA segment from minimal starting material (64). This powerful and versatile method forms the basis of many applications in research, medicine, forensics and biotechnology (65). The core principle of PCR is its ability to mimic the natural process of DNA replication in a controlled, cyclic manner. By repeatedly heating and cooling the reaction mixture, PCR enables the enzymatic synthesis of DNA in three main steps: denaturation, annealing and extension. During denaturation, the double-stranded DNA template is heated to around 94–98 °C, breaking the hydrogen bonds between complementary bases and resulting in single-stranded DNA molecules. In the annealing step, the temperature is lowered (typically to 50–65 °C) to enable short synthetic primers to bind, or anneal, to their complementary sequences flanking the target region. In the final step, the temperature is increased to 72 °C, which optimises the activity of a thermostable DNA polymerase, most commonly Taq polymerase (66). This enzyme extends the primers by adding nucleotides complementary to the template strand, synthesising a new DNA strand. These three steps constitute one PCR cycle, and each cycle theoretically doubles the amount of target DNA in comparison to the previous cycle. After 25–40 cycles, this exponential amplification results in a substantial quantity of the specific DNA fragment of interest. The amplified DNA product can be analysed using electrophoretic methods and fluorescent dyes to detect the production of the correctly sized DNA product.

The Polymerase Chain Reaction (PCR) has had a profound influence on the diagnosis and management of infectious diseases. In the early stages of research into its application for the detection of *Mycobacterium tuberculosis*, it was revealed that PCR achieved sensitivity, specificity, and positive/negative predictive values comparable to those of traditional culture methods (67). Furthermore, results were reported to be available in approximately 6.5 hours. Conversely, culture-based diagnostics for *Mycobacterium tuberculosis* have been shown to require up to 14 days for detection (68), underscoring the clinical value of PCR in significantly reducing time-to-diagnosis and potentially enhancing patient outcomes.

https://doi.org/10.7795/110.20260518

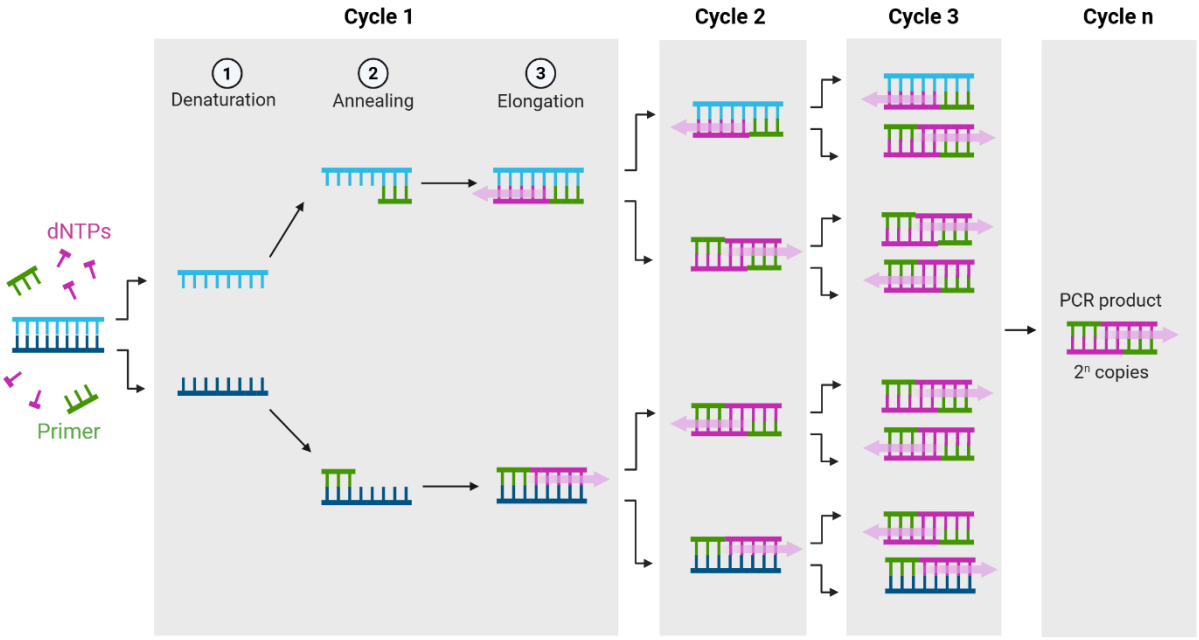

Figure 7: Schematic representation of the PCR reaction.
The reaction consists of repeated thermal cycling steps: (1) denaturation of double-stranded DNA; (2) annealing of primers to complementary target sequences and (3) elongation by DNA polymerase. Each cycle doubles the number of DNA molecules, resulting in the exponential amplification of the target sequence and yielding 2^n) copies after n cycles.

The adaptability and versatility of PCR in the field of infectious disease diagnostics are demonstrated across a wide range of applications. This method has been shown to facilitate the sensitive detection of pathogen DNA in biological specimens that are often challenging to collect or contain low concentrations of the organism, such as cerebrospinal fluid (CSF), amniotic fluid, urine, saliva, and respiratory secretions (69). Modifications of the standard PCR protocol, such as nested PCR, which involves two successive rounds of amplification using distinct primer sets, have been successfully employed for detecting Plasmodium species in epidemiological studies (70).

Furthermore, a significant body of research has demonstrated the efficacy of PCR targeting bacterial 16S ribosomal DNA, a technique commonly referred to as broad-range PCR. This method has gained widespread acceptance within the domain of clinical bacteriology, serving as a fundamental approach for subsequent microbiome analyses (67). It is also possible to adapt the technique so that it can be used to amplify complex DNA templates, including those with a high GC content. Furthermore, multiplex PCR facilitates the concurrent detection of multiple gene targets within a single reaction. This approach has been shown to conserve reagents and reduce turnaround time, while also facilitating the identification of associations between multiple targets (71). The simplicity, speed and high sensitivity of PCR have made it an indispensable tool in areas such as genetic engineering, pathogen detection, genotyping and forensic analysis (72).

https://doi.org/10.7795/110.20260518

1.3.1 Quantitative real-time PCR (qPCR)

The development of quantitative real-time PCR (qPCR) represented a significant advancement in the evolution of conventional PCR, allowing for the simultaneous amplification and detection of DNA within a single reaction (73). A significant benefit of PCR amplification in real time is that it eliminates the necessity for post-PCR analysis using electrophoretic gels, thereby markedly reducing the overall time required to obtain results.

qPCR is based on the same fundamental principles as conventional PCR, yet it possesses the additional capability of tracking DNA amplification in real time. This is achieved by detecting changes in fluorescence after each cycle, which reflect the accumulation of double-stranded DNA (dsDNA). Fluorescence can be measured using intercalating dyes, such as SYBR® Green, which bind non-specifically to dsDNA, or through sequence-specific fluorescent probes like hydrolysis probes (Figure 8). The utilisation of labelled probes facilitates real-time detection and enhances the specificity of the assay, as these probes bind exclusively to the target DNA sequence. Consequently, probe-based qPCR has become increasingly prevalent for the purpose of infectious disease diagnostics (74). Furthermore, the availability of a range of fluorophores with different emission spectra enables the detection of multiple targets simultaneously in a single multiplex reaction.

The process of fluorescent signal detection commences at the point at which the signal first exceeds the background levels, a phenomenon referred to as the quantification cycle (Cq) (75). The Cq value is defined as the PCR cycle number at which the target sequence is detected, thereby serving as a threshold for the confirmation of amplification. Whilst qPCR can be used to determine the presence or absence of a target, it also allows for precise quantification. This is typically achieved by comparing the Cq value of an unknown sample to a standard curve generated from a dilution series of a known calibrator. The resulting curve, which plots Cq values against the logarithm of known DNA quantities, enables accurate determination of target concentration in the sample (74, 76). In order to ensure reliable quantification, it is imperative that the standard is adequately characterised, free from any inhibitors, and closely resembles the composition of the test sample.

https://doi.org/10.7795/110.20260518

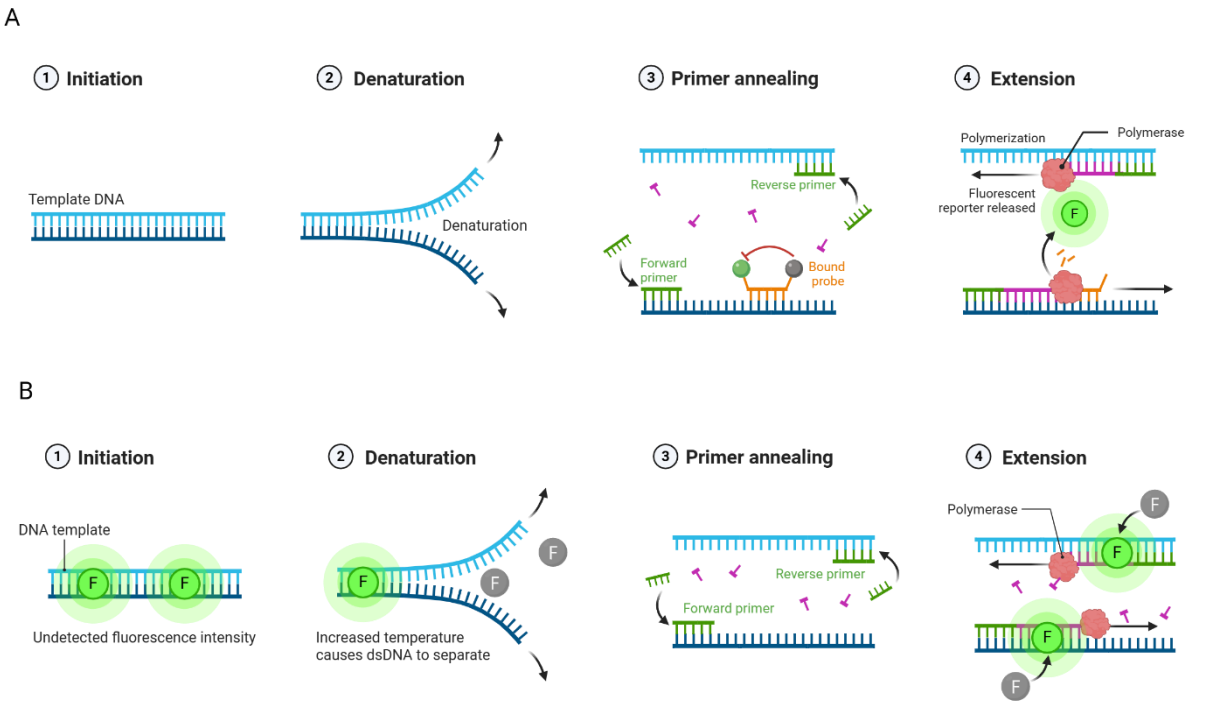

Figure 8: Principles of fluorescent probe–based and dye–based quantitative PCR (qPCR).
The amplification cycle for both methods consists of (1) Initiation, where the double-stranded DNA (dsDNA) template is present before denaturation; (2) Denaturation, in which heating separates the dsDNA into single strands; (3) Primer annealing, where forward and reverse primers bind to their complementary target sequences; and (4) Extension, where DNA polymerase synthesises new strands. In probe–based qPCR (A), a sequence-specific fluorescent probe binds the DNA, probe cleavage during extension separates the fluorescence reporter from the quencher, generating a fluorescence signal. In dye–based qPCR (B), fluorescence is produced when fluorescence dye intercalates into double-stranded DNA.

In the contemporary scientific community, qPCR is widely recognised as the gold standard for nucleic acid quantification. The instrument's capacity to measure pathogen load with high sensitivity and specificity has rendered it indispensable in the diagnosis and management of infectious diseases. When employed in conjunction with reverse transcription (RT-qPCR), the method facilitates the quantification of viral RNA, thereby providing critical insights into viral load for pathogens such as HIV-1, hepatitis C virus, and coronaviruses. This quantitative information plays an important role in assessing transmission risk, guiding treatment strategies, and monitoring disease progression (77-79).

From a metrological perspective, qPCR has the advantage of a wide dynamic range of 8–9 logs (80), high throughput capacity, and well-established protocols across diagnostic and research laboratories. Nevertheless, the primary restriction of this method is its relative nature, which renders quantification contingent on external calibration curves. Consequently, this introduces variability and measurement uncertainty. This dependency also weakens traceability, since calibration standards must themselves be validated against higher-order reference materials, and differences in PCR efficiency can significantly affect results (81). Consequently, the inter-laboratory reproducibility of quantitative polymerase chain reaction (qPCR) is often compromised, with reported variability in the range of 10- to 50-fold differences when compared to digital PCR reference values (82). The number of cycles is another major

https://doi.org/10.7795/110.20260518

source of error propagation — small deviations in amplification efficiency or Cq determination are magnified exponentially across 30–40 cycle (83-85).

Although qPCR remains the gold standard for sensitive and high-throughput nucleic acid quantification, its reliance on calibration standards and amplification efficiency introduces significant sources of uncertainty and limits metrological traceability, underscoring the need for more absolute and reproducible quantification methods.

1.3.2 Droplet digital PCR (ddPCR)

First described in the 1990s (86), digital PCR (dPCR) has emerged over the past decade as a precise method for quantifying nucleic acids (75). The technique involves partitioning a PCR reaction into numerous micro-reactions, some of which contain the target nucleic acid and some of which do not. Amplification occurs in each partition using fluorescence-based chemistries, most commonly hydrolysis probes. The number of positive partitions, relative to the total number of partitions, is used to calculate the absolute target concentration via Poisson statistics (76). dPCR has found applications in virology, bacteriology, mycology and parasitology. In virology, for example, it has been used to measure viral loads in pathogens such as HCMV (87) and HIV-1 (88), to detect rare drug-resistance mutations in influenza (89) and to evaluate chromosomally integrated herpesviruses (90). dPCR has also been used for the detection of bacteria, such as Staphylococcus spp., Mycobacterium tuberculosis and Chlamydia trachomatis, as well as fungi, helminths and protozoa (91-95).

Commercial dPCR platforms can be broadly divided into fixed-volume chamber systems and droplet-based oil-partitioning systems. These offer thousands to millions of partitions, depending on the technology (96). Unlike qPCR, dPCR provides standard curve-free quantification and is highly sensitive to low-copy targets. It also supports multiplexing for the simultaneous detection of multiple sequences (97).

From a metrology perspective, digital droplet PCR (ddPCR) aligns more closely with the principles of the International System of Quantities, as quantification is directly based on the counting of events, thereby avoiding reliance on external calibrators (81). A substantial body of research has demonstrated the efficacy of ddPCR in delivering more reproducible and accurate measurements, particularly in the context of low-copy targets or complex matrices (82, 98). This highlights its potential as a robust reference measurement procedure for nucleic acid quantification.

https://doi.org/10.7795/110.20260518

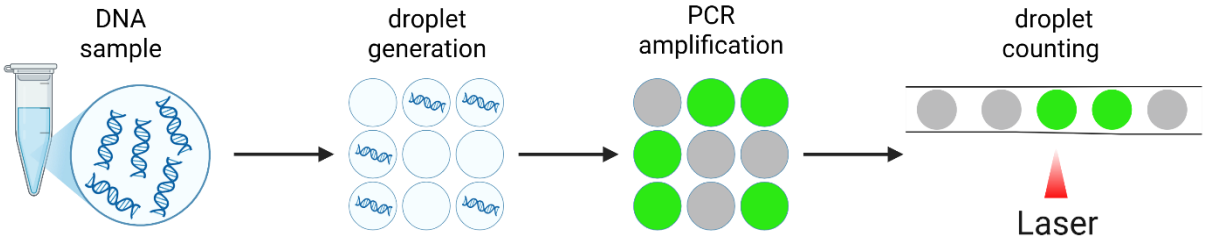

Figure 9: ddPCR principle.
Sample partitioning, thermal cycling and detection of fluorescence. A total reaction volume containing the DNA template is divided into multiple droplets. In each droplet, an individual PCR amplification takes place. The resulting fluorescence signal is detected. Droplets are counted as positive or negative. Generated with Biorender.

In contrast to qPCR, droplet digital PCR (ddPCR) is, to a considerable extent, independent of the number of amplification cycles. In ddPCR, amplification occurs within thousands of discrete droplets, and each droplet is evaluated in a binary manner, classified simply as positive or negative for the target sequence. Quantification is therefore based on the absolute count of positive droplets relative to the total number of partitions, following Poisson statistical principles, rather than on the continuous monitoring of fluorescence kinetics or the determination of a cycle threshold value. Nevertheless, ddPCR is subject to certain limitations, including a comparatively lower dynamic range (4–5 logs), higher costs, and longer processing times when compared to qPCR (99).

In summary, ddPCR represents a highly precise and metrologically robust advancement in nucleic acid quantification. It enables the ability to count, is calibration-free and has a superior reproducibility and traceability compared to qPCR, despite its narrower dynamic range, higher cost, and longer processing time.

1.4 Human Cytomegalovirus

The human cytomegalovirus (HCMV), also called human herpesvirus 5, is one of the largest (in terms of its physical dimension) viruses to cause clinical diseases (100). HCMV is prevalent worldwide, displaying a seroprevalence ranging from 40% to 100% among the adult population. In Germany, seroprevalence is reported to be between 40% and 50%, while in developing countries like Brazil and India over 90% of the population tests positive for HCMV (101, 102). While HCMV infection in healthy individuals is often mild or asymptomatic, it can be the cause for life-threating complications in immunocompromised patients (103, 104). After infection, HCMV establishes lifelong latency within the host. The understanding of the latent state's impact on conditions like cancer, vascular diseases and others remains limited (105-107). Congenital HCMV infection is linked to significant neurological complications, encompassing conditions such as hearing loss, mental disorders and even infant mortality.

https://doi.org/10.7795/110.20260518

Remarkably, it stands as the most prevalent congenital viral infection to date, impacting 20,000 to 30,000 infants annually in the United States (108).

The mature HCMV virions consist of a double stranded DNA genome (109) which is surrounded by an icosahedral capsid, followed by the tegument and an outermost lipid envelope (110, 111). In addition to virions, HCMV-infected cells also produce defective viral particles, namely non-infectious enveloped particles (NIEPs) and dense bodies (DBs) (112).

1.4.1 HCMV infected cells produce Virions, NIEPs and DB

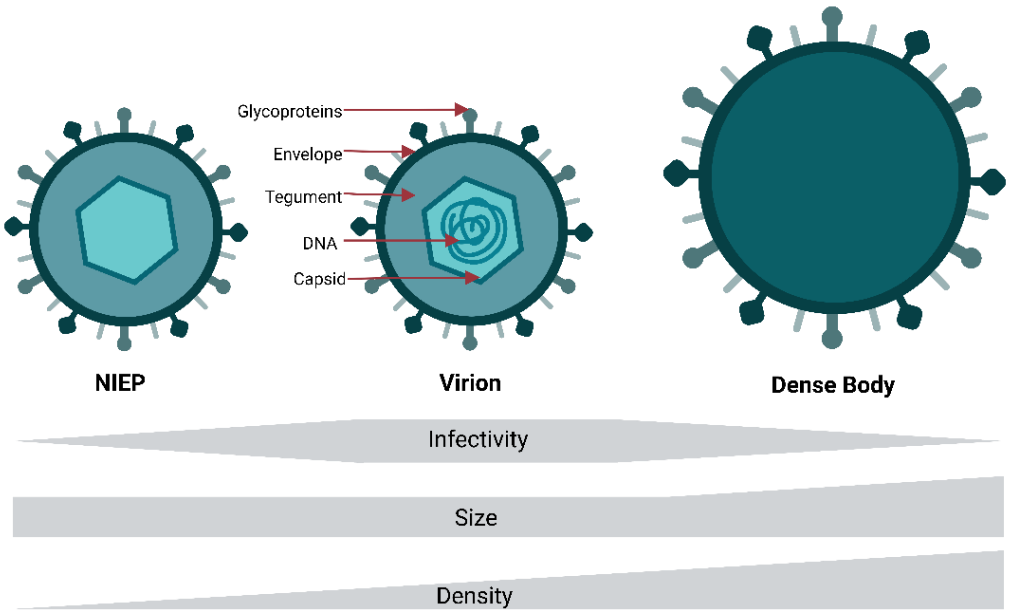

Figure 10: HCMV infected cells produce NIEPs, virions and DBs.
Virions and NIEPs share a similar size, measuring approximately 230 nm, whereas DBs are larger, ranging from 250 to 600 nm in size. While virions represent the fully mature and infectious particles, both NIEPs and DBs are considered as non-infectious. DBs have greater density compared to virions and NIEPs.

The HCMV virion is spherical, about 230 nm in diameter and comprises four components: a double-stranded DNA genome (~230 kb) in its inner core, an icosahedral capsid protecting the genome, a proteinaceous layer surrounding the capsid known as the tegument, and a lipid bilayer envelope that encloses the tegument and contains viral glycoproteins important for attachment and entry into host cells (Figure 10) (113).

https://doi.org/10.7795/110.20260518

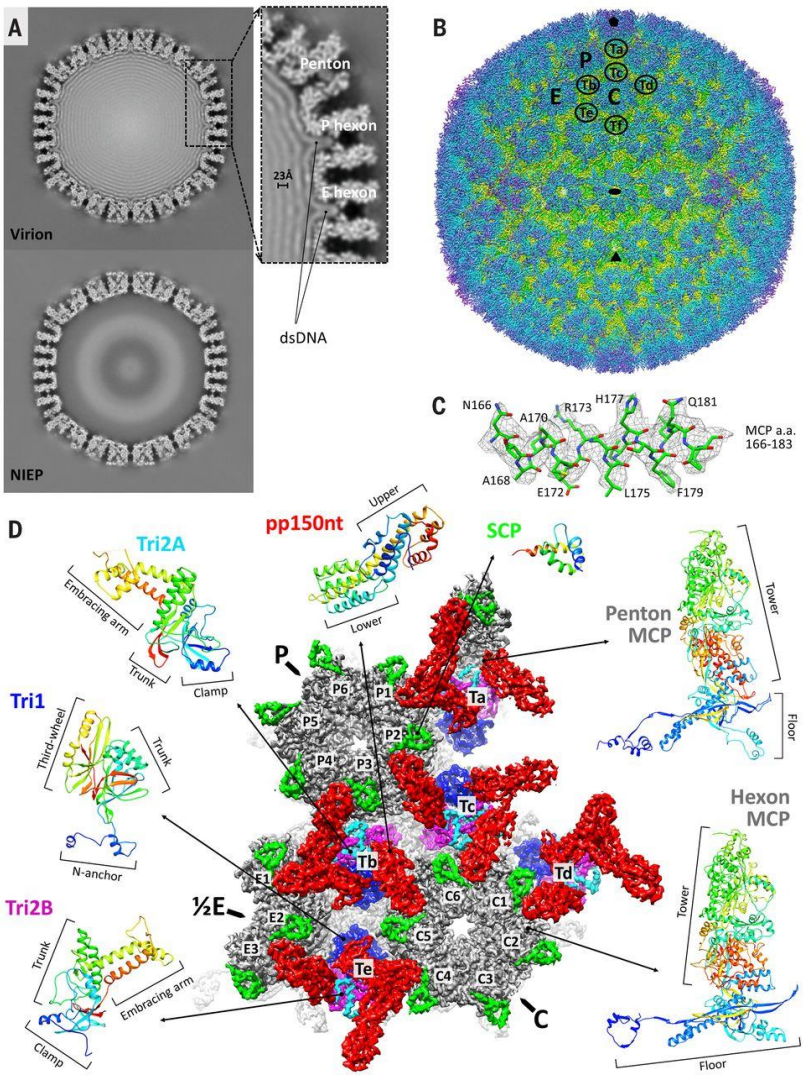

Figure 11: CryoEM reconstruction and atomic modeling of HCMV.
*(A) Central slices of HCMV virion (top) and noninfectious enveloped particle (NIEP, bottom) reconstructions at 15 Å. The inset shows a 23-Å dsDNA interlayer distance and dsDNA density within hexon channels. (B) Radially colored HCMV reconstruction at 3.9-Å resolution viewed along a twofold axis. Fivefold, threefold, and twofold axes are denoted by a pentagon, triangle, and oval, respectively. P (peripentonal), C (center), and E (edge) denote hexons and Ta to Tf denote triplexes that together contribute to an asymmetric unit. (C) Density map (mesh) and atomic model of an MCP helix illustrate side chain features. A, alanine; E, glutamic acid; F, phenylalanine; H, histidine; L, leucine; N, asparagine; Q, glutamine; R, arginine; a.a., amino acids. (D) Asymmetric unit colored by protein subunit type. MCPs (gray) make up pentons and hexons. Triplexes are heterotrimers composed of Tri1 (blue) and a Tri2A (cyan)–Tri2B (magenta) dimer. SCPs (bright green) bind to all MCPs, whereas pp150 tegument proteins (red) cluster above triplexes. Rainbow ribbon models show individual proteins and conformers (blue N terminus through green and yellow to red C terminus). pp150nt, N-terminal one-third of pp150.(from Xuekui Yu et al., Atomic structure of the human cytomegalovirus capsid with its securing tegument layer of pp150.Sci-ence**356**,eaam6892(2017).DOI:10.1126/science.aam6892 (119))*

In addition to intact, infectious virions, HCMV infected cells produce two different types of defective particles, known as DBs and NIEPs (Figure 10). The different densities of these HCMV particle types enable their isolation through ultracentrifugation methods (112, 114, 115). NIEPs share a similar size with virions but lack the viral genome, making them less dense than virions (112). DBs are larger than virions and NIEPs, with a diameter ranging from approximately 250-600 nm. They display a higher

https://doi.org/10.7795/110.20260518

density compared to virions and NIEPs. DBs contain many of the structural proteins found in mature virions. However, despite the presence of capsid proteins in DBs, these proteins are not organised into a protective capsid, thus a viral genome cannot be packaged. A more in-depth analysis of protein and phosphoprotein contents in HCMV particles revealed that DBs and NIEPs contain numerous viral and host proteins (114, 116).

The primary roles of the HCMV capsid are to protect the viral genome, transport it within the host, and ensure delivery of the genome to the host cell nucleus (117, 118). Cryo electron microscopy studies reveal the structure of HCMV capsids (Figure 11). The HCMV capsid comprises 60 asymmetric units. Each unit contains 16 copies of the major capsid protein (MCP), each of which is topped by a corresponding copy of the smallest capsid protein (SCP). Each unit also contains five copies of the triplex protein 1 (Tri1) and ten copies of the triplex protein 2 (Tri2) triplex dimer protein (119).

1.4.2 The virus replication cycle

The replication cycle of human cytomegalovirus (HCMV) is composed of two phases: a productive lytic phase and a non-productive latent phase. Occasionally, herpesviruses reactivate from latency and re-enter the lytic cycle. This strategy enables efficient viral propagation and lifelong persistence in the host (120). During lytic infection, which typically occurs in specific cell types such as epithelial, endothelial, fibroblastic or macrophage cells, the expression of viral genes is tightly regulated. This leads to extensive replication of the viral genome, viral protein expression and the production of large numbers of de novo assembled infectious progeny virions. In contrast, when HCMV infects undifferentiated myeloid cells, including $CD34^+$ haematopoietic progenitor cells, the virus establishes latency. This state is characterised by near-complete silencing of viral gene expression and the absence of viral genome replication and infectious particle production. This latent reservoir enables the virus to evade the immune system while retaining the ability to reactivate and re-enter the lytic cycle when appropriate physiological or immunological conditions are met (121).

Infection begins when HCMV enters host cells by either directly fusing its envelope with the plasma membrane or via endocytosis, depending on the target cell type (120). Viral entry is mediated by a complex set of envelope glycoproteins that engage cellular receptors and trigger membrane fusion (122). Following entry, the tegumented capsid is released into the cytoplasm and transported along the microtubule network to the nucleus, where the viral genome is delivered from the capsid through the nuclear pore complex (123). Although the viral DNA is linear within the virion, it circularises upon nuclear entry, a requirement for genome replication during lytic infection via the rolling circle mechanism (124). Viral gene expression then proceeds in a highly ordered temporal cascade that coordinates

https://doi.org/10.7795/110.20260518

DNA replication and capsid assembly within the nucleus. Newly formed capsids exit the nucleus involving budding at the inner nuclear membrane. Once in the cytoplasm, the capsids acquire additional tegument proteins and are transported to the viral assembly complex in the cytoplasm, which is a reorganised membranous compartment derived from the endoplasmic reticulum and the Golgi apparatus. At this assembly site, viral glycoproteins and tegument components are incorporated to form mature virions. Mature virions are ultimately released from the cell within secretory vesicles through budding and membrane fusion events. These coordinated steps together define the HCMV replication cycle and underpin its capacity for both productive replication and lifelong persistence (121).

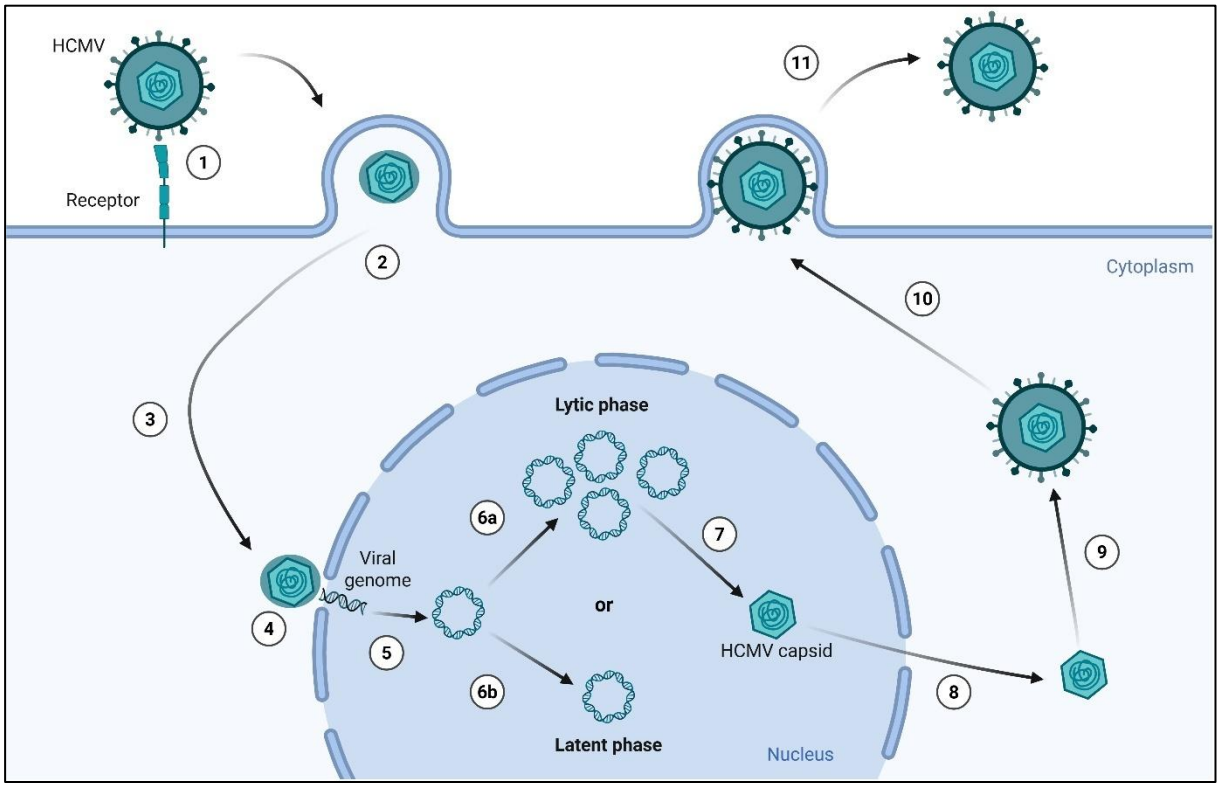

Figure 12: HCMV replication cycle.
(1) Viral glycoproteins bind to cell surface receptors and mediate entry via fusion with the plasma membrane or endocytosis (not shown). (2) Tegument proteins (represented as blurry circle around the capsid) and the capsid containing the viral genome are released into the cytoplasm. (3) The capsid with the associated inner tegument is transported via microtubules to dock at the nuclear pore complexes, through which the viral genome enters the nucleus (4). (5) The viral genome circularises to an episome and enters a latent phase (6b) or a lytic phase, leading to the expression of time-regulated genes and the replication of the viral genome (6a). (7) The newly synthesized viral genome is then packaged into the capsid and (8) leaves the nucleus by budding from the nuclear membranes, incorporating inner viral tegument proteins. (9) The capsids then travel to the viral assembly compartment (not shown in detail) where the mature viruses are formed. (10) Mature viruses travel to the plasma membrane and (11) are released via exocytosis.

1.4.3 Laboratory methods for HCMV diagnosis

Several laboratory methods are available for HCMV detection and diagnosis. These include the isolation or growth of the virus from blood, urine, or biopsy samples, the detection of HCMV specific

https://doi.org/10.7795/110.20260518

antibodies and antigens by immunological methods, and viral nucleic acid amplification and detection (100, 125, 126).

A reliable testing method in clinical virology for confirming the presence of infectious HCMV is through its isolation in cell culture. This approach offers a level of certainty, eliminating the possibility of false positives or negatives associated with antigen and nucleic acid detection. To carry out virus isolation in culture, various types of samples like blood, tissue, and urine can be utilized (127). However, it is important to note that this testing method has some limitations.

Table 1: Methods for the diagnosis of HMCV infection

Method	Principle	Results and clinical uses	Limitation
Nucleic acid tests	PCR, detects and quantifies HCMV DNA	Reported as copies of HCMV per mL sample A rapid and sensitive method for diagnosing HCMV infection and monitoring HCMV DNA decline during therapy	Lack of consensus threshold that is applicable across patients and clinical settings Lack of standardisation (different limits of detection and range of quantification, sample type, gene target and amplicon size) Patients with different risk profiles will likely have different viral thresholds Also detects latent virus
Antigenemia	Detection of pp65	Reported as number of pp65-positive cells per number of leukocytes counted Sensitive, early diagnosis of HCMV infection	Lack of assay standardisation Labor intensive Lack of automation Subjective interpretation
Virus culture	Detects typical cytopathic effect on human fibroblasts (conventional cell culture)	Highly specific for the diagnosis of CMV infection	Low sensitivity Slow turn-around time
Serology	Detection of antibody against CMV (IgG, IgM)	HCMV-IgG indicates past HCMV infection HCMV-IgM implies acute or recent infection	Complete interpretation may require paired acute- and post-infection sera Not helpful in immunocompromised patients who have attenuated and delayed antibody production

It typically requires a lengthy processing time of approximately 21 days to observe changes in virus-induced cell morphology. Additionally, the sensitivity of the test can vary depending on the specific isolation technique or method (128). The reported sensitivity and specificity of HCMV isolation in culture range from 45% to 78% and 89% to 100%, respectively (129).

Serological tests are employed for diagnostic purposes by monitoring changes in IgM and IgG antibody levels over time through the comparison of acute- and convalescent-phase paired sera, typically measured 2 to 4 weeks apart. In the case of HCMV, IgM antibody levels tend to rise within 2 to 6 weeks

https://doi.org/10.7795/110.20260518

following the initial infection and usually decline within 2 to 3 months in healthy individuals. IgM antibodies are rarely detected during HCMV reactivation (130). The presence of a recent HCMV infection is indicated by a significant, at least four-fold, increase in IgG antibody levels in paired sera with reported sensitivity and specificity ranging from 98% to 100% and 95% to 99%, respectively (129). However, it is important to note that high IgG antibody levels persist throughout the lifetime of individuals infected with HCMV, and fluctuations in HCMV-IgG antibody levels due to virus reactivation are typically small. As a result, serum antibody tests are useful for screening individuals who may be susceptible to HCMV reactivation but may not be the optimal choice for evaluating acute infections, including HCMV reactivation.

The antigenemia assay detects specific viral proteins (antigens) in infected blood cells using immunostaining techniques. This technique identifies HCMV phosphoprotein 65 (pp65) in blood samples, which is the most abundant tegument protein in HCMV viral particles (131). Isolated leukocytes are labelled with antibodies against pp65 allowing visualisation of pp65-positive leukocytes by immunofluorescence. This assay detects pp65 in leukocytes however, this does not indicate the presence of active viral replication since HCMV does not replicate within these cells. The presence of pp65-positive leukocytes is associated with the risk of disease, but the specific threshold number that predicts disease varies depending on the clinical context (132). The HCMV pp65 antigenemia is a clinically useful assay, but it has several important methodological limitations. The assay relies on immunofluorescence staining, a process that is labour-intensive and time-consuming. It involves multiple manual steps, including leukocyte isolation, cytospin preparation, fixation, antibody incubation and microscopic evaluation.

Furthermore, the assay is not automated, meaning that result interpretation depends heavily on operator expertise. The subjective nature of microscopic evaluation of stained cells leads to inter-observer and inter-laboratory variability. Differences in antibody clones, staining protocols, the number of cells examined and the criteria used to define a positive cell further contribute to inconsistent results. Consequently, there is no universally accepted standard for assay performance, result reporting or clinical cut-off values, which makes comparisons between different labs difficult.

Most clinical laboratories use PCR-based techniques for detecting copies of viral DNA in blood or plasma. Due to its sensitivity and its speed, this method has been automated in numerous laboratories to handle multiple samples efficiently (133). For standardization within and between clinical labs, a reference material from the National Institute of Standards and Technology (NIST) is available. It consists of pure Towne strain CMV DNA cloned into a bacterial artificial chromosome (BAC). As a certified reference material, SRM 2366 fulfils a number of functions that can improve measurement quality, including calibration, estimation of method uncertainty, method validation or verification, quality

https://doi.org/10.7795/110.20260518

control, and proficiency testing. However, its main function is to serve as a primary reference material, thereby ensuring metrological traceability for the calibrants employed in various CMV qPCR assays. (134). Furthermore, in recent years, reference measurement procedures using droplet digital PCR have been introduced for the quantification of viral copies without the need for a reference material or calibrator (135-137). Therefore, the future need and use of this material may be limited to method development and for QA/QC purposes.

Despite the availability of multiple laboratory methods for diagnosing HCMV, direct, metrologically traceable quantification of viral burden is lacking. None of the assays used in routine practice measure intact HCMV virions, instead, infection is inferred indirectly through the detection of viral components (DNA or antigens), host immune responses (antibodies) or virus-associated cellular changes. These surrogate measurements introduce variability and uncertainty, which is particularly problematic in cases of active, latent or reactivated virus, as current methods cannot reliably distinguish between latent viral genomes and actively reactivating viruses. PCR detects viral DNA regardless of replication status, antigenemia reflects viral protein uptake rather than productive infection and serology cannot identify reactivation events. Combined with inconsistent calibration, limited traceability and the absence of standardised reference measurement procedures, these factors hinder comparability across assays and laboratories and complicate the definition of clinically meaningful thresholds. These limitations together underscore the need for robust, standardised, metrologically robust approaches that can provide reproducible, biologically relevant quantification of HCMV infection, including the early detection of viral reactivation from latency.

1.5 Scope of the thesis

Viral load is a critical parameter in clinical diagnostics, epidemiological surveillance and public health decision-making, especially during viral outbreaks and pandemics. In principle, viral load refers to the concentration of complete viral particles in a biological sample. In practice, however, viral load cannot be measured directly. Instead, it is defined through surrogate measurands, most commonly viral nucleic acids or proteins, which are quantified using routine analytical methods. Consequently, viral load measurement currently lacks a clearly defined reference measurement system.

A key metrological limitation of current viral load measurements is the lack of a traceable and unbroken chain of measurement to the International System of Units (SI). Consequently, differences in analytical methodology, calibration strategy and sample processing result in systematic biases between laboratories and platforms, which limits comparability and makes it difficult to establish universally applicable diagnostic thresholds.

https://doi.org/10.7795/110.20260518

This lack of traceability is exacerbated by the absence of agreed higher-order standards for direct viral load measurement. Currently, there is no internationally harmonised framework that defines the measurand, the reference measurement procedures and the reference materials that are required in order to link routine clinical methods, such as qPCR, to SI units. Furthermore, significant variability is introduced prior to the analytical measurement due to differences in sample collection, storage, inactivation, extraction, and target selection. From a metrological perspective, these pre-analytical factors represent additional sources of uncertainty that are rarely quantified or controlled systematically.

Reference materials are a key component of any traceable measurement system; however, the production of viral reference materials presents substantial challenges. Such materials must be sufficiently homogeneous and stable, commutable across measurement procedures and have assigned values using traceable reference methods. In the case of viral load, the biological heterogeneity of virus preparations introduces additional complexity, including the presence of incomplete or defective particles, free nucleic acids, and non-stoichiometric relationships between viral components. These factors complicate the definition of the measurand and the assignment of reference values with well-characterised uncertainties.

This thesis aims to contribute to the development of an SI-traceable reference measurement framework for viral load by addressing these challenges at the level of primary measurement procedures. Specifically, it focuses on developing and applying two complementary primary reference measurement procedures: droplet digital PCR for absolute viral DNA quantification and isotope dilution mass spectrometry for viral structural protein quantification. Both methods can deliver results that are traceable to SI units through well-defined calibration strategies and uncertainty evaluation.

By integrating these independent measurements and applying biological stoichiometry, the known quantitative relationship between viral genome copies and structural protein content, the thesis aims to derive a more robust estimate of the concentration of viral particles by amount of substance. This combined approach is intended to reduce reliance on single-component surrogate measurands and provide a stronger metrological link between measured quantities and the intended measurand of viral particle concentration.

To this end, the thesis covers the production and characterisation of virus samples suitable for metrological investigation, the development and validation of an isotope dilution mass spectrometry method for viral protein quantification and the establishment of precise, reproducible droplet digital PCR measurements for viral DNA.

This work addresses an issue that has not yet been systematically resolved due to the inherent difficulty of combining biological systems with the specific demands of primary measurement procedures. The establishment of traceable viral load measurements requires the integration of virology, analytical

https://doi.org/10.7795/110.20260518

chemistry and metrology, as well as the development of robust reference methods and materials. Therefore, the ambition of this thesis is not to standardise routine clinical assays immediately, but to provide a scientifically and metrologically sound foundation upon which future reference materials, calibration hierarchies and harmonised viral load measurement systems can be developed.

https://doi.org/10.7795/110.20260518

2 Material and Methods

2.1 Material

2.1.1 Chemicals and reagents

Table 2: List of chemicals and reagents

Chemical/reagent	Order number	Source
0.1 % FA in acetonitrile ULC/MS	1934101	Biosolve
0.1 % FA in water ULC/MS	23244101	Biosolve
6M HCl (Pierce)	11541074	Thermo Fisher Scientific
Acetic acide (98-100 %)	100264	Merck KGaA
Acetonitrile for LC-MS	CSO.2697.1000	Th. Geyer GmbH & Co. KG
Agar	214010	BD Bioscience Pharmingen
Agarose	A9539	Sigma-Aldrich Chemie GmbH
Ammonium acetate	AP131114.1211	Merck KGaA
Ammonium hydroxide	5002	Sigma-Aldrich Chemie GmbH
Ampicilline (100 mg/mL)	A5354	Sigma-Aldrich Chemie GmbH
ddPCR droplet generation oil for probes	1864110	Bio-Rad Laboratories GmbH
ddPCR droplet reader oil	1863004	Bio-Rad Laboratories GmbH
ddPCR supermix for probes (no dUTP)	R-M10	Bio-Rad Laboratories GmbH
Dinatrium hydrogenphosphat	13472-35-0	Merck KGaA
Dithiothreitole (≥99%)	10708984001	Sigma-Aldrich Chemie GmbH
DMEM, high glucose	41965120	Gibco™ Life Technologies
dNTP set, 100 mM, Fermentas	R0181	Thermo Fisher Scientific
dNTP set, 100 mM, Fermentas	R0181	Thermo Fisher Scientific
EDTA Dinatriumsalz Dihydrat	1.316.691.209	AppliChem GmbH
Ethanole absolut	1.410.860.716	AppliChem GmbH
FastDigest Buffer (10x), Fermentas	B72	Thermo Fisher Scientific
FastDigest Buffer (10x), Fermentas	11946389	Thermo Fisher Scientific
Formaldehyde	7398.1	Carl Roth GmbH + Co. KG
GeneRuler 1-kb Plus DNA ladder	SM1331	Thermo Fisher Scientific
Glycerole	2039.1000	Th. Geyer GmbH & Co. KG
GoTaq™ qPCR master mix (2x)	A6001	Promega
hydrochloric acid (6N), Sequencing Grade	044921.K2	Thermo Fisher Scientific
Iodacetamide	I1149	Sigma-Aldrich Chemie GmbH
Isopropanol for LC-MS	1178-1L	Th. Geyer GmbH & Co. KG
JetPEI™ transfection reagent	101000020	Polyplus
Methanol für LC-MS	1439-2.5L	Th. Geyer GmbH & Co. KG
Midori Green	MG03	Nippon Genetics Europe GmbH
Monosodium phosphate	13472-35-0	Sigma-Aldrich Chemie GmbH
Nuclease-free water	AM9932	Thermo Fisher Scientific
Nycodenz®	1002424	Axis-Shield, Oslo, Norway
PBS, pH 7.4	10010023	Gibco™ Life Technologies

https://doi.org/10.7795/110.20260518

Chemical/reagent	Order number	Source
Penicillin Streptomycin	15070063	Gibco™ Life Technologies
Phenole	W322318	Sigma-Aldrich Chemie GmbH
Potassium chloride (> 99 %)	231-211-8	Sigma-Aldrich Chemie GmbH
Rapigest	186002123	Waters, Milford, MA, US
Sodium chloride	9265.1	Carl Roth GmbH + Co. KG
Sodium tartrate	121719.1211	AppliChem GmbH
Trifluoroacetic acid	808260	Sigma-Aldrich Chemie GmbH
Trizma® base (≥ 99,9 %)	201-064-4	Sigma-Aldrich Chemie GmbH
Tryptone	244020	BD Bioscience Pharmingen
Yeast extract	4.036.871.210	AppliChem GmbH

2.1.2 Kits

Table 3: List of kits

Kit	Order number	Source
BCA assay	UP40840B	Interchim
High Pure Viral Nucleic Acid Ki	11858 874 001	Roche
NucleoBond® Xtra Midi Kit	12752653	Macherey-Nagel
NucleoSpin® Gel and PCR Clean-up Kit	740609.50	Macherey-Nagel
NucleoSpin® Plasmid DNA purification (Mini) Kit	740.588.250	Macherey-Nagel
Rapid DNA Ligation Kit (Fermentas)	K1423	Thermo Fisher Scientific

2.1.3 Consumables

Table 4: List of materials

Material	Order no	Source
6-well cell culture plates	CLS3516	Corning Life Sciences
96-well cell culture plates	CLS3596	Corning Life Sciences
Autosmapler vials ND9	7658886	Th. Geyer GmbH & Co. KG
Bacterial petridishes (10 cm)	Z666254	Greiner Bio-One
Cell culture dishes	CLS430167	Corning Life Sciences
Cell scraper, 25 cm	179693	Thermo Fisher Scientific
ddPCR DG8 96 well plates	12001925	Bio-Rad Laboratories GmbH
ddPCR DG8 cartridge	1864008	Bio-Rad Laboratories GmbH
ddPCR DG8 cartridge holder	1863051	Bio-Rad Laboratories GmbH
ddPCR DG8 gaskets	1864007	Bio-Rad Laboratories GmbH
ddPCR pierceable foil heat seals	17005225	Bio-Rad Laboratories GmbH
epT.I.P.S.® 0,1 – 10 µL	30073754	Eppendorf AG
epT.I.P.S.® 0,1 – 5 mL	30071662	Eppendorf AG
epT.I.P.S.® 0,5 – 20 µL	30073797	Eppendorf AG
epT.I.P.S.® 2 – 200 µL	30073819	Eppendorf AG

https://doi.org/10.7795/110.20260518

Material	Order no	Source
epT.I.P.S.® 50 – 1000 µL	30073851	Eppendorf AG
LightCycler® 480 Multiwell plate 96, white	4729692001	Roche
Microplates, PS, 96 well, chimney, white	655094	Greiner Bio-One
PierceTM C18 Tips	87784	Thermo Fisher Scientific
Protein LoBind® Tubes, 1.5 mL	30108116	Eppendorf AG
Protein LoBind® Tubes, 2.0 mL	30108132	Eppendorf AG
Protein LoBind® Tubes, 5.0 mL	30108302	Eppendorf AG
Reaction tubes, 0.2 mL, 8x strip	G002	Kisker Biotech GmbH
Reaction tubes, Falcon™ (50 mL)	10788561	Thermo Fisher Scientific
T-175 Flasks	431466	Corning Life Sciences
T-25 Flasks	431463	Corning Life Sciences
T-75Flasks	431464	Corning Life Sciences
Ultra-clear™ centrifuge tube	344060	Beckman Coulter®
Waters Essential Sample Vial, 2mL	186011407	Waters Corporation
Waters Essential Sample Vial, 300 µL	186002804	Waters Corporation

2.1.4 Enzymes

Table 5: List of enzymes

Enzyme	**Order number**	**Source**
FastDigest NcoI	FD0574	Thermo Fisher Scientific
FastDigest NdeI	FD0583	Thermo Fisher Scientific
HF Phusion DNA polymerase	F530S	Thermo Fisher Scientific
Trypsin (bovine pancreas)	07.07.9002	Sigma-Aldrich Chemie GmbH

2.1.5 Buffers and solutions

Table 6: List of buffers and solutions

Buffers and solutions	**Components**
Agarose gel	0,8 - 1% agarose in 1x TAE buffer
10% Nycodenz	10% Nycodenz® dissolved in TN buffer at 70 °C autoclaved and stored protected from light at RT
TAE buffer, 1x	40 mM Tris base 20 mM acetic acid 1 mM EDTA in MQ
TN buffer	50 mM Tris 100 mM NaCl in MQ pH 7.4, filter seril
Buffers and solutions	**Components**

https://doi.org/10.7795/110.20260518

0.4 M sodium phospate buffer	35.6 g Na_2HPO_4*$2H_2O$, 31.2 g NaH_2PO_4 *$2H_2O$, 500 mL MQ
35% Na-tartrate	35% Na-tratrate, in sodium phosphate buffer
Water, MQ	18 MΩ·cm

2.1.6 Amino acids and peptides

Certified reference amino acids were obtained from the National Metrology Institute of Japan and were gravimetrically prepared using a microbalance to 7 nmol/mg stock solutions. The labelled amino acids were purchased from Cambridge Isotope Laboratories Inc. and gravimetrically prepared to 0.7 nmol/mg stock solutions.

Table 7: Certified reference materials and isotopically labelled amino acids used for amino acid analysis

Amino Acids	**Molar Mass (g/mol)**		
Certified reference material		**Certified value (kg/kg)**	
L-Isoleucine (NMIJ CRM 6013-a)	131.17	0.997 ± 0.002	
L-Leucine (NMIJ CRM 6012-a)	131.17	0.999 ± 0.002	
L-Phenylalanine (NMIJ CRM 6014-a)	165.19	0.999 ± 0.002	
L-Proline (NMIJ CRM 6016-a)	115.13	0.999 ± 0.002	
L-Valine (NMIJ CRM 6015-a)	117.15	0.998 ± 0.002	
Isotopically labelled		**Purity (%)**	
		Chemical	**Isotopical**
L-Isoleucine-13C6 (CIL CLM-2248)	137.13	98	99
L-Leucine-13C6 (CIL CLM-2262)	137.13	98	99
L-Phenylalanine-13C915N (CIL CNLM-575)	175.10	98	99
L-Proline-13C515N (CIL CNLM-436)	121.09	98	99
L-Valine-13C515N (CIL CNLM-442)	123.10	98	99

Peptides were custom synthesized by JPT Peptides Technologies GmbH (Berlin). 700 nmol/g solutions (estimated) were prepared in ultrapure water.

https://doi.org/10.7795/110.20260518

Table 8: Peptide list associated with HCMV measurement

Name	Protein	Sequence	Molar Mass (g/mol)	Purity in % (by JPT)
Pep01	Tri1	DPADEDNELVTALK	1529.61	97.4
Pep02	Tri1	SVELGDFR	922.01	96.5
Pep03	Tri2	LSIADVGK	801.94	96.1
Pep04	Tri2	LVAAVVPIPQR	1162.45	96.0
Pep05	MCP	ETFEGTILDK	1152.25	96.5
Pep06	MCP	IDFVDALK	920.08	98.8
Pep07	MCP	NTEEIIAANK	1102.19	97.6
Pep08	MCP	VQDLFR	776.9	97.7
Isotopically labelled				
Pep09	Tri1	DPADEDNELVTALK*	1537.55	95.3
Pep10	Tri1	SVELGDFR*	931.93	97.1
Pep11	Tri2	LSIADVGK*	809.88	95.0
Pep12	Tri2	LVAAVVPIPQR*	1172.37	98.6
Pep13	MCP	ETFEGTILDK*	1160.19	94.5
Pep14	MCP	IDFVDALK*	928.02	97.1
Pep15	MCP	NTEEIIAANK*	1110.13	97.9
Pep16	MCP	VQDLFR*	786.28	94.4

* Isotopically labelled amino acid; arginine (R): U-$^{13}C_6$, U-$^{15}N_4$; lysine (K): U-$^{13}C_6$, U-$^{15}N_2$

Table 9: Pepmix – peptides used as instrument controls, purchased from Sigma-Aldrich

	Amino acid sequence	Product no.
Insulin-Cain-B-Ox	FVNQHLCGSHLVEALYLVCGERGFFYTPKA	I6383
Glu-Fibrinopeptide B	EGVNDNEEGFFSAR	F3261
Bradykinin	RPPGFSPFR	D42722
Angiotensin I	DRVYIHPFHL	A9650
Angiotensin II	DRVYIHPF	A9525
MRFA	MRFA	M1170

2.1.7 Plasmids and oligonucleotides

Oligonucleotides were purchased from Integrated DNA Technologies IDT (Leuven, Belgium).

https://doi.org/10.7795/110.20260518

Table 10: List of plasmids

Plasmid	Description	Source
pGEM ®-T vector	Cloning vector, ampicillin resistance	Promega (A3600)
pYB01	HCMV lab standard for qPCR assay	This study

Table 11: List of oligonucleotides

ID	Oligo name	Sequence (5'-3')	Restriction site/modification	Usage
OLYB001	UL54_F	GGCCGTTACTGTCTG-CAGGA	none	qPCR/ddPCR
OLYB002	UL54_R	GGCCTCGTAG-TGAAAATTAATGGT	none	qPCR/ddPCR
	UL54_Probe	CCG-TATTGGTGCGCGATCT GTTCAA	5'-FAM, 3'-BHQ1	qPCR/ddPCR
OLYB003	UL54_NcoI_F	TGGA**C-CATGG**CCAGAAAAATC GGC	NcoI	cloning
OLYB004	UL54_NdeI_R	TATT**CATATG**ACAC-GCCGCAACGGAATTTT	NdeI	cloning
P2329	M13_For	GTAAAACGAC-GGCCAGT	none	sequencing
P2331	M13_Rev	GGAAACAGCTATGAC-CATG	none	sequencing

2.1.8 Eukaryotic cells and cell culture media

All cells were cultured at 37 °C in a humidified 7.5% CO2 incubator. Cells were maintained and routinely passaged by trypsinization every 2-3 days.

https://doi.org/10.7795/110.20260518

Table 11: List of cell lines

Cell line	Description	Groth media	Source
MRC-5	Human fibroblast cell line derived from normal lung tissue	DMEM high glucose 8% FBS 1x P/S	ATCC® CCL-171™
HFF-1	Primary human foreskin fibroblasts	DMEM high glucose 15% FBS 1x P/S 1x non-essential amino acids	ATCC® SCRC-1041™

2.1.9 Bacteria and growth media

Table 12: Bacterial strains

Bacteria	Description	Strain genotype
Escherichia coli DH10B	Chemically competent DH10B strain of *E. coli*	F– mcrA Δ(mrr-hsdRMS-mcrBC) Φ80lacZΔM15 ΔlacX74 recA1 endA1 araD139 Δ (ara-leu)7697 galU galK λ– rpsL (StrR) nupG

Table 13: Bacterial growth media

Bacterial medium	Components
LB medium*	10 g/L tryptone 5 g/L yeast extract 7 g/L NaCl ddH2O, pH 7.5
SOC medium	2% tryptonr 0.5% Yeast extract 10 mM NaCl 10 mM MgCl2 10 mM MgSO4 20 mM Glucose

*When necessary, LB medium was supplemented with 16 g/L agar to prepare solid plates

2.1.10 Viruses

Table 14: List of viral strains

Virus	**Description**
HCMV TB40/E WT	Human cytomegalovirus TB40/E-BAC4 (GenBank accession number EF999921.1)

https://doi.org/10.7795/110.20260518

HCMV-eGFP	HCMV TB40/E expressing the enhanced green fluorescent protein (eGFP) under the control of the murine CMV-MIEP. The eGFP sequence was inserted into the gpt-BAC cassette of HCMV TB40/E-BAC4 (138)

Table 15: Virus samples used in this study

Virus prep	Virus	Preparation date	Purification method	BCA assay (mg/mL)				Usage
				WVM*	NIEPs	Virions	DBs	
VYB04	WT	2021.08.31	Nycodenz	0.313	n.a.	n.a.	n.a.	Proteomics
VYB05	GFP	2021.11.22	Nycodenz	n.a.	n.a.	n.a.	n.a.	proteomics
VYB06	GFP	2021.12.07	Nycodenz	0.274	n.a.	n.a.	n.a.	Proteomics
VYB07	GFP	2021.12.16	Nycodenz	0.230	n.a.	n.a.	n.a.	Proteomics
VYB08	GFP	2022.03.11	Nycodenz	0.161	n.a.	n.a.	n.a.	Method development
VYB09	GFP	2022.08.13	Nycodenz	n.a.	n.a.	n.a.	n.a.	Method development
VYB10	GFP	2022.08.13	Nycodenz	n.a.	n.a.	n.a.	n.a.	Method development
VYB11	WT	2022.12.14	Nycodenz	n.a.	n.a.	n.a.	n.a.	Method development
VYB12	WT	2023.02.01	Na-tartrate	n.a.	0.355	0.090	0.102	Viral load estimation

*Whole virus material; n.a. not applicable

2.1.11 Devices

Table 16: List of Devices

Device	**Company**
Nitrogen evaporator vapostat	Barkey
Microbalance (ME6.6S-000-DM)	Sartorius Lab Instruments GmbH & Co. KG
Analytical balance (Cubis MA225S)	Sartorius Lab Instruments GmbH & Co. KG
ddPCR C1000 Touch™ Thermal Cycler	Bio-Rad Laboratories GmbH

https://doi.org/10.7795/110.20260518

ddPCR PX1 PCR Plate Sealer	Bio-Rad Laboratories GmbH
ddPCR QX200 droplet generator	Bio-Rad Laboratories GmbH
ddPCR QX200 droplet reader	Bio-Rad Laboratories GmbH
HERAcell VIOS 160i	Thermo Fisher Scientific
Kühlfalle (CT 04-50 SR)	Martin Christ Gefriertrocknungsanlagen GmbH
Rotations-Vakuum-Konzentrator (RVC 2-33 IR)	Martin Christ Gefriertrocknungsanlagen GmbH
Heraeus Multifuge X3R (50 mL)	Thermo Fisher Scientific
Agilent™ 1100 Series LC	Agilent Technologies Inc.
Agilent™ 1200 Series LC	Agilent Technologies Inc.
LTQ Orbitrap Elite	Thermo Fisher Scientific
LC-1100-MSD	Agilent Technologies Inc.
Incucyte S3 live cell analysis system	Sartorius Lab Instruments GmbH & Co. KG
Infinite F200 Pro microplate reader	Tecan, Männedorf, Switzerland
Gradient mixer MX 10	Beranek Laborgeräte
Gerstel-MultiPurposeSampler MPS Robot	Gerstel GmbH & Co.KG
Xevo TQ-XS	Waters, Milford, MA, US
Acquity UPLC M-Class	Waters, Milford, MA, US
Optima L-90K ultracentrifuge	Beckmann Coulter

2.1.12 Columns

Table 17: List of columns

Name	**Order No**	**Source**
iKey BEH C18 (130A 1,7µM - 150µM x 50mm)	186006764	Waters, Milford, MA, US
Trap column NanoEase C18 (100A 5µm 300µm x 50mm)	186009250	Waters, Milford, MA, US
iKey Infusion Device	186007049	Waters, Milford, MA, US
Jupiter 300 C18 column (150×2.1 mm, 5 µm)	00F-4396-B0	Phenomenex
SeQuant ZIC-HILIC column (3.5 µm, 150 mm x 2.1 mm)	1504420001	Merck

2.1.13 Software

Table 18: Software list

Software	Version	Source
GUM WorkBench	2.4.1.392	Metrodata GmbH
Light Cycler 96	1.1.0.1320	Roche Diagnostics International Ltd
PatternLab V	5.0.0.195	Laboratory for Computational and Structural Proteomics - Fiocruz
Prism	9.2.0 (332)	GraphPad
QuantaSoftTM Anlaysis Pro	1.0.596	BioRad

https://doi.org/10.7795/110.20260518

Skyline	v25.1	MacCoss Lab
SnapGene	4.1.9	Dotmatics (former GSL Biotech LLC)
Thermo XCalibur	2.2 SP1.48	Thermo Scientific

2.2 Methods

2.2.1 Generation of study material

2.2.1.1 Cell culture

Work involving eukaryotic cells was conducted in laminar flow cabinets to ensure sterile culture conditions. All cells were maintained at 37 °C with 5% or 7.5% CO_2 in a humidified incubator (HERAcell VIOS 160i, Thermo Fisher Scientific). Cell cultures were maintained by passaging three times per week. When passaging or seeding cells for experiments, they were washed with PBS and then dissociated by incubating them in Trypsin–EDTA at 37 °C for 5 minutes. Trypsin activity was then stopped by adding a culture medium containing FCS. The cells were then resuspended and transferred to fresh culture vessels containing medium.

2.2.1.2 Virus stock preparation

Virus reconstitution from BAC DNA

To reconstitute the virus, high-purity, endotoxin-free HCMV BAC DNA was purified from the *E. coli* GS1783 strain using a NucleoBond® Xtra Midi EF kit. The DNA was then dissolved in 50 µL of endotoxin-free water. MRC-5 cells were seeded at a density of 4 x 10^5 cells per well in a 6-well plate and incubated overnight at 37 °C with 7.5% CO_2. The following day, the transfection mixtures were prepared. For each transfection, 5 µL of BAC DNA was diluted with 45 µL of 150 mM NaCl. Separately, a JetPEI solution was prepared by mixing 4 µL of JetPEI reagent with 96 µL of NaCl (150 mM) and brief vortexing to ensure homogeneity. Then, 50 µL of the JetPEI solution was added to each BAC DNA dilution. The mixtures were mixed gently and incubated for 25 minutes at room temperature to allow complex formation. Meanwhile, the culture medium was replaced with 2 mL of fresh medium. The transfection mixture was then added dropwise to the cells. The plates were then centrifuged at 300 x g for eight minutes and subsequently incubated for six hours at 37 °C and 7.5% CO_2. After incubation, the medium was replaced with 2 mL of fresh medium. The cells were monitored daily for the appearance of plaques, which typically developed within 7–9 days post-transfection. The supernatant was then harvested for virus propagation.

Virus growth purification for IDMS for proteomics studies

https://doi.org/10.7795/110.20260518

To prepare the virus stocks, 1–2 mL of infectious supernatant was harvested from BAC-transfected MRC-5 cells, diluted in 5 mL of fresh HFF-1 medium, and added to a T25 flask containing 3 x 10^6 HFF-1 cells. The cells were then incubated at 37 °C with 7.5% CO_2 and inspected regularly. After 3-4 days, 3 mL of fresh HFF-1 medium was added to the infected cells. The cells and the supernatant were harvested once around 100% of the cells exhibited high cytopathic effect, infected cells appear and enlarged (after 7–10 days). This was followed by centrifugation at 2,465×g for 20 minutes at 4 °C to pellet the cell debris. The supernatant containing infectious HCMV was diluted 1:2 with fresh HFF-1 medium and used to infect two T175 flasks (2 x 10^7 HFF-1 cells per flask in 30 mL of medium). The next day, the supernatant was removed, and 30 mL of HFF-1 medium was added to each flask. The supernatant was harvested when at least 80% of the cells showed a cytopathic effect (CPE). This step was repeated every three to five days until 100% of the cells showed high CPE (this step could usually be performed three times). For the final harvest, the cells were scraped into the supernatant. The supernatant, including the cells, was then collected, after which the sample was centrifuged at 2,465xg for 20 minutes at 4 °C to pellet the cell debris. The supernatant was then subjected to further centrifugation at 26,000xg for three hours at 4 °C to pellet the virus. After discarding the supernatant, 1.5 mL of cold complete medium was added to each pellet and the mixture was incubated overnight at 4 °C. The next day, the virus particles were layered on a 10% Nycodenz cushion and then centrifuged at 46,000×g for 4 hours at 4 °C. The purified, pelleted virus was resuspended in 2 mL of cold TN buffer and divided into 50 µl and 20 µl stocks. The vials were stored at -70 °C for further utilisation.

Virus growth and gradient purification for IDMS and ddPCR measurements

One day before infection, HFF-1 were seeded at a density of 1.8 x 10^6 /flask in twenty T-175 cm^2 flasks. For infection, the cell culture medium was removed (stored for later use) and a virus inoculum was prepared by mixing 0.5 mL of HCMV WT or HCMV GFP supernatant harvested from from BAC-transfected MRC-5 cells with 3.5 mL of DMEM. Per flask, 4 mL of virus inoculum was added to the cells and allowed to adsorb for 1.5 h at 37 °C. Then, 16 mL of the stored cell culture medium was added to the cells. After 7 days post infection, when the cells showed a complete cytopathic effect (enlarged, rounded cells), the supernatant from the infected cells was harvested for gradient purification. First, cellular debris was removed by centrifugation for 10 min at 1,300xg in 50 mL tubes. The supernatant was transferred to Beckman Coulter® 70 mL polycarbonate centrifuge bottles and centrifuged at 95,000×g for 70 minutes at 10 °C using a type 45Ti rotor to pellet the viral particles. During the final 15 minutes of centrifugation, two glycerol/tartrate gradients were pre-formed in a Beckman Coulter® Ultra-clear™ centrifuge tube using a two-chamber gradient mixer. The feed chamber was filled with 5 mL of 15% sodium tartrate and the mixing chamber was filled with 4 mL of 35% sodium tartrate. After

https://doi.org/10.7795/110.20260518

centrifugation, the pellets were resuspended in a total of 2 mL TN buffer. 1 mL of virus suspension was added to each gradient and centrifuged for 60 minutes at 90,000 x g and 10 °C in a SW41Ti swing bucket rotor without deceleration. Under these conditions, virions, NIEPs and DBs sediment to form three well separated light scattering bands. Each fraction was isolated with a needle (24G x 1) from the side and transferred to a Beckman Coulter® Ultra-clear™ centrifuge tube. Each fraction was washed with 10 mL TN buffer and pelleted by centrifugation (90 min; 10 °C; 100,000 g). Each pellet was resuspended in 500 µL TN buffer and stored at -80 °C until further use. The virus sample were used for DNA extraction, BCA assay and heat inactivation.

https://doi.org/10.7795/110.20260518

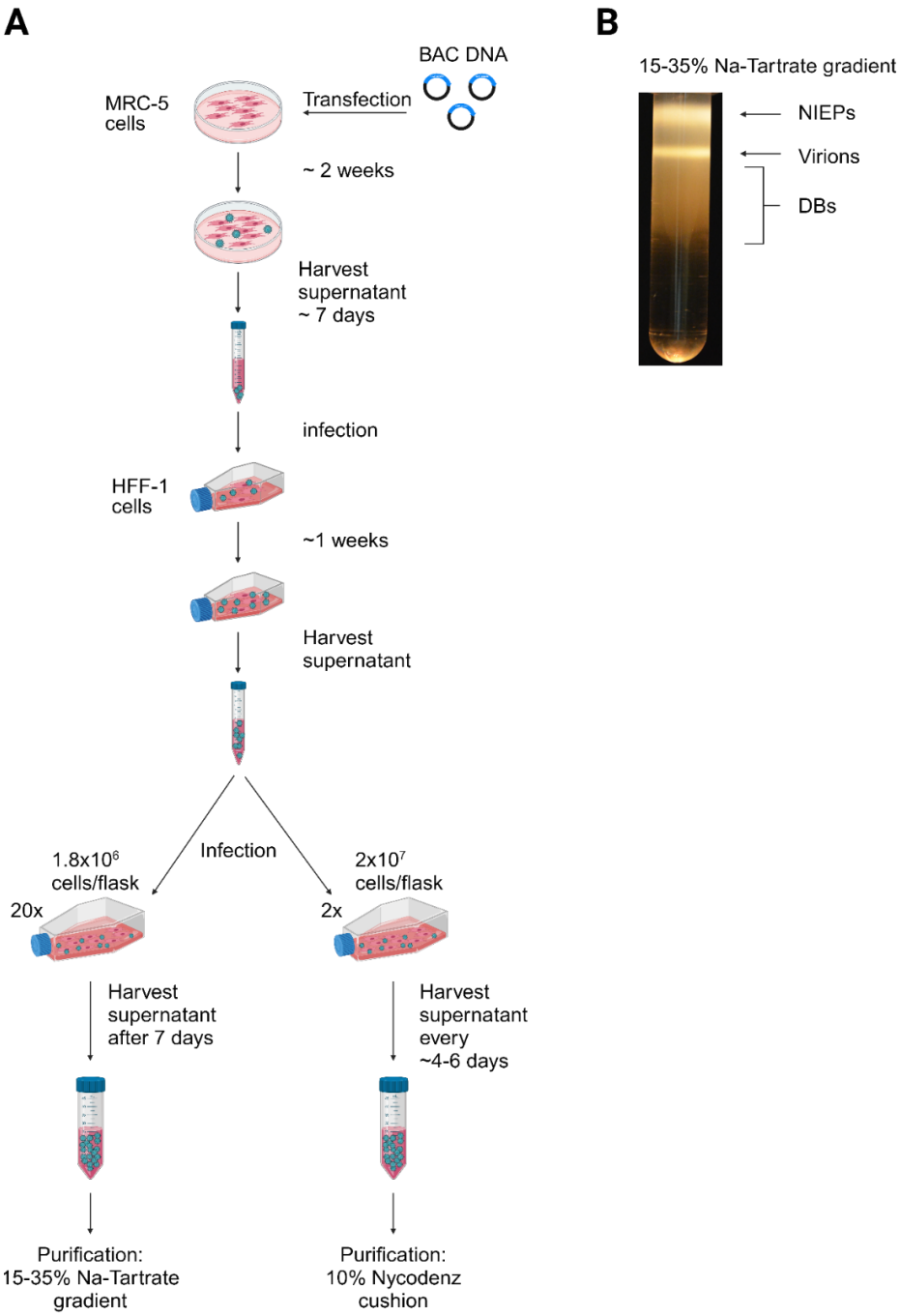

Figure 13: A. Virus production and purification scheme.
HCMV BACs were reconstituted by transfection of MRC5 cells with purified BAC DNA. The reconstituted virus was propagated in HFF-1 cells and afterwards either purified on a 10% Nycodenz cushion or on a 15-35% Na-Tartrate gradient B. Gradient purification of viral particles. Clarified medium from HCMV infected HFF cells was layered over a glycerol-tartrate gradient and centrifuged in a Beckman SW41Ti rotor. After centrifugation, two light scattering bands, referred to as non-infectious enveloped particles (NIEPs) and virions, and a broad area of dense bodies (DBs) are formed.

Heat inactivation of virions

500 µL of virus suspension (HCMV WT or HCMV GFP) was incubated at 70 °C for 120 minutes, shaking (1,000 rpm) on an Eppendorf ThermoMixer F1.5. To demonstrate that this condition is suitable for virus inactivation, HFF-1 cells were infected with heat-treated HCMV GFP. For infection, 5 x10^3

https://doi.org/10.7795/110.20260518

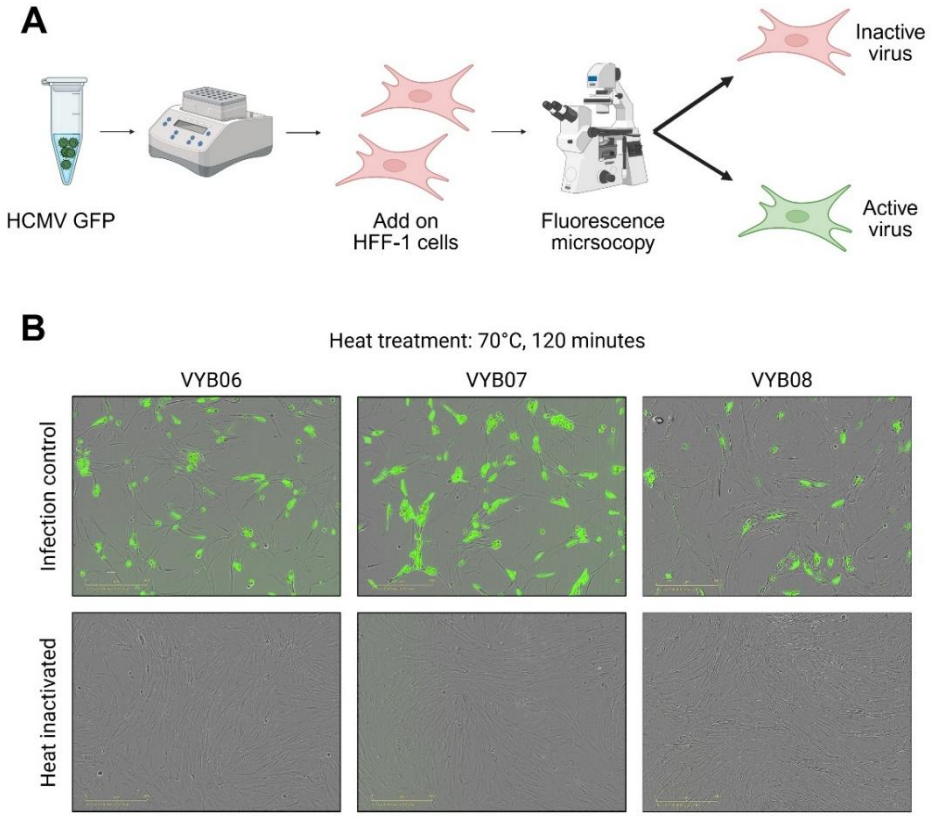

Figure 14: HCMV heat inactivation.
A. Experimental scheme for heat inactivation testing. HCMV-GFP suspension was heat treated, added to HFF-1 cells and incubated at 37 °C and 7.5% CO2 for 2-3 days. Infected cells were observed by fluorescence microscopy. Cells infected with actively replicating HCMV are indicated by expression of GFP. B. Fluorescence microscopy of cells infected with HCMV GFP that was heat treated at 70 °C for 120 minutes. Three independent virus preparations (VYB06 -08) were heat treated and added undiluted to HFF-1

cells/well were seeded onto a 96-well plate one day before infection. On the day of infection, cell culture medium was removed and 90 µL of HCMV GFP in different dilutions (undiluted, 10^{-1}, 10^{-2}, 10^{-3}, 10^{-4}, 10^{-5}, 10^{-6}) was added to the cells. After incubation for 3 hours at 37 °C and 7.5% CO_2, the virus inoculum was replaced with fresh cell culture medium and incubated for 2-3 days at 37 °C and 7.5% CO_2. Fluorescence microscopy was performed to visualize GFP-positive cells on an IncuCyte S3 live-cell analysis system (Sartorius). Only cells showing viral replication would express GFP, while the absence of fluorescence indicated effective inactivation of the virus.

2.2.1.3 Extraction of viral DNA

Viral DNA extraction was performed using a High Pure Viral Nucleic Acid Kit according to the manufacturer's instructions with 1 µL of virus suspension. DNA extraction was performed immediately after virus purification and before heat inactivation.

https://doi.org/10.7795/110.20260518

2.2.1.4 BCA assay

The bicinchoninic acid (BCA) assay was used to determine the total protein content of virus suspensions according to the supplier's instructions. Absorbance was measured at 562 nm using an Infinite F200 Pro microplate reader.

2.2.1.5 Cloning lab standard for qPCR assay

A 1077 bp UL54 gene fragment (Gene ID 307750, nucleotide position 665-1740) was amplified from HCMV TB40-BAC4 DNA (EF999921.1) by standard PCR using HF Phusion DNA polymerase. The PCR components are shown in Table 19 and the thermocycler conditions in Table 20.

Table 19: Composition of PCR reactions used for cloning

Component	Volume/Amount
DNA template (HCMV BAC DNA)	200 ng
OLYB002 (10 µM)	2.5 µL
OLYB003 (10 µM)	2.5 µL
dNTP mix (10 mM)	1 µL
5x Phusion HF buffer	10 µL
Phusion DNA polymerase	0.5 µL
Molecular-grade H_2O	ad 50 µL

Table 20: Thermocycler conditions used for cloning

Step	Temperature	Time	Cycles
Initial denaturation	98 °C	30 sec	1
Denaturation	98 °C	10 sec	
Annenaling	58 °C	20 sec	30
Extension	72 °C	35 sec	
Final extension	72 °C	5 min	1

The separation of PCR products was conducted on 1% agarose gels by conventional electrophoresis, followed by visualisation under UV. The desired PCR product was purified with the NucleoSpin®PCR Clean-up kit system. The obtained PCR product and the destination vector, pGEM-T vector (Promega), were digested as shown in Table 21 for 30 min at 37 °C.

Table 21: Composition of restriction digest for PCR product and vector

Component	PCR product	Destination vector
PCR product or vector	25 µL	2 µg
Fermentas FastDigest Buffer (10x)	3 µL	2 µL
FDNcoI	1 µL	1 µL
FDNdeI	1 µL	1 µL
Molecular-grade H_2O	ad 30 µL	ad 20 µL

https://doi.org/10.7795/110.20260518

The digested vector was separated on a 1% agarose gel, excised and purified together with the digested PCR product. For the ligation reaction, 6.5 µl of the digested PCR product and 1 µl of the digested destination vector were combined with 0.5 µl of T4 DNA Ligase (5 U/µl) in 1× T4 DNA ligase buffer. The mixture was then subjected to an incubation process at ambient temperature for 30 minutes. Subsequently, the ligation mixture was added to 50 µl of chemically competent E. coli DH10α cells. Following a one-hour incubation on ice, the cells were subjected to heat shock at 42 °C for 30 seconds, after which they were returned to ice for a duration of two minutes. Subsequently, 500 µl of SOC medium (2% Trypton, 0.5% yeast extract, 10mM NaCl, 10mM $MGCl_2$, 10 mM $MgSO_4$, 20 mM Glucose) was added, and the cells were incubated at 250 rpm for 1 hour at 37 °C. The cells were then plated on LB agar containing 100 µg/mL ampicillin and incubated overnight at 37 °C. Colonies were screened by colony PCR with primers P2329 and P2331 (Table).

Table 22: Composition of colony PCR reactions

Component	Volume/Amount
DNA template (material of bacterial colony)	1 colony
P2329 (10 µM)	0.5 µL
P2331 (10 µM)	0.5 µL
PCR 2x Master Mix (Thermo Scientific)	10 µL
Molecular-grade H_2O	9 µL

Positive colonies were cultivated in LB medium with 100 µg/mL ampicillin (Sigma-Aldrich), and plasmid DNA was extracted with the NucleoBond® Xtra Midi kit (Macherey-Nagel). The verification of insertion sequences was conducted through full sequencing (Eurofins Genomics) utilising the primers P2329 and P2331 listed in Table . The concentration of DNA was value assigned by ddPCR.

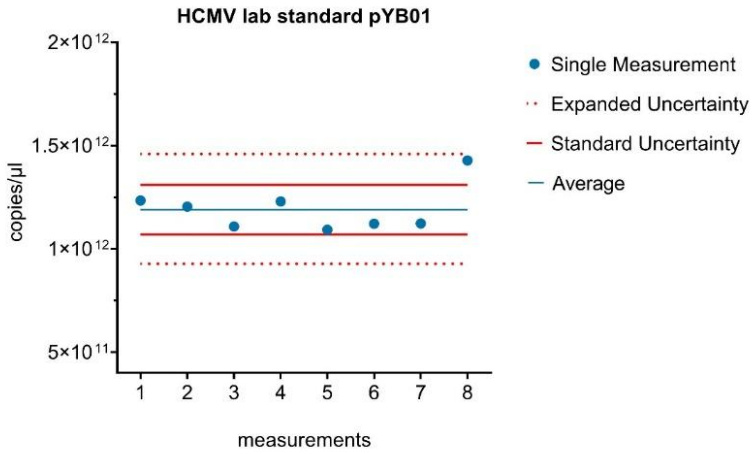

Figure 15: Vector copies of the HCMV laboratory standard.
Quantification of the HCMV UL54 lab standard (pYB01) via ddPCR, showing eight independent measurements of vector copy number (copies/µL). The blue dots represent individual measurements, the blue line shows the mean copy number and the red solid lines indicate the standard uncertainty. The red dotted lines show the expanded uncertainty.

https://doi.org/10.7795/110.20260518

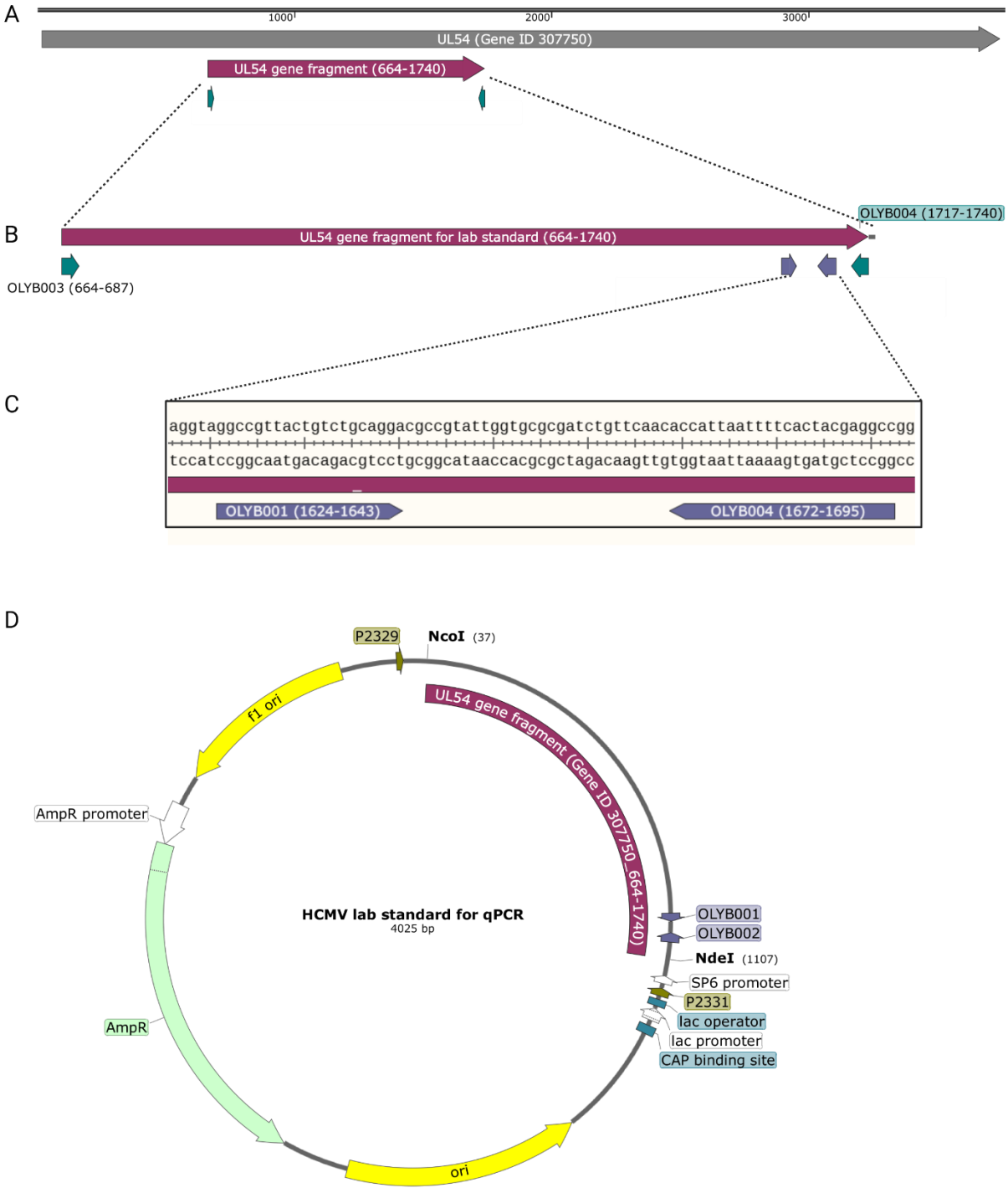

Figure 16: Construction of the HCMV UL54 laboratory standard.
A. A schematic representation of the UL54 gene (Gene ID: 307750), showing the region selected for the generation of the internal lab standard. B. A 1077 bp UL54 gene fragment (nucleotides 664–1740) was amplified by PCR from HCMV TB40-BAC4 DNA (EF999921.1). Green arrows indicate the primers used for fragment amplification and purple arrows represent the primers used for qPCR. C. A detailed view of the qPCR amplicon sequence region, highlighting the primer binding sites in purple (OLYB001 and OLYB004). D. Plasmid map of the final HCMV UL54 laboratory standard showing the cloned UL54 fragment within the pGEM-T vector (Promega) backbone. Figure generated with SnapGene

https://doi.org/10.7795/110.20260518

2.2.2 Instrument settings for LC–MS/MS

To ensure consistent performance of the instrument throughout the analytical sequence, a control peptide mixture containing oxidized Insulin Chain B oxidised, Glu-Fibrinopeptide B, Bradykinin, Angiotensin I, Angiotensin II and MRFA was analysed regularly. These peptides were chosen due to their varying sequence lengths and physicochemical properties, which cover a wide spectrum of characteristics commonly found in LC-MS/MS measurements. The mixture was injected at the beginning, intermittently between samples and at the end of each measurement sequence. The peak shape, retention time and signal intensity of each peptide were continuously monitored to verify stable chromatographic and mass spectrometric conditions. Deviations were interpreted as signs of potential technical problems. Runs were aborted and the data were excluded from further evaluation if any of the following issues occurred: a shift in retention time exceeding 0.5 min, significant broadening of the chromatographic peaks, signal loss of more than 30% across all peptides, disappearance or severe distortion of individual peaks (example chromatogram, see Figure A9 und A10). When such deviations were observed, the LC-MS/MS system was inspected and cleaned. Analytical measurements were only resumed after successful verification of system stability by reinjection of the control peptide mixture.

	Amino acid sequence	**Concentration of ready-to-use solution**	
		Orbitrap	Xevo TQ-XS
Insulin-Cain-B-Ox	FVNQHLCGSHLVEALYLVCGERGFFYTPKA	0.4 pmol/µL	100 fmol/µL
Glu-Fibrinopeptide B	EGVNDNEEGFFSAR	4.8 pmol/µL	200 fmol/µL
Bradykinin	RPPGFSPFR	2.9 pmol/µL	10 fmol/µL
Angiotensin I	DRVYIHPFHL	1.0 pmol/µL	10 fmol/µL
Angiotensin II	DRVYIHPF	1.2 pmol/µL	1 fmol/µL
MRFA	MRFA	4.7 pmol/µL	1 fmol/µL

2.2.3 Proteomics

2.2.3.1 Proteolysis of virus samples for mass spectrometry

30 µg of virus stock (VYB04, VYB06, VYB07 or VYB08) was subjected to lyophilization and subsequently resuspended in 80 µL of Rapigest™ (Waters, 1 mg/mL in 50 mM NH_4HCO_3 buffer). Afterwards, 10 µL of DTT (50 mM) was added. Subsequently, the mixture was incubated at 60 °C for 30 minutes, followed by cooling to room temperature. Thereafter, 10 µL of iodoacetamide (150 mM) was added for alkylation. Then, the mixture was incubated at room temperature ~~and~~ in the dark for one hour. Thereafter, 2 µL of trypsin (Sigma, 10 mg/mL in 50 mM acetic acid) was added and the mixture was incubated at 37 °C while shaking for a period of 24 hours. The proteolysis was stopped by adding 10 µL HCl (1M).

https://doi.org/10.7795/110.20260518

2.2.3.2 LC-MS/MS

The LTQ Orbitrap Elite mass spectrometer (Thermo Scientific) combined with an on-line Agilent 1200 series LC and Phenomenex Jupiter 300 C18 column (150×2.1 mm, 5 µm) was used for peptide mapping studies. For LC-coupled MS analysis, 10 µL of the digested samples were separated by reverse phase chromatography using two mobile phases eluent A (MilliQ water/ 0.1 % formic acid (FA)) and eluent B (acetonitrile/ 0.1 % FA) as follows: 0-30 min 99% A, linear gradient from 30-120 min 99-78% A, 120-150 min 78-62% A, 150-170 min 62-20% A, 170-175 min 20% A, 175-185 min 20-99% A, 185-200 min 99% A (Figure 17). The flow rate was set at 0.2 mL/min, and the oven temperature was set to 25 °C.

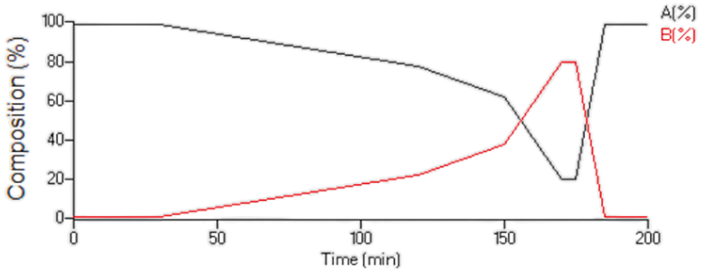

Figure 17: LC gradient profile used for proteomic peptide separation.
Gradient elution scheme showing solvent composition over time. Solvent A consisted of 0.1% formic acid (FA) in water, and solvent B was acetonitrile containing 0.1% FA. The gradient started with 0% B, gradually increased to enrich hydrophobic peptides, and was followed by a high-organic wash and re-equilibration step to initial conditions.

The important basic settings of the LTQ Orbitrap Elite mass spectrometer are listed in Table 23 and Table 24.

Table 23: Tune method

Tune File Values	
Source Type	HESI (Heated Electrospray Ionization)
Capillary Temperature [°C]	300
Source Heater Temperature [°C]	300
Sheath Gas Flow [L/min]	35
Aux Gas Flow [L/min]	10
Ion Trap Zoom AGC [ions]	3 000
Ion Trap Full AGC [ions]	30 000
Ion Trap SIM AGC [ions]	10 000
Ion Trap MSn AGC [ions]	10 000
FTMS Full AGC [ions]	1 000 000
FTMS SIM AGC [ions]	100 000
FTMS MSn AGC [ions]	200 000
Positive Polarity	
Source Voltage [kV]	3
Source Current [uA]	100
S-Lens RF Level [%]	61
Multipole RF Amplifier (Vp-p)	800
Ion Trap Mirco Scans (Zoom, Full, SIM, MSn)	1

https://doi.org/10.7795/110.20260518

Ion Trap Zoom Max Ion Time [ms]	50
Ion Trap Full Max Ion Time [ms]	300
Ion Trap SIM Max Ion Time [ms]	50
Ion Trap MSn Max Ion Time [ms]	500
FTMS Mirco Scans (Full, SIM, MSn)	1
FTMS Mi Max Ion Time (Full, SIM, MSn) [ms]	500

Table 24: Instrument method

FTMS settings	
Resolution at *m/z* 200	60 000
Scanning range [*m/z*]	200 - 2000
ITMS settings	
MSMS	Top10
Activation Type	CID
Min Signal Required (counts)	2000
Isolation Width [*m/z*]	2
Normalized Collision Energy [eV]	30
Default Charge State	2
Data Dependent Settings	
Neutral loss in top	3
Product in top	3
Global Data Dependent Settings	
Exclusion Mass Width [*m/z*]	3
Parent Mass Width [*m/z*]	1
FT SIM scan mass width low [*m/z*]	5
FT SIM scan mass width high [*m/z*]	5
Neutral Loss Mass Width [*m/z*]	1
Product Mass Width [*m/z*]	1

2.2.3.3 Peptide identification

Peptide identification was performed using the PatternLab V software (139). To this end, the individual identified product ion data in raw file format were compared with HCMV AD169 sequences in fasta file format.

2.2.4 Amino acid analysis

2.2.4.1 Blend preparation

The sample and calibration blends were prepared gravimetrically on a microbalance (ME6.6S-000-DM, Satorius) and an analytical balance (Cubis MA225S, Satorius) as follows: The sample blend contained a known mass of the target proteotypic peptide solution of interest at an unknown concentration. A mixed solution of labelled amino acids was prepared so that the amount of each labelled amino acid was carefully matched to the expected molar ratio of the individual amino acids in the target peptide.

https://doi.org/10.7795/110.20260518

The ratio of the labelled to natural amino acids were iteratively altered until the measured ratio of the labelled to natural for each amino acid on the mass spectrometer was one. This was achieved by gravimetrically adding the labelled amino acid solution until unity was observed. For each peptide, a calibration blend was prepared containing the reference amino acids at the amount concentration they were expected to be released by hydrolysis of the respective peptides. Using the same labelled amino acid solution, the labelled amino acids were spiked into this blend using the same mass as used to prepare the sample blend. The use of this exact matching method would correct for any bias caused by incomplete isotopic enrichment of the labelled amino acids (5). For each peptide, three calibration and sample blends were prepared on three different days.

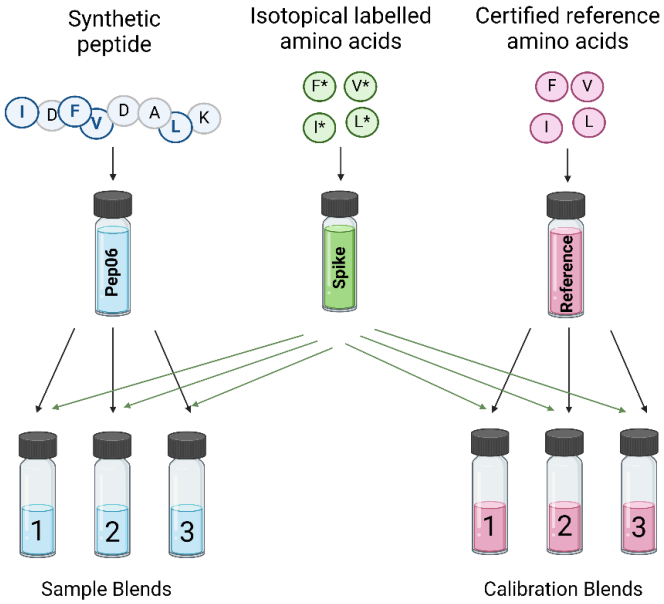

Figure 18: Schematic illustration of the preparation of blends for the exact matching of isotope dilution mass spectrometry (IDMS) for the quantification of synthetic peptides.
Synthetic peptide (here Pep06) and isotopically labelled amino acids (Spike) are combined to generate sample blends, while calibration blends are prepared by mixing certified reference amino acids (Reference) with the same isotopically labelled amino acids. These blends allow for the precise quantification of peptide-derived amino acids based on the principles of exact-matching IDMS.

2.2.4.2 Peptide Hydrolysis

For hydrolysis, the prepared blends were transferred to a hydrolysis tube (Pierce, 6 mL, 10 mm x 150 mm). The solvent was removed by applying nitrogen (1 bar) at 35 °C. The dried blends were resuspended by adding 400 µL of 6M HCl containing 0.1% Phenol. After freezing the content by placing the bottom of the tube in liquid nitrogen, the hydrolysis tube was evacuated. The tube was allowed to warm to room temperature prior to placing it in a heating block at 130 °C for 24 hours for hydrolysis. Then, HCl was removed using a constant stream of nitrogen (nitrogen, 35 °C) on a nitrogen evaporator,

https://doi.org/10.7795/110.20260518

the residue was resuspended in 200 µL of MQ water and 800 µL acetonitrile in preparation for LC-MS analysis for the individual amino acids.

2.2.4.3 LC-MS analysis

Isotope ratio measurements on the individual amino acids were performed on a liquid chromatography-electrospray ionization quadrupole mass spectrometry (LC/ESI-Q MS) system (Agilent 1100 LC/MSD). Amino acid separation was achieved using a ZIC-HILIC column paired with a corresponding HPLC guard column (ZIC-HILIC Optiguard). The mobile phase consisted of eluent A (5 mM ammonium acetate in water) and eluent B (acetonitrile). After equilibrating the column at 80% B, a gradient from 80% to 40% B was applied over 16 minutes at a flow rate of 0.1 mL/min. The ESI source conditions were selected as follows: nebulizer pressure 20 psi, drying gas flow 10 L/min, drying gas temperature 350 °C, fragmentor 30 V. Amino acid detection was performed via low-resolution mass spectrometry in selected ion monitoring (SIM) mode. The peak area ratios of natural and labelled amino acids were determined using the following SIM races for the $[M + H]^+$ of the natural and labelled amino acids using the 'Data Analysis, Integrate' software module: *m/z* 116.1/122.1 (proline), *m/z* 118.1/124.1 (valine), *m/z* 132.1/138.1 (leucine and isoleucine), and *m/z* 166.1/176.1 (phenylalanine). Each sample blend was injected four times onto the system with each injection being bracketed by an injection of the respective calibration blend. The concentration of each amino acid in the peptide was determined using the reduced form of the double IDMS equation (Equation 2). The average of the measured ratios was calculated for the bracketing calibration blends.

$$\kappa_x = \frac{\kappa_z * \frac{m_z}{m_{yc}} * \frac{m_y}{m_x} * \frac{R'_B}{R'_{BC}}}{number\ of\ aa\ in\ peptide}$$

Equation 2: IDMS equation used to calculate the amount of substance content for each amino acid.

where κ_x is the concentration of the analyte in the sample, κ_z is the concentration of the reference amino acid solution, m_z is the mass of the reference amino acid solution added to the calibration blend, m_x is the mass of the peptide solution used in the sample blend, m_{yc} is the mass of the isotopically labelled amino acid solution added to the calibration blend, m_y is the mass of the isotopically labelled amino acid solution added to the sample blend, R'_B is the measured ratio (peak area amino acid derived from the hydrolysed peptide/peak area isotopically labelled amino acid) of the sample blend, and R'_{BC} is the average measured ratio (peak area reference amino acids/peak area isotopically labelled amino acids) of the calibration blend injected before and after the sample.

https://doi.org/10.7795/110.20260518

2.2.4.4 Uncertainty calculations according

The standard uncertainty u of each amino acid measurement was calculated according to the GUM. Since the measurement is based on a fully defined equation (see Equation 2), the associated uncertainty of each measurement can be expressed as follows:

$$u = \kappa_x \sqrt{\left(\frac{u_{\kappa_z}}{\kappa_z}\right)^2 + \left(\frac{u_{R_B}}{R_B}\right)^2 + \left(\frac{u_{R_{BC}}}{u_{R_{BC}}}\right)^2 + \left(\frac{u_{m_x}}{m_x}\right)^2 + \left(\frac{u_{m_y}}{m_y}\right)^2 + \left(\frac{u_{m_z}}{m_z}\right)^2 + \left(\frac{u_{m_{yc}}}{m_{yc}}\right)^2}$$

Equation 3: Uncertainty calculation for individual IDMS measurements for each amino acid.

κ_x	Amount of substance content of sample
κ_z	Amount of substance content of reference amino acid (natural) stock
u_{κ_z}	Standard uncertainty associated with the preparation of the reference stock
u_{R_b}	Standard deviation of ratio R_B
R_B	Mean measured ratio of sample blend (n=4)
$u_{R_{BC}}$	Standard deviation of ratio R_{BC}
R_{BC}	Mean measured ratio of calibration blend (n=4)
u_{m_x}	Uncertainty associated with the mass of sample solution used
m_x	Mass of sample solution used
u_{m_y}	Uncertainty associated with the mass of labelled amino acid solution added to the sample
m_y	Mass of labelled amino acid added to the sample
u_{m_z}	Uncertainty associated with the mass of natural amino acid solution added to the calibration blend
m_z	Mass of natural amino acid solution added to the calibration blend
$u_{m_{yc}}$	Uncertainty associated with the mass of labelled amino acid solution added to the calibration blend
m_{yc}	mass of labelled amino acid solution added to the calibration blend

The final measurement uncertainty for each amino acid was calculated by combing the average uncertainty $\bar{u}$ associated with each of the three replicates with the standard deviation of the mean $u(\bar{x})$.

$$u(aa) = \sqrt{\bar{u}^2 + u(\bar{x})^2}$$

Equation 4: Total uncertainty of amino acid measurements

with

$$u(\bar{x}) = \frac{s}{\sqrt{n}}$$

https://doi.org/10.7795/110.20260518

s	Standard deviation
n	Number of measurements

Equation 5: Standard deviation of the mean

The total measurement uncertainty of the peptides was defined as the standard deviation of the mean of the of the amino acids measured.

2.2.5 Method development for peptide-based protein quantification

To improve sensitivity and selectivity the proteotypic peptides were analysed using a targeted analytical method. The peptides were separated using a 2D capillary reversed phase LC followed by MS detection using a triple quadruple mass spectrometer operating in multiple reaction monitoring (MRM) mode.

2.2.5.1 LC separation

For the separation of the proteotypic peptides, a two-dimensional LC system operated in a trapping function was used. The trap was operated in a backflush manner using a 6-port switching valve and two separate gradient capillary LC pumps. The samples were separated by an integrate chromatographic separation and ESI emitter device (iKey waters) using a binary mobile phase elution consisting of A (0.1 % FA in water, ULC/MS, Biosolve) and eluent B (acetonitrile in 0.1 % FA, ULC/MS, Biosolve). Before analytical separation, 2 µL of sample was loaded onto a trap column (NanoEase). The trap column was operated in a trapping configuration using 99% solvent A and 1% solvent B at 8 µL/min for 5 minutes. During trapping, the flow-through was directed to waste. After loading, the trap column was switched in-line with the ionKey analytical column The elution gradient used was as follows: 0-7 min 95 % A, linear gradient from 7-17 min 95-80 % A, 17-20 min 80-5 % A, 20-30 min 5% A, 30.1 95 % A. The flow rate was set at 2 µL/min, and the oven temperature was set to 30 °C.

2.2.5.2 Optimization of MRM transitions by direct infusion

For tuning of the collision energy, 10 pmol of the respective peptide in 50:50 % v/v acetonitrile: water 0.1% formic acid was directly infused through the ikey infusion tile (infusion flow rate: 5 µL/min) to the mass spectrometer. The MRM transitions for the signature peptides were optimised on a Waters Xevo TQ-XS triple quadrupole mass spectrometer equipped with an ionkey source. Optimization steps included precursor ion identification, product ion scanning, and optimisation of collision energy (CE) to yield the maximum intensity for the chosen product ion for use in the MRM experiments.

https://doi.org/10.7795/110.20260518

2.2.5.3 Instrument Parameters

The mass spectrometer was operated under the following conditions: capillary voltage +3 kV, source temperature 100 °C, collision gas flow 6 mL/h, and cone gas flow 80 L/h. Cone voltage and collision energy were optimized as described below.

2.2.5.4 Precursor Ion Determination

A full scan (MS mode) was performed over an *m/z* range of 200–1000 in positive ion mode. The most intense ion, typically corresponding to $[M + 2H]^{2+}$, was selected as the precursor ion. Cone voltage was varied between 15 and 40 V to determine the optimal transmission settings, based on peak height.

2.2.5.5 Product Ion Scanning and CE optimization

The collision energy (CE) was optimized by varying the CE in 2–5 eV increments across a range of between 10–40 eV to identify abundant and structurally relevant fragment ions. The most intense product ions at the respective CE were selected for MRM development.

2.2.5.6 Final Transition Selection

Final MRM transitions were selected based on intensity, selectivity, and reproducibility. Two to three transitions were chosen per natural and labelled peptide. Each transition was assigned to an optimized collision energy. The instrument dwell time was set to 0.100 sec. Cone voltage was set to 20 V.

2.2.5.7 Injection reproducibility

To evaluate injection reproducibility, 5 different mixtures of the synthetic peptides Pep01-16 (10, 20, 40, 80 and 100 fmol on column) were injected in total 225 (45 time each) consecutive times under identical conditions. Data were acquired in MRM mode using the scan conditions shown in table 5.1. The data was analysed for retention time and transition ratios. Reproducibility was assessed by calculating the coefficient of variation (CV%).

2.2.5.8 LOD/LOQ

Calibration curves were used for the determination of the limits of detection (LOD) and the limits of quantitation (LOQ). To provide this information, three sets of peptide mixtures were meticulously prepared gravimetrically. These mixtures contained isotopically labelled peptides (Pep09-16) at 7 fmol/g and 9 calibration points with increasing amounts of natural peptides (Pep01-08) at concentrations ranging from 0-15 fmol/mg. For LC-MS/MS analysis, 2 µL of the peptide mixtures was used per injection. The observed ratio of the peak area of the natural peptides divided by the peak area of the labelled peptides was plotted against the gravimetric amount of natural peptide on column.

https://doi.org/10.7795/110.20260518

2.2.5.9 Time course experiment

For the assessment of the release of the target peptides from the intact viral protein preparations, 30 pmol of Pep09-16 was added to 30 µg total viral protein of VYB12. The mixture was lyophilized (Christ, RVC 2-25 CDplus, 15 mbar, 30 °C) and resuspended in 240 µL of Rapigest™ (Waters, 1 mg/mL in 50 mM NH_4HCO_3 buffer). Afterwards, 30 µL of DTT (50 mM, Sigma) was added. Subsequently, the mixture was subjected to incubation at 60 °C for 30 minutes, followed by cooling to room temperature. Thereafter, 30 µL of iodoacetamide (Sigma, 150 mM) was added for alkylation. Then, the mixture was incubated at room temperature and in the dark for one hour.

Proteolysis was performed on a Gerstel-MultiPurposeSampler MPS Robot and started by adding 20 µL of trypsin solution (10 mg/mL) and incubating the mixture at 37 °C whilst shaking. Samples of 20 µL were drawn after 1, 2, 3, 4, 5, 6, 8, 10, 12,16, 24, 32, 48 hours. Proteolysis was stopped by addition of 20 μL of HCl (150 mmol/L). After each sample was withdrawn, a fresh aliquot of trypsin (20 µL) was added to the reaction mixture. The samples were desalted using solid-phase extraction (SPE) C18 tips (Pierce™ C18 Tips) according to the manufacturers protocol. Briefly, samples were adjusted to 0.1% TFA. The tip was activated by aspirating twice with100 µL of 50 % acetonitrile. Afterwards, the tip was equilibrated by aspirating twice with 100 µL of 0.1% TFA, followed by dispensing and aspirating the sample for 10 cycles. After washing twice with 100 µL 0.1% TFA/5%ACN, samples were eluted with 30 µL 0.1% FA in 80% ACN, lyophilised, resuspended in 0.1 FA and proceeded to LC-MS/MS.

2.2.6 Viral load quantification

2.2.6.1 Droplet digital PCR

Droplet digital PCR was performed as described previously (140). Primer and probes (Table 25) were used as described in Sassenscheidt et al. (141). In detail, the genome copy number of the extracted DNA from the virus samples was measured using a QX200 system (Bio-Rad). Assays targeting the UL54 gene of the human cytomegalovirus (HCMV) genome were performed using primers at a concentration of 600 nM and hydrolysis probes at a concentration of 200 nM (ITD Technologies, see Table).

Table 25: Primer and probes used for ddPCR

Name	Sequence (5’-3’)	Labelling
UL54_For	GGCCGTTACTGTCTGCAGGA	n.a.
UL54_Rev	GGCCTCGTAGTGAAAATTAATGGT	n.a.
UL54_Probe	CCGTATTGGTGCGCGATCTGTTCAA	5’-FAM, 3’-BHQ1

https://doi.org/10.7795/110.20260518

PCR was performed using a C1000 Touch Thermal Cycler (Bio-Rad). The cycling protocol consisted of an initial 2-minute step at 50 °C, followed by a 10-minute step at 95 °C, and then 45 cycles of 15 seconds at 95 °C and 1 minute at 60 °C. An additional 10-minute step at 98 °C was included at the end.

Reaction volumes of 20 µL were prepared consisting of: 10 µL of 2× Master Mix (ddPCR™ Supermix for Probes, Bio-Rad, 1863024); 0.33 µL of each primer and probe; 1 µL of nuclease-free water (Pierce, AM9337); and 8 µL of sample. To reduce pipetting errors associated with small volumes, a bulk reaction mix was prepared in a single tube and then distributed into several tubes, each containing 12 µL of the mix. DNA samples were analysed in quadruplicates, with each replicate added separately to the 12 µL mix.

Data analysis was performed using QuantaSoft Analysis Pro software. Thresholds for distinguishing positive and negative droplets were manually established (more than three positive droplets were considered a positive sample). Only reactions with more than 10,000 accepted droplets were included in the analysis. A droplet volume of 0.85 nL was used to calculate the DNA copy numbers in the samples.

2.2.6.2 Quantification of viral capsid proteins MCP, Tri1 and Tr2

Blend preparation

The sample and calibration blends were prepared gravimetrically on a microbalance (ME6.6S-000-DM, Satorius) and an analytical balance (Cubis MA225S, Satorius) as follows: The sample blend contained the virus sample, spiked with the corresponding amount concentration of the labelled peptides, which were expected to be released from the virus during the proteolysis step. A calibration blend was prepared containing the synthetic peptides at the amount concentrations they were expected to be released by complete proteolysis of the virus sample. This blend was spiked with the same labelled peptide solution using the same mass as used to prepare the sample blend. The blends were lyophilized (Christ, RVC 2-25 CDplus, 15 mbar, 30 °C) and resuspended in 240 µL of Rapigest™ (Waters, 1 mg/mL in 50 mM NH_4HCO_3 buffer). Afterwards, 30 µL of DTT (50 mM, Sigma) were added. Subsequently, the mixture was subjected to incubation at 60 °C for 30 minutes, followed by cooling to room temperature. Thereafter, 30 µL of iodoacetamide (Sigma, 150 mM) were added for alkylation. Then, the mixture was incubated at room temperature and in the dark for one hour. Proteolysis was performed on a Gerstel-MultiPurposeSampler MPS Robot and started by adding 20 µL of trypsin solution (10 mg/mL) and incubating the mixture at 37 °C, with constant shaking. After 1, 2, 3, 4, 5, 6, 8, 10, 12,16, 24, 32, 48 hours, a fresh aliquot of trypsin (20 µL) was added to the reaction mixture. Proteolysis was stopped by the addition of 20 μL of HCl (150 mmol/L).

https://doi.org/10.7795/110.20260518

LC-MS/MS

Settings were used as described in Chapter 2.2.5. Each sample blend was injected four times onto the system with each injection being bracketed by an injection of the respective calibration blend. The peak area ratios of natural and labelled peptides transitions (Table 29) were determined using the Skyline.

2.2.6.3 Uncertainty calculations

ddPCR measuremnts

The uncertainty in the measurement of the ddPCR assay was determined by performing three independent DNA extractions. For each extraction, the uncertainty was calculated based on two main components: pipetting error and the standard deviation of replicate ddPCR measurements.

$$u_{ex_x} = \sqrt{{u_{p_x}}^2 + {u_{gc_x}}^2}$$

Equation 6: Uncertainty calculation for ddPCR measurements per DNA extraction sample.

$\mathrm{u_{p_x}}$	Pipetting error
$\mathrm{u_{gc_x}}$	Relative standard deviation

Pipetting errors were derived from critical volume transfer steps including the elution of DNA during extraction, the first dilution step to adjust the DNA concentration prior to PCR setup and the subsequent dilution step during PCR preparation.

$$u_{p_x} = \sqrt{{u_{p_1}}^2 + {u_{p_2}}^2 + {u_{p_3}}^2}$$

Equation 7: Uncertainty due pipetting error

u_{p_1}	Elution step during DNA extraction
u_{p_2}	Dilution before PCR preparation
u_{p_3}	Dilution during PCR reaction mix preparation

Pipetting uncertainties were derived from the manufacturer's specifications for the pipettes and volumes used. The uncertainty arising from replicate ddPCR measurements represented the assay's analytical repeatability. An individual uncertainty budget was established for each DNA extraction, and the overall measurement uncertainty of the ddPCR method was obtained by combining the uncertainties of all three extractions.

https://doi.org/10.7795/110.20260518

$$u_{genome\ copies_{VYB12}} = \sqrt{{u_{ex_1}}^2 + {u_{ex_2}}^2 + {u_{ex_3}}^2}$$

Equation 8: Combined uncertainty calculation for ddPCR measurement of VYB12

All uncertainty budgets and combined uncertainty calculations were performed using GUM Workbench. The expanded uncertainty with k = 2.2 within a 95% confidence interval was calculated as follows:

$$U = k \times u_{VYB12}$$

Equation 9: Expanded uncertainty calculation for VYB12

K was calculated using the TINV function in Microsoft Excel, a function that returns the two-tailed inverse of the Student's t-distribution, with n=12.

IDMS measurements

The measurement uncertainty of the number of viral capsids determined by IDMS was calculated based on three structural capsid proteins: MCP, Tri1 and Tri2.

One representative signature peptide was analysed for each protein. The uncertainty for each protein was derived from the combined uncertainties of the corresponding peptide measurement. Each peptide was quantified using two or three selected transitions. The uncertainty was calculated according to Equation 3 in chapter 2.2.2.4. The uncertainty of each transition was based on the response ratio of the sample blend and the calibration blend. Additionally, the uncertainty of the assigned concentration of the reference peptide standard was included. The reference peptide concentration was prepared by gravimetry, and the mass determination during weighing contributed to the overall uncertainty. This weighing uncertainty included the calibration uncertainty of the analytical balance used. For each capsid protein, the uncertainties of all transitions belonging to its peptide were calculated to obtain the overall protein-specific uncertainty $u(\overline{p_x})$ as follows:

$$u(\overline{p_x}) = \frac{s}{\sqrt{n}}$$

Equation 10: Calculation of peptide standard uncertainty

s	Standard deviation of all transition measurements
n	Number of observations

The uncertainty of the peptide-based capsid number was calculated by combining the uncertainty of the peptide measurement with the uncertainty of the conversion factor (based on Herzik et al., 2019 (142)).

https://doi.org/10.7795/110.20260518

$$u_{capsid_{pep(x)}} = \sqrt{u(\overline{p_x})^2 + {u_{CF}}^2}$$

Equation 11: Uncertainty of capsid numbers based on one peptide/protein

$u(\overline{p_x})$	Uncertainty from peptide quantification of the respective peptide
u_{CF}	Uncertainty of conversion factor

The final measurement uncertainty of the calculated capsid number was determined via the standard deviation of the mean value of the individual capsid protein values (equation 9).

$$u(\overline{capsid_{final}}) = \frac{s_{capsid}}{\sqrt{n}}$$

Equation 12: Uncertainty of final capsid numbers

s	Standard deviation of capsid number based on the different peptides
n	Number of observations

Final viral load

The viral load was estimated by averaging the numbers of gene copy results from ddPCR and of capsid numbers based on peptide-based protein measurements. The standard deviation of the two measurement was used as the estimator for the standard measurement uncertainty

https://doi.org/10.7795/110.20260518

3 Results and discussion

3.1 Proteomics for peptide discovery

In this study, proteomics was essential for two main reasons: firstly, to identify viral proteins; and secondly, to determine which proteins and peptides would be suitable for peptide-based protein quantification. Ribosome profiling studies, which detect actively translated open reading frames by sequencing ribosome-protected mRNA fragments during HCMV infection, have shown that the human herpesvirus 5 (HCMV) encodes over 200 proteins (143). However, not all of them have been observed via mass spectrometry to date (144). Therefore, it was essential to choose proteins and peptides for quantification based on experimental data that were generated in our laboratory.

For selecting proteins for viral load quantification, it is important to know which protein reliably correlates with the number of viral particles. The answer is simple: the protein must be present in the same proportion in each virus particle and the stoichiometric ratio of the number of proteins to the virus particle must be known. For instance, tegument proteins are less suitable, as their composition can be influenced by factors such as the used strain and the infected cell type (145). In contrast, it has been demonstrated that the capsid proteins exhibit a fixed stoichiometry (119) and therefore may act as good targets for protein quantification methods as the amount of substance of content of the detected peptide can be related directly to the virus particle number via the known copies of peptide per protein, the number of each protein present in the virus capsid and Avogadro's constant.

In addition to the selection of proteins, the corresponding peptides that are to be used for quantification must also be determined. Peptides vary greatly in their performance across many aspects of targeted MS analysis. These variations include synthesis, stability after digestion, solubility, recovery (completeness of release from the protein), and their respective ionization efficiencies in the mass spectrometer. Therefore, the choice of specific peptides is critical for developing accurate and sensitive methods.

3.1.1 HCMV proteomics and protein selection

To identify suitable proteins and tryptic signature peptides for quantification, viral samples were enzymatically digested using trypsin. Tryptic peptides have an optimal length for analysis and form doubly or triply charged ions when ionised and detected using ESI MS, which provide useful sequence information through CID fragmentation. The peptide monoisotopic masses and their respective production ions obtained after the tryptic digestion of the isolated virus proteins were

https://doi.org/10.7795/110.20260518

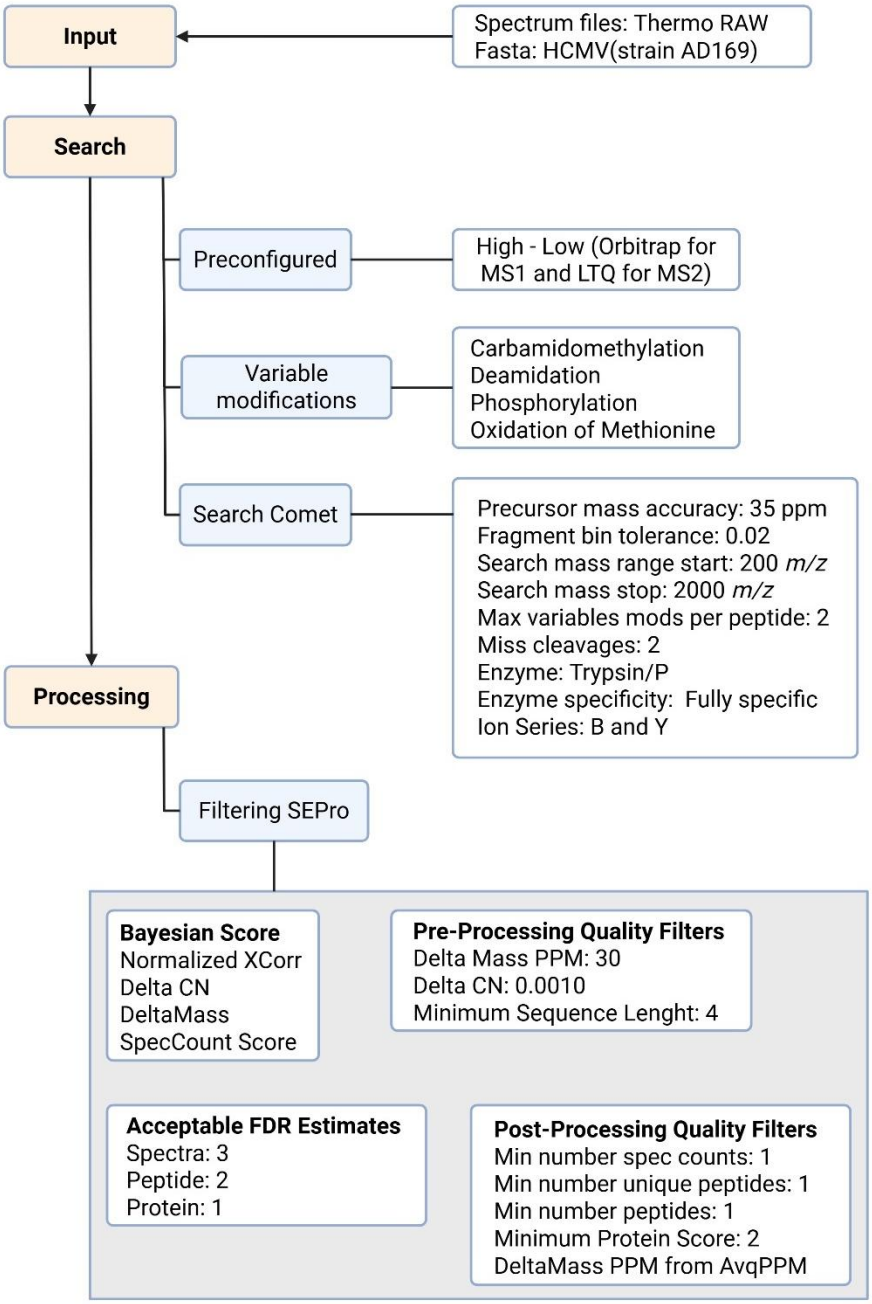

Figure 19: Peptide identification workflow using PatternLab for Proteomics.
Schematic overview of the peptide identification pipeline performed with PatternLab V software (141). Raw spectral data acquired in Thermo RAW format were searched against the HCMV (strain AD169) protein database (FASTA). The workflow involved preconfigured search parameters for high–low mass spectrometry (Orbitrap for MS1 and LTQ for MS2) and considered variable modifications including carbamidomethylation, deamidation, phosphorylation, and methionine oxidation. Searches were executed using the Comet engine with defined precursor and fragment mass tolerances, enzyme specificity (trypsin/P), and ion series (b and y). Identifications were subsequently filtered through SEPro, applying Bayesian scoring, pre- and post-processing quality filters, and false discovery rate (FDR) thresholds to ensure confident peptide and protein identification

used to identify proteins from databases entries of the TB40 strain using PatternLab V (139). This analysis identified 17 tegument, 5 envelope, 4 non-structural and 4 capsid proteins (Figure 21). To ensure that the identified proteins were not dependent on the batch (virus preparation), three independent

https://doi.org/10.7795/110.20260518

biological replicates (VYB04, VYB06-07) were analysed. In order to correlate the viral proteins to the total number of viral particles, the number of viral proteins per viral particle has to be known. Therefore, the choice of proteins for quantification is essential. Previous proteomics studies have shown different numbers for specific tegument, envelope or non-structural proteins (112, 139, 142, 143). For capsid proteins, there are different cryogenic electron microscopy studies reporting a consistent stoichiometry of capsid proteins of 16:16:10:5 (MCP:SCP:Tri2:Tri1) (115, 144-146). As capsid proteins were observed during this proteomics study, they were selected as the ideal targets for protein quantification and subsequent viral load determination. Next, for a peptide-based protein quantification, the capsid signature peptides were selected.

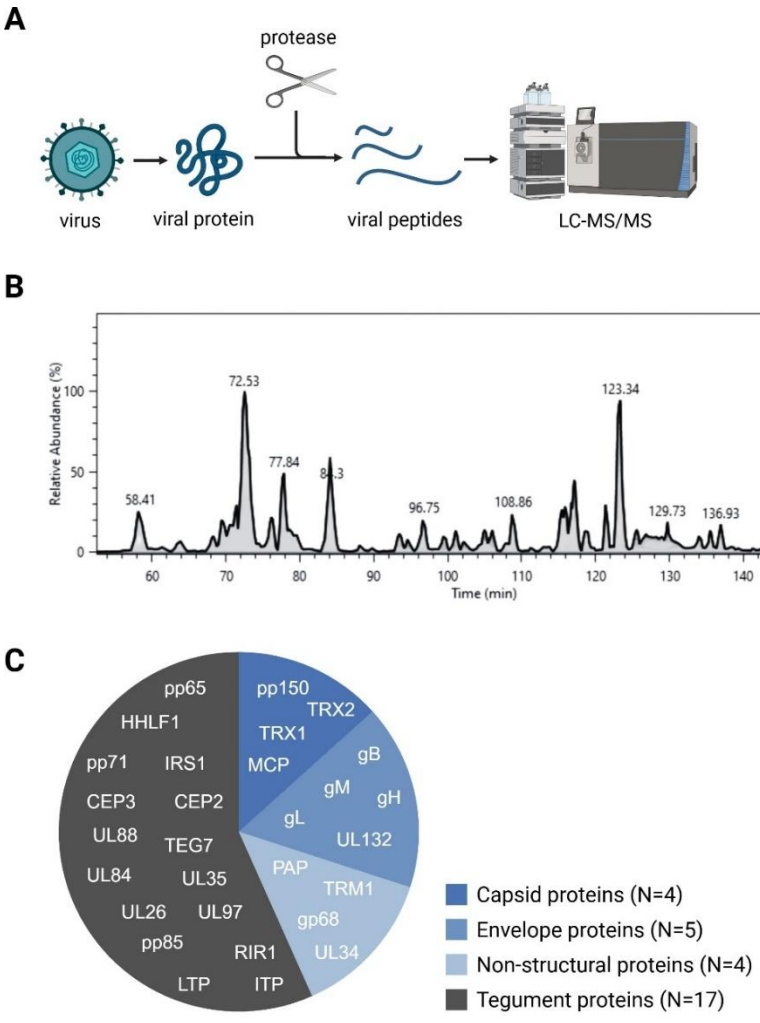

Figure 20: Proteomic workflow and protein identification from HCMV samples.
A. Schematic overview of the proteomic workflow. Viral proteins were digested with trypsin to generate peptides, which were then analysed using LC–MS/MS. B. Representative total ion chromatogram (TIC) showing the elution profiles of peptides over time during the LC–MS/MS measurement of virus prep VYB04. C. Classification of HCMV proteins identified by peptide mapping using PatternLab V software. Shown are proteins that were consistently detected across all virus preparations (VYB04, VYB06, VYB07 and VYB08). Each viral preparation was analysed in triplicate. The proteins are grouped according to their functional category

https://doi.org/10.7795/110.20260518

3.1.2 Signature peptide selection for capsid protein quantification

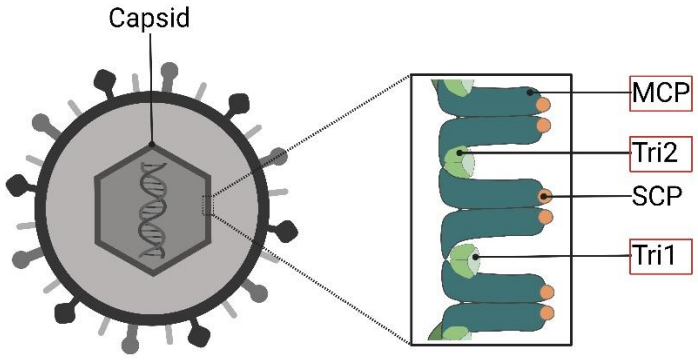

Figure 21: Viral Capsid proteins.
A Scheme of viral proteins forming the viral capsid. It comprises 60 asymmetric units. Each unit contains 16 copies of MCP (dark green), each of which is topped by a copy of the SCP (orange). Each unit also contains five copies of the Tri1 (light green) and ten copies of the Tri2 (green). The red rectangles indicate the chosen proteins for protein quantification.

As revealed from the proteomic study above, viral capsid proteins MCP, Tri1 and Tri2 were chosen for peptide-based protein quantification (Figure 17). To ensure the accuracy of protein quantification, ideally greater than three different peptides, from different regions of the protein (e.g. close to c-terminus, middle of protein, close to n-terminus), should be chosen but often less peptides can be used due to stability issues. Each peptide could give an independent value assignment of the protein amount concentration. Confirmation between two or more values from different peptides can be used to suggest that digestion has progressed to completion, but digestion curves showing the evolution of the peptides during proteolysis are still essential.

For the peptide selection different criteria, described in Hoofnagle et al., 2016, were applied. The chosen peptides have to be specific for the protein of interest, should be 6-20 amino acids long and observable by MS. Furthermore, possible miscleavage sites (e.g. Lys-Lys and Arg-Arg) have be avoided, because they may result in variable digestion yields. Moreover, amino acid residues that may be susceptible to modifications during sample preparations should be avoided (e.g. methionine, cystine) (63). These criteria served as a guideline and represent the ideal case scenario. The ideal peptides were selected, and then additional candidates were added that exhibited most of the criteria considered favourable for selection. In total 8 peptides were selected, 4 for the MCP, and two each for Tri1 and Tri2 (Table 26). All of them were observed in MS analysis of three independent virus stock preparations (VYB04, VYB06 and VYB07), showed a fragmentation pattern consistent with that expected from the peptide sequence (y- and b- ions, checked manually) (Figure S1) and were analysed regarding uniqueness by blast search against the proteome of HCMV (UP000008991), the human proteome

https://doi.org/10.7795/110.20260518

(UP000005640) because the virus was produced in a human cell line, and the bovine proteome (UP000009136) since fetal calf serum was a supplement of the cell culture medium.

Table 26: Selected HCMV signature peptides for quantification of viral capsid proteins MCP, Tri1 and Tri2

Name	HCMV Protein	*m/z*	Amino acid position of the respective protein	Sequence
Pep01	Tri1	1528.72	12-25	DPADEDNELVTALK
Pep02	(P16783)	921.45	280-287	SVELGDFR
Pep03	Tri2	801.45	16-23	LSIADVGK
Pep04	(P16728)	1161.72	27-37	LVAAVVPIPQR
Pep05		1151.57	141-150	ETFEGTILDK
Pep06	MCP	919.50	440-447	IDFVDALK
Pep07	(P16729)	1101.56	1267-1276	NTEEIIAANK
Pep08		776.41	1110-1115	VQDLFR

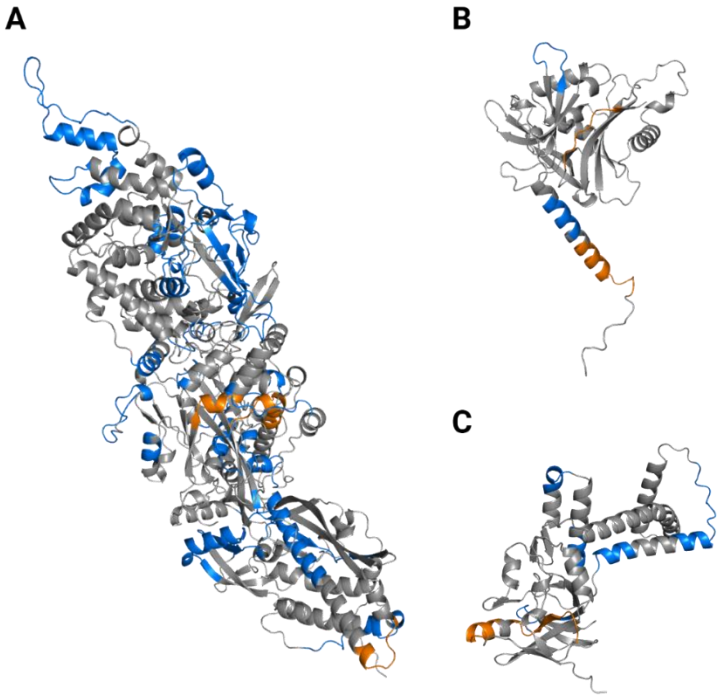

Figure 22: Structural mapping of HCMV capsid proteins identified by LC-MS/MS.
The three-dimensional structures of the viral capsid proteins were visualised using PyMOL: (A) MCP (UniProt ID: P16729), (B) Tri1 (UniProt ID: P16783), (C) Tri2 (UniProt ID: P16728). The peptides identified by LC–MS/MS are highlighted in blue, while orange indicates the signature peptides that were selected for quantitative analysis. The identified and selected peptides are distributed throughout the protein structures.

https://doi.org/10.7795/110.20260518

In summary, the proteomics data presented provides a crucial analytical framework for selecting both viral proteins and corresponding peptides, enabling precise viral quantification in downstream applications.

3.2 Quantification of reference peptides via amino acid analysis

SI-traceable peptide-based protein quantification methods require peptide or protein reference standard solutions that have been value-assigned with a known amount content and associated measurement uncertainty to act as calibrators. Peptide reference standards are synthetic peptides, that are produced by a process called solid phase peptide synthesis (SPPS). The peptide chain is built from the C-terminus towards the N-terminus. SPPS involves selective protecting and then removing the reactive moieties of the coupled amino acid and the residue already attached to the growing peptide chain (146). The presence of salt and excipients and the high-water content impact on any subsequent gravimetric preparation of standards using dried “purified” peptides. Therefore, it is essential to value-assign the synthetic peptide solutions for their amount of substance content of the peptide of interest. The method of choice for SI-traceable quantification of the purified peptides is amino acid analysis by exact matching isotope dilution mass spectrometry (EM-IDMS) after acid hydrolysis (16, 22). Certified reference materials of pure amino acid are available and provide traceability to the SI. Complete hydrolysis allows the amount of substance concentration of peptides to be derived by determining the amino acid concentrations. As impurities in synthetic peptides are usually deletion products missing a single amino acids or even whole sequence parts, amino acid analysis is only reliable for high-purity peptides, known to contain an insignificant amount of peptide related impurities (147). The estimation of measurement uncertainty associated with the amino acid analysis significantly impacts the total measurement uncertainty assigned to the peptide calibration standards. To ensure the most precise peptide reference value, it is essential to reduce this uncertainty. Additionally, as uncertainties propagate down the traceability chain, the uncertainty of the peptide reference standards used is a substantial factor in total protein measurement uncertainty. Consequently, reducing the uncertainty associated with the amino acid analysis not only reduces peptide measurement uncertainty but also improves the precision of protein quantification.

3.2.1 Impurity check

Structural impurities, such as deletion products or missing single amino acids, could be a source of error in determining peptide concentration. Although the peptides were ordered to be >98% pure, their purity was verified by analysing Pep01-Pep08 on a Thermo Scientific LTQ Orbitrap Elite mass spectrometer. One hundred femtomoles of each peptide were injected onto the column, either

https://doi.org/10.7795/110.20260518

separately or as a mixture of all of them. None of these analyses detected any structural impurities at this level (Figure 23).

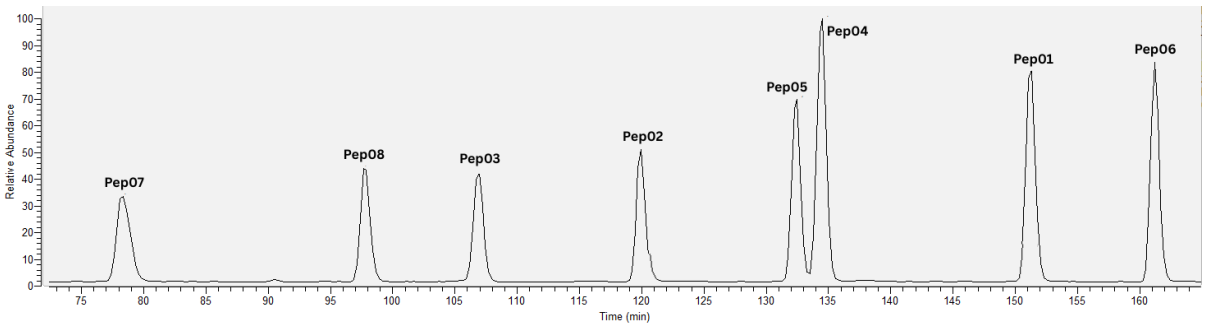

Figure 23: LC–MS/MS analysis of peptide standards (Pep01–Pep08) for purity assessment.
Chromatogram of individual peptide showing distinct and well-separated peaks for each peptide. No structural impurities were detected.

3.2.2 Value-assigning of the reference peptides

It is known that complete acid hydrolysis of peptides results in molar ratios of the released amino acids relative to the parent peptide being studied and therefore the concentration of the peptide can be determined from the concentrations of its constituent amino acids (16, 22). However, it is essential to select suitable amino acids for quantification. The reference amino acids calibrators and the isotopically labelled amino acids are not identical to the peptide of interest and may behave differently during hydrolysis, particularly if they are susceptible to degradation. Therefore, the IDMS procedure is only compensating for difference/losses after the peptide has been hydrolysed. The direct molar correlation between peptide concentration and amino acid concentration remains valid only if the monitored amino acids are fully released and remain stable without degradation over time. This excludes amino acids with reactive side chains, like methionine and cysteine, and leaves those with alkyl and amino side chains (148, 149).

For peptide quantification, the final result was obtained by averaging the individual amino acid measurements. At this stage, it was essential to confirm the complete release of amino acids, which was verified through equimolar results. Two or three amino acids (depending on the peptide sequence) were therefore used for quantification. An exception was Pep07 (see Table 6 and Figure 20), which could not be quantified this way, as it contained only isoleucine as a quantifiable amino acid. In addition to its suboptimal amino acid composition, this peptide also exhibited solubility issues. These factors likely contributed to the high uncertainty in the assigned value. Consequently, Pep07 was not used for protein quantification. For all other peptides, the relative standard uncertainty ranges between 0.5% and 2.5% (Table 27).

https://doi.org/10.7795/110.20260518

A well-established procedure traceable to the International System of Units (SI) was used to quantify synthetic reference peptides by amino acid analysis with exact-matching isotope-dilution mass spectrometry (EM-IDMS), following acid hydrolysis. Certified reference materials

Table 27: Results of amino acid analysis of reference peptides – quantification of amino acids of the respective peptide

Peptide	Amino acid	Amount of content (nmol/mg)		
		content	u	u in %
Pep01	Leucine	659,1	29,7	4,5
	Proline	672,8	7,2	1,1
	Valine	673,7	41,6	6,2
Pep02	Leucine	648,9	26,6	4,1
	Phenylalanine	657,1	28,3	4,3
	Valine	634,7	14,3	2,3
Pep03	Leucine	667,7	19,9	3,0
	Valine	681,4	22,4	3,3
Pep04	Leucine	645,3	17,6	2,7
	Isoleucine	669,4	24,0	3,6
Pep05	Leucine	660,8	21,4	3,2
	Isoleucine	659,1	20,5	3,1
	Phenylalanine	654,2	20,2	3,1
Pep06	Leucine	614,4	5,6	0,9
	Phenylalanine	598	19,6	3,3
	Isoleucine	604,9	15,8	2,6
Pep07	Isoleucine1	616,2	15,0	2,4
	Isoleucine2	442,9	4,4	1,0
	Isoleucine3	670,5	58,5	8,7
Pep08	Leucine	797,1	99,8	12,5
	Phenylalanine	805,4	114,6	14,2
	Valine	814,6	174,1	21,4

for amino acids, each of which is traceable to the International System of Units (SI), and isotopically labelled internal standards were used to assign peptide amount content values with demonstrated

https://doi.org/10.7795/110.20260518

traceability. This traceability establishes the metrological basis for SI-traceable peptide-based protein quantification.

Reliable quantification results were achieved through careful gravimetric preparation of samples and calibration blends, complete hydrolysis and repeated LC-MS measurements. For most of the analysed peptides, the relative measurement uncertainty ranged from 0.6% to 4% (Table 28, Figure 24), confirming the method's precision and suitability for reference material assignment.

Table 28: Results of amino acid analysis of reference peptides – summary

Peptide	Amount of content (nmol/mg)				
	κ (nmol/g)	u	u in %	U	U in %
Pep01	668,5	4,7	0,7	9,4	1,4
Pep02	646,9	6,5	1,0	13,1	2,0
Pep03	674,6	6,8	1,0	13,7	2,0
Pep04	657,4	12,1	1,8	24,1	3,7
Pep05	658,0	2,0	0,3	4,0	0,6
Pep06	605,8	4,8	0,8	9,5	1,6
Pep07	576,5	68,6	11,9	137,3	23,8
Pep08	805,7	5,1	0,6	10,1	1,3

However, one exception was Pep07, which exhibited high uncertainty due to an unfavourable amino acid composition (only one quantitative amino acid) and solubility issues, and was therefore excluded from use in protein quantification. By ensuring that peptide quantification results are traceable to the SI, this work directly contributes to reducing measurement uncertainty in downstream protein quantification. Accurate value assignment of peptide reference standards is therefore a critical step in establishing a reliable traceability chain for protein quantification workflows, supporting reproducibility and comparability across laboratories (Figure 2).

https://doi.org/10.7795/110.20260518

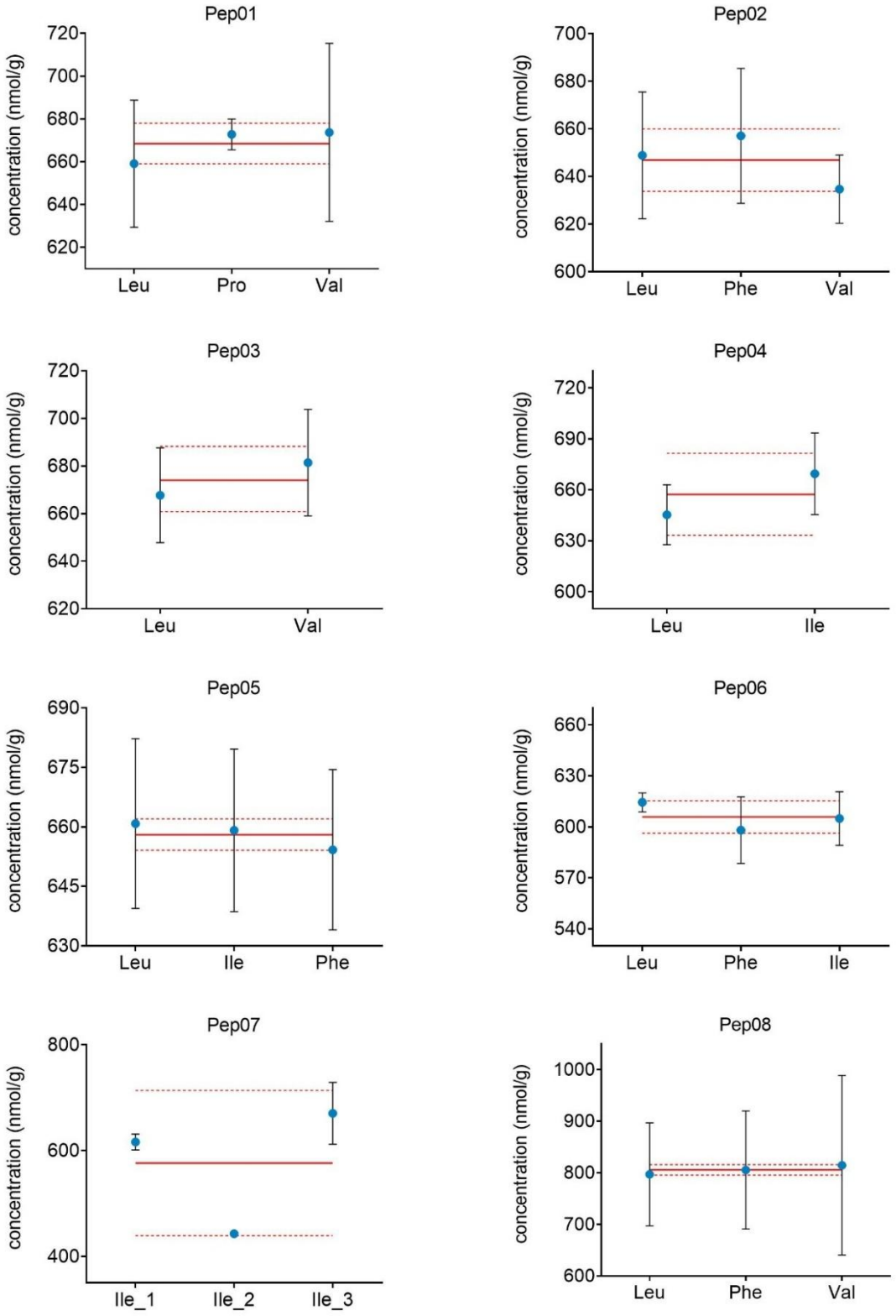

Figure 24: IDMS results for peptide quantification. Each plot shows the final results for each peptide.
Error bars represent standard uncertainty of the amino acid from 3x4 measurements, except for Pep07, here they represent 1x4 measurements. The thick red line indicates the average value for the peptide and the red dotted line the upper/lower expanded uncertainty value of the peptide value.

https://doi.org/10.7795/110.20260518

3.3 Method development for peptide-based protein quantification

Tandem mass spectrometry (MS/MS) is an important tool in clinical laboratories (150-153). This is largely due to its sensitivity and specificity, which are essential for detecting biomolecules that are often present at extremely low concentrations. However, challenges arise due to the structural complexity and wide dynamic range of protein mixtures. Peptide-based protein quantification is preferred over whole protein analysis because peptides are more stable, easier to ionize, and better suited to mass spectrometry, leading to higher sensitivity, specificity, and reproducibility (154-156). However, complex peptide mixtures still pose analytical challenges, such as competition for ionization and potential ion suppression, especially in biological matrices. During electrospray ionization (ESI), peptides typically form doubly or triply charged ions, which brings their mass-to-charge ratios into the optimal range for conventional mass analysers. While this improves detectability, the distribution of signals across multiple charge states can reduce the intensity of any single peak, especially when analyte concentration is low.

Selected reaction monitoring (SRM), also known as multiple reaction monitoring (MRM), has become the technique of choice in quantitative proteomics. SRM, particularly when performed on triple quadrupole mass spectrometers, is well-established in clinical laboratories for the precise quantification of molecules in complex biological samples such as serum and plasma (157, 158). Due to the limited mass range of triple quadrupole instruments (2000 – 4000 *m/z*), proteins must be enzymatically digested, followed by quantification of signature peptides. The success of SRM analysis heavily depends on ionization and fragmentation efficiency, therefore a careful selection of signature peptides and their transitions is critical. Although peptides carrying two or three charges are typically measured, there is no universal rule for predicting which peptides and transitions will produce strong MS signals. Therefore, it is standard practice to experimentally identify those that generate the strongest responses under differing MS conditions. Once these peptides and transitions are selected, SRM parameters, such as source voltages and collision energies, have to be fine-tuned individually for each peptide.

Accurate and precise peptide-based protein quantification relies on intensive method development. It is necessary to select the MRM parameters on a triple quadrupole to receive selective, stable and reproducible transitions signals for quantification. Furthermore, the limit of detection (LOD) and limit of quantification (LOQ) are determined. Lastly, time-course experiments were conducted to confirm the complete release of peptides during digestion. This is important because incomplete digestion would compromise the quantification of peptides as a measure of protein, since 1 mol of peptide equals 1 mol of protein.

https://doi.org/10.7795/110.20260518

3.3.1 Transition selection and optimisation

In peptide-based protein quantification, accurate and reproducible quantification by LC-MS/MS is highly dependent on the careful selection of precursor to product ion transitions in MRM mode. Transition selection is critical to achieving both sensitivity and specificity, as it allows the instrument to focus on distinct fragmentation patterns unique to the target peptide. By selecting transitions that yield high-intensity product ions while avoiding those prone to interference or exhibiting a low signal intensity, it is possible to improve the method's ability to detect and quantify peptides even at low concentrations in complex biological matrices. In addition, proper optimisation of transitions reduces the likelihood of co-eluting isobaric interferences, contributing to improved quantitative accuracy and method robustness. Two to three transitions per peptide should be chosen depending on the selectivity and measurement uncertainty required. Transition selection begins with the identification of suitable precursor ions - typically the doubly or triply charged peptide ions that exhibit strong MS1 signal intensity of the precursor ions. Once the precursor ion has been selected, product ions are selected based on their fragmentation behaviour, favouring y or b ions that are abundant and unique to the peptide sequence. Fragment ions should ideally be in the higher *m/z* range to reduce interference from background noise and maximise specificity.

For transition selection and optimisation, 10 pmol of a peptide solution was infused into the mass spectrometer via the iKey infusion tile. After selecting the most intense precursor ion, the corresponding product ions were selected. The collision energy was optimised to obtain the most abundant product ion signal for each individual transition. Table 29: Precursor and product ions (transitions) summarises the selected transitions used for targeted peptide quantitation. For each peptide, the table lists the precursor ion *m/z*, the corresponding product ion *m/z* (transition) and the optimised collision energy (CE) that were monitored over the expected chromatographic elution time for each peptide. This table provides the basis for developing a robust MRM assay by ensuring that each transition is both analytically sensitive and specific to the target peptide sequence. Control measurements (0.1% FA+labelled peptide, 0.1% FA+natural peptide, 0.1 FA%) show no interfering or overlapping traces, confirming that there is no interference between the isotopically labelled and natural traces.

https://doi.org/10.7795/110.20260518

Table 29: Precursor and product ions (transitions)

Protein	Peptide	Sequence	Precursor (*m/z*)	T1 (*m/z*)	T2 (*m/z*)	T3 (*m/z*)	CE (eV)
Tri1	Pep01	DPADEDNELVTALK	765.4^{+2}	1246.6	432.3		28
Tri1	Pep09	DPADEDNELVTALK*	769.4^{+2}	1254.6	440.3		28
Tri1	Pep02	SVELGDFR	461.7^{+2}	736.4	607.3	494.2	15
Tri1	Pep10	SVELGDFR*	466.7^{+2}	746.4	617.3	504.2	15
Tri2	Pep03	LSIADVGK	401.7^{+2}	689.4	602.4	498.3	15
Tri2	Pep11	LSIADVGK*	405.7^{+2}	697.4	610.4	497.3	15
Tri2	Pep04	LVAAVVPIPQR	581.9^{+2}	709.4	610.4		18
Tri2	Pep12	LVAAVVPIPQR*	586.9^{+2}	719.4	620.4		18
MCP	Pep05	ETFEGTILDK	576.8^{+2}	775.6	646.4		20
MCP	Pep13	ETFEGTILDK*	580.8^{+2}	783.6	654.4		20
MCP	Pep06	IDFVDALK	460.8^{+2}	807.4	692.4		14
MCP	Pep14	IDFVDALK*	464.8^{+2}	815.4	700.4		14
MCP	Pep07	NTEEIIAANK	551.8^{+2}	887.5	758.4		18
MCP	Pep15	NTEEIIAANK*	555.8^{+2}	895.5	766.4		18
MCP	Pep08	VQDLFR	389.2^{+2}	678.4	550.3		14
MCP	Pep16	VQDLFR*	394.2^{+2}	688.4	560.3		14

To evaluate the suitability of the chosen MRM transitions (Table 29), a peptide mixture comprising Pep01–Pep16 was analysed using LC-MS/MS. Each peptide was injected at a concentration of 100 fmol on-column. The resulting total ion chromatograms (TIC) show distinct, well-resolved peaks for all analytes, indicating stable chromatographic separation and reliable signal detection (Figure 22). Furthermore, the natural and isotopically labelled peptide pairs exhibited similar retention behaviour and comparable peak shapes, confirming the anticipated co-elution of both forms. These results demonstrate that all monitored transitions perform as intended and can be reliably used for quantitative analysis.

https://doi.org/10.7795/110.20260518

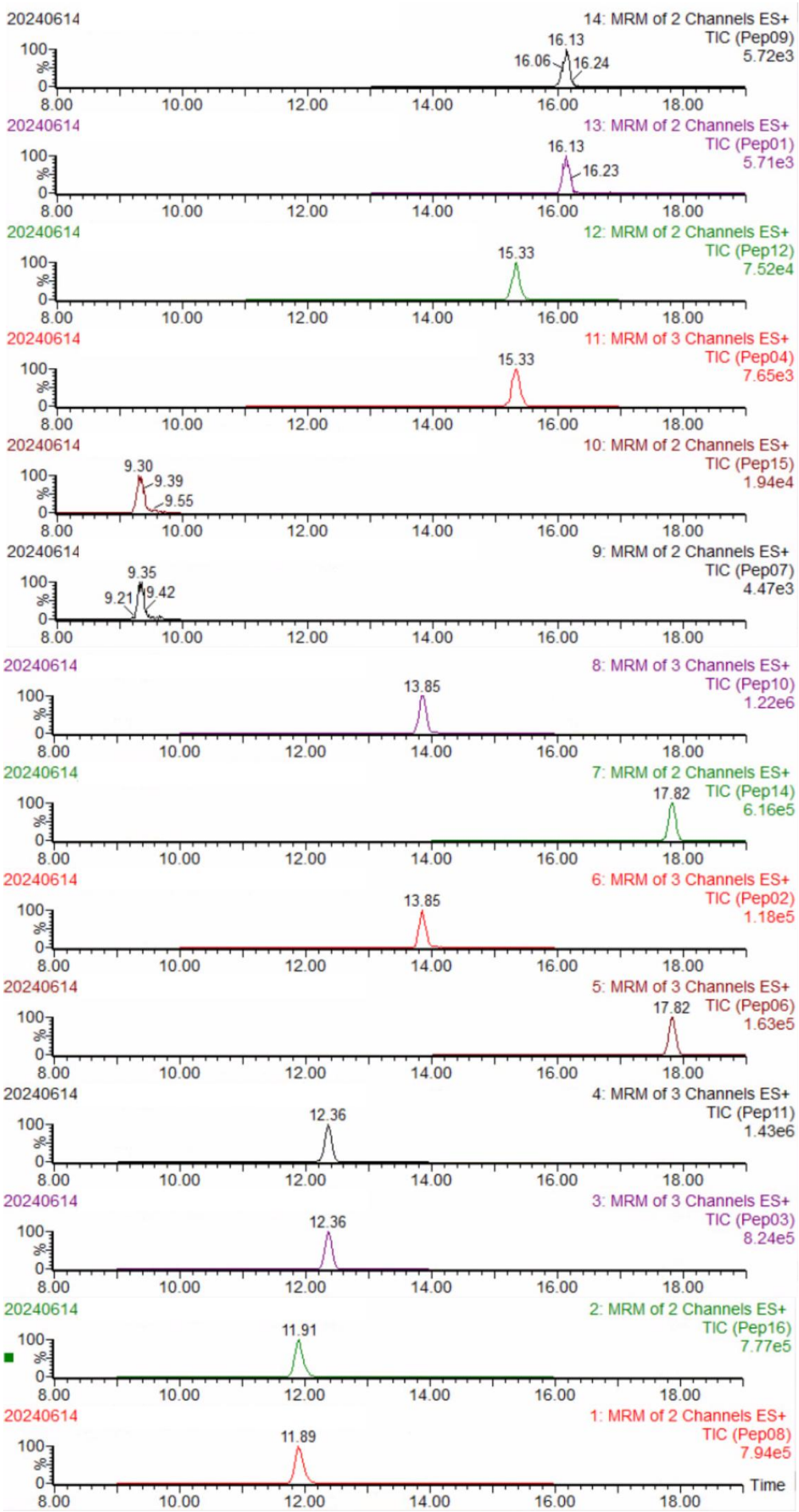

https://doi.org/10.7795/110.20260518

Figure 25: Total ion chromatograms (TICs) of peptides Pep01–Pep16 acquired by LC-MS/MS in MRM mode.
A mixture of all sixteen peptides was injected, with 100 fmol of each peptide loaded onto the column. Each trace represents the monitored transitions listed in Table 7. The chromatograms show distinct, well-resolved peaks with consistent retention times, demonstrating stable chromatographic performance and reliable signal detection. The corresponding natural and isotopically labelled peptide pairs exhibited identical retention behaviour and comparable peak shapes, confirming correct chromatographic alignment and the expected co-elution of labelled and unlabelled forms. The y-axis shows the signal intensity and the x-axis represents the retention time in minutes.

3.3.2 LOD and LOQ determination

The limit of detection (LOD) is the lowest analyte concentration at which the signal is distinguishable from the noise or can be detected with confidence (159). The LOD is a relevant performance parameter that reflects the sensitivity of an analytical method. In peptide quantitation by LC-MS/MS, especially in complex biological matrices such as plasma or tissue extracts, peptides are often present at very low concentrations. A low LOD ensures that even small amounts of target peptides can be detected, which is essential for applications such as biomarker discovery, pharmacokinetics and disease diagnostics. Accurate detection at low levels is particularly important when studying low-abundance proteins, post-translationally modified peptides or early-stage diseases where biomarkers are present at very low levels. An inadequate LOD can lead to false negatives or the complete omission of biologically relevant signals, thus compromising the scientific or clinical utility of the data (160). The lower limit of quantitation refers to the lowest concentration of the analyte at which quantitative measurements can be made and as with the LOD, it is important when measuring low-abundance peptides in complex biological matrices.

The LOD and LOQ capability for the developed MRM assay were practically assessed. The LOD and LOQ was determined according to the ICH guideline "Validation of analytical Procedures" (161). The ratio of the peak area of the natural peptide to that of the labelled peptide was plotted against the amount of natural peptide loaded on the column (Figure 26). The LOD and LOQ was calculated based on the standard deviation of the response and the slope of the calibration curve. The LOD and LOQ was calculated as follows:

$$LOD = \frac{3.3\,\sigma}{S}$$

Equation 15: Calculation of LOD

$$LOQ = \frac{10\,\sigma}{S}$$

Equation 16: Calculation of LOQ

https://doi.org/10.7795/110.20260518

Where σ is the standard deviation of natural/labelled (nat/lbld) ratio at 2 fmol on column and S is the slope of the calibration curve. The LOD for all peptides was below 2 fmol on column and the LOQ was below 8 fmol on column (Table 30). The R^2 for Pep02, Pep03, Pep06, and Pep08 proposing a good fit. For Pep04 and Pep01, the error bars are high and the R^2 is below 0.95. The quantification in such low concentrations have to be treated with caution. The LOD/LOQ for Pep05 could not be determined, because it could not be separated by LC under the same conditions as the other peptides. Therefore, it was not used for further investigations.

Table 30: LODs/LOQs

Peptide	LOD (fmol on column)	LOQ (fmol on column)
Pep01	1.08	3.28
Pep02	0.87	2.65
Pep03	0.84	2.54
Pep04	2.37	7.18
Pep06	0.95	2.88
Pep07	0.73	2.22
Pep08	0.04	0.12

https://doi.org/10.7795/110.20260518

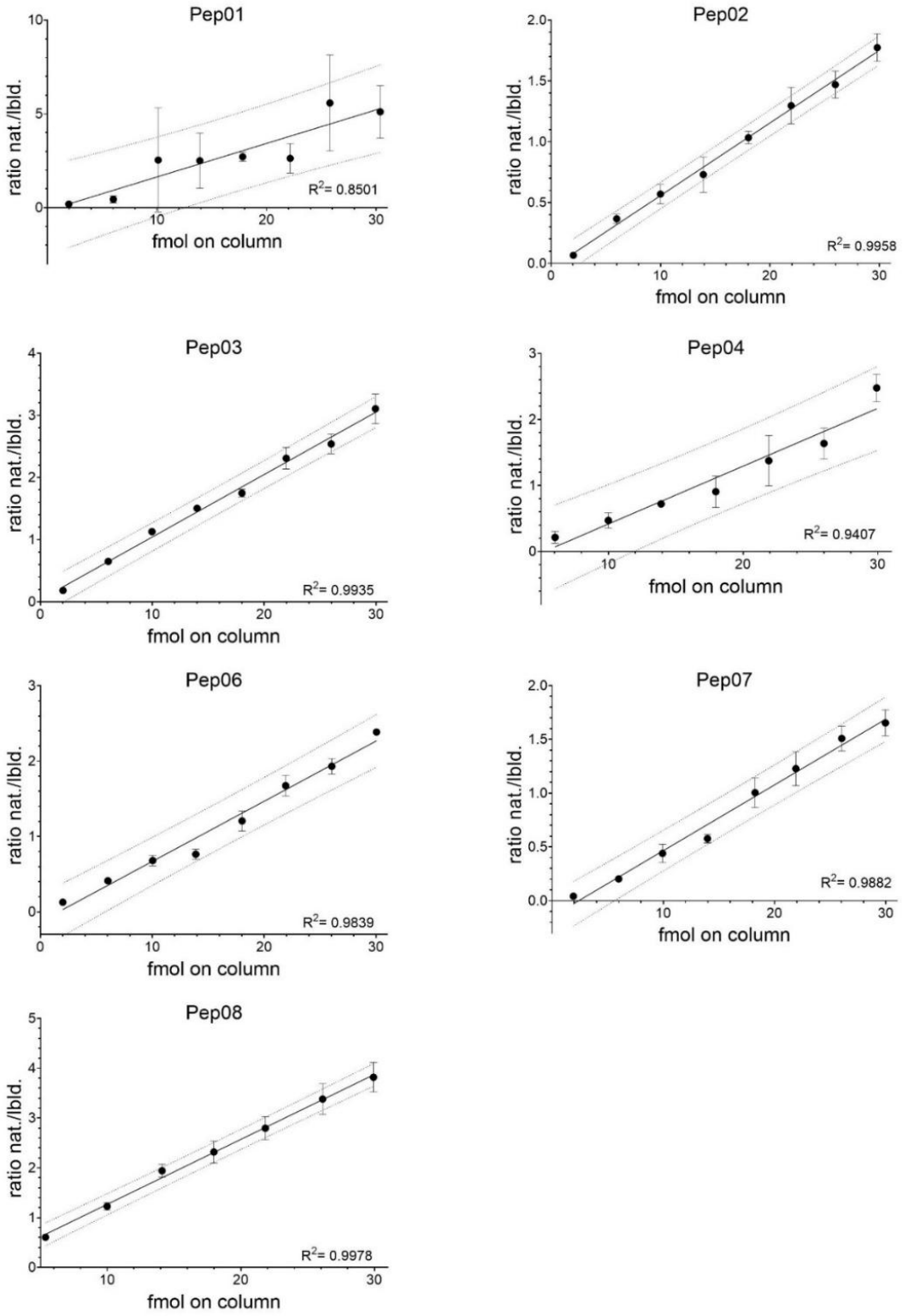

Figure 26: Calibration curves for LOD/LOQ determination.
Dotted lines describe the 95% confidence interval. Solid line: linear regression curve. Error bars represent the standard deviation from three different experiments, measured four times each. The y-axis shows the ratio of natural peak area to labelled peak area. The x-axis represents the amount of substance concentration of the natural peptide on column. Plots were generated with Graph Path Prism.

https://doi.org/10.7795/110.20260518

3.3.3 Reinjection reproducibility

Reinjection reproducibility in LC-MS/MS assays is a key quality parameter that ensures the reliability of sample analysis even over a longer run time. Reproducibility assesses whether the reinjected samples give the same quantitative results as the first injection, taking into account sample stability and instrument stability in terms of retention time, ionisation and fragmentation performance. To assess the reproducibility of reinjection, five different Pep01-16 mixtures (10-100 fmol) were reinjected 45 times, for a total of 225 times over the entire run. For retention time, the average retention time for each peptide over the 225 injections was calculated. The coefficient of variation (CV) was calculated by dividing the standard deviation of the retention time by the mean and then multiplying by 100. For all peptides the CV was less than 1 %, which is below the recommendation of the C62 guideline for Liquid chromatography-mass spectrometry methods (162). The average retention time was similar for all natural and isotopically labelled peptide pairs. Transition ratios were analysed to evaluate fragmentation robustness. There are regulatory guidelines regarding ion ratio tolerances and these recommendations vary across organizations such as the United Nations (UN), the European Union (EU), and the United States of America (USA). The UN stipulates an ion ratio tolerance of ±20% for the analysis of illicit drugs in seized materials and biological samples (163). The European Commission Decision 2002/657/EC prescribes a tolerance range of ±20% to ±50%, depending on ion intensities, for analytical methods applied to official samples in control laboratories (164). In the United States, the Department of Agriculture enforces a ±20% tolerance for ion transition ratios (165), whereas the Food and Drug Administration (FDA) specifies tolerances of ±20% and ±30% when monitoring two and three diagnostic ions, respectively (166). A notable limitation of these guidelines, however, is that the specified tolerances are not derived from empirical evidence but are instead arbitrarily defined (167). For the peptide pair (nat/isotopically labelled) Pep02/Pep10 and Pep03/Pep11 three transitions were measured. For all other peptide pairs, two transitions were measured. The observed transition ratios variations for the different peptides were between 14 and 48 %. The threshold CV for good reinjection reproducibility was set to 30% for those peptides with three measured transitions and to 20% for two measured transitions. Therefore, the peptide pairs Pep01/Pep09, Pep07/Pep15 and Pep08/Pep16 (in red) were not considered for further experiments (Table 31).

In general, transitions or LC gradients could have been optimised by selecting the best conditions for the different peptides so that none had to be excluded. But the aim was to find the best conditions for measuring as many peptides as possible with a single injection. This allowed all peptides to be analysed under the same conditions, facilitating better comparisons between these proteins. Multiple measurements introduce run-to-run variation, which can reduce quantitative reliability. A single, combined measurement reduces sample consumption and protein degradation.

https://doi.org/10.7795/110.20260518

Table 31: Reinjection Reproducibility
In red, peptides that were not used for quantification, in green, peptides that were used for quantification

Protein	Peptide	Retention Time		Transition ratio	
		Average (min)	CV (%)	Average	CV (%)
Tri1	Pep01	16.39	0.41	0.74	35.40
Tri1	Pep09	16.39	0.39	0.56	43.14
Tri1	Pep02	13.92	0.27	0.13	24.36
Tri1	Pep10	13.92	0.26	0.08	20.12
Tri2	Pep03	12.58	0.33	0.03	21.43
Tri2	Pep11	12.58	0.35	0.02	23.62
Tri2	Pep04	15.93	0.27	0.39	16.98
Tri2	Pep12	15.92	0.27	0.33	19.01
MCP	Pep06	17.98	0.23	0.51	14.78
MCP	Pep14	17.98	0.25	0.48	15.49
MCP	Pep07	9.50	0.66	1.65	47.39
MCP	Pep15	9.50	0.66	1.76	33.71
MCP	Pep08	11.93	0.36	0.24	16.64
MCP	Pep16	11.93	0.36	0.24	23.76

3.3.4 Time course experiments for proteolysis confirmation

In peptide-based protein quantification by LC-MS/MS, complete and reproducible proteolysis is essential to ensure consistent peptide generation. Quantification relies on measuring the abundance of specific peptides as surrogates for their parent proteins. Incomplete digestion can lead to underestimation of protein levels, increased variability and poor reproducibility. Time course proteolysis experiments were performed to define the optimal digestion time that ensures complete peptide release without introducing degradation artefacts.

The virus sample VYB12 was spiked with isotopically labelled peptides (Pep09-16) and digested using trypsin under standardized conditions using the MPS robot. Aliquots were collected after 1, 2, 3, 4, 5, 6, 8, 10, 12,16, 24, 32 and 48 hours. Samples were analysed via LC-MS/MS and the peak area ratios of natural to labelled peptide signal were plotted over time. To ensure that no degradation occurs over time, peptide controls (pure peptides) were treated in parallel. For all proteins, a plateau was reached after 10-12 hours (Figure 27).

https://doi.org/10.7795/110.20260518

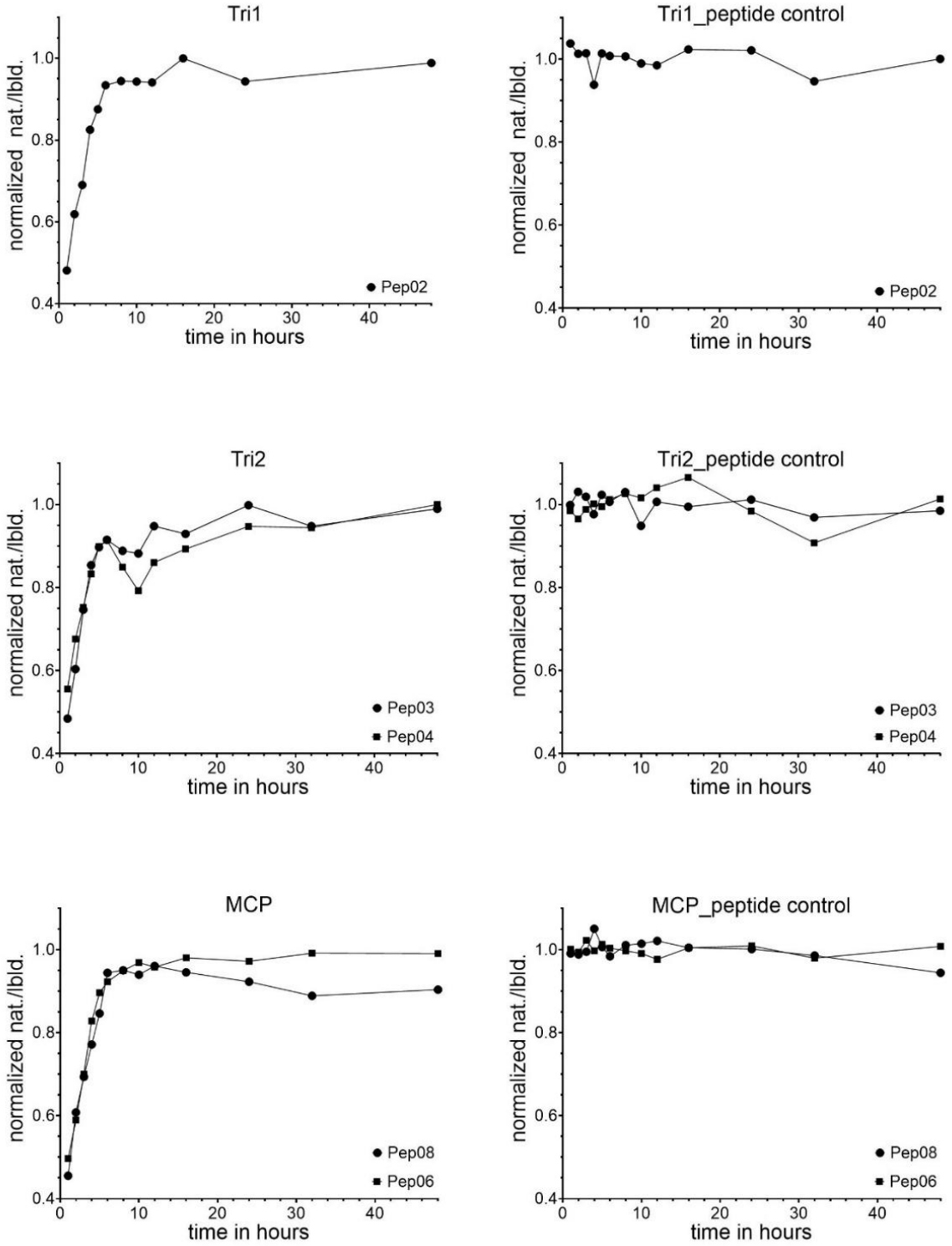

Figure 27: Time course digestion curves.
Plotted data are from 3 different experiments, proceeded on three different days. Data was normalized to the maximum ratio of nat./lbld.. Plots were generated with Graph Path Prism.

To obtain the best precision during the measurement process it is preferential to obtain similar intensities between the calibration standards and samples. Therefore, it is common practice to perform the

https://doi.org/10.7795/110.20260518

same sample preparation on the calibration blend as will be used on the sample. In this instance the calibrators are free peptides that have been spiked with isotopically labelled peptides. However, in the virus preparation sample, the natural peptides are incorporated in the proteins, and the labelled peptides are spiked as free peptides. Therefore, equilibration of the natural and labelled peptides can only occur after complete release of the peptide. This is a considerable weakness in the peptide-based IDMS approach for protein quantification. As the instability of the peptides can cause error or bias, in the final result, it is essential to prove that peptides spiked at the beginning of the digestion procedure are stable until equilibration is possible. To assess this the evolution of the peptides was monitored over the digestion time. The natural peptide signal from the sample digest (represented by circles in Figure 28) initially increased and then stabilised, indicating successful digestion with no signs of degradation. The signals from the peptide controls (the natural peptide, represented by triangles, and the isotopically labelled peptide, represented by squares) remained stable throughout the incubation period. The minor decreases in the control peptide signals over time can be attributed to dilution effects during digestion, given that samples were drawn and fresh trypsin was added at each time point. These data confirm the stability of the peptide during digestion. For all three capsid proteins, a 12 hour digestion provides a complete peptide release. This time point was chosen for peptide-based quantification of HCMV capsid proteins.

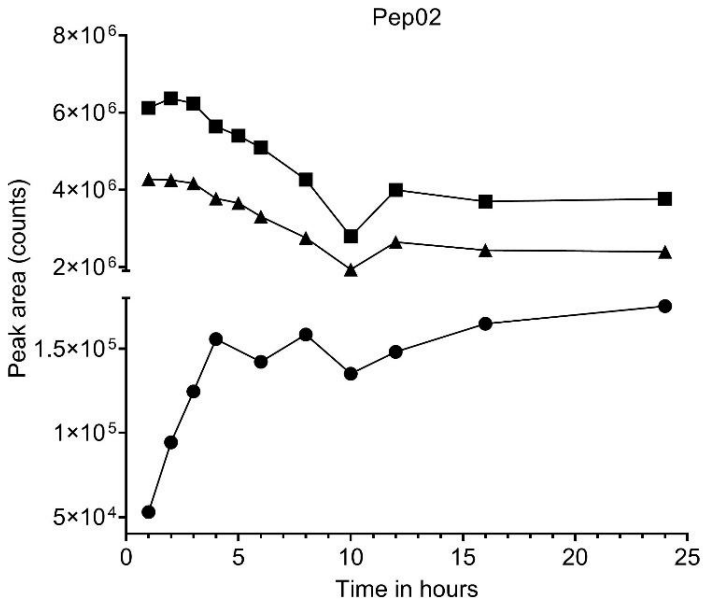

Figure 28: Example of time profiles of individual signals.
Circles: natural signal from sample digest. Triangle: signal from natural peptide in peptide control. Square: signal from isotopically labelled peptide in peptide control

https://doi.org/10.7795/110.20260518

Following the assignment of the SI traceable amount of substance concentration to the primary calibrators and assessment of the peptide stability during extraction and digestion we began the systematic development of a robust and sensitive method for peptide-based quantification of HCMV capsid proteins. The method leverages the advantages of tandem mass spectrometry for detecting low-abundance peptides, where peptide-based analysis is favoured over whole proteins due to better stability, ionization efficiency, and reproducibility.

3.4 Viral load estimation by combining ddPCR and IDMS measurements

The developed method was assessed for the quantitative characterisation of gradient purified viral particles (HCMV virions) of the VYB12 sample. The quantity of interest, the measurand, is the number of viral particles. However, as there is no direct method to count them, their quantification relies on indirect measurements. Therefore, two primary reference measurement procedures were employed: droplet digital PCR (ddPCR) for quantifying viral DNA genomes, and isotope dilution mass spectrometry (IDMS) for measuring the amount of substance of capsid protein signature peptides. Combining these complementary methods provided a robust estimate of both genome copy numbers and capsid protein content, offering an integrated estimation of total virion number in the sample. The DNA and protein samples generated were used to assess the molecular quantification methods using the IDMS and ddPCR. Furthermore, the known stoichiometries of the HCMV capsid architecture (119) were used to infer virion numbers from peptide-based protein measurements. In addition to methodological implementation, the variability between biological replicates and an assessment of between genome- and protein-based quantifications agreement was performed. Together, these analyses provide comprehensive, validated measurements of virion load, demonstrating proof of concept for combining orthogonal quantification approaches in viral metrology.

3.4.1 DNA quantification of virus sample VYB12

The three independent DNA extractions of VYB12 virions were diluted (1:1000) with nuclease-free water before proceeding the ddPCR protocol. Each extraction was measured in four replicates on three different days (Figure 29).

https://doi.org/10.7795/110.20260518

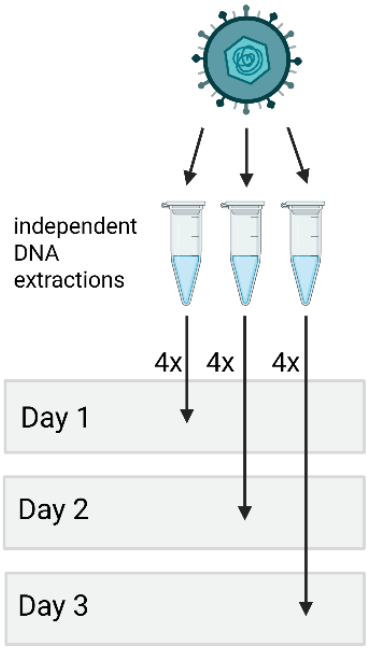

Figure 29: Experimental design of the droplet digital PCR (ddPCR) analysis for the VYB12 sample.
Three independent viral DNA extractions were performed; each extraction was analysed on three different days (Day 1–3). Four technical replicates were analysed per extraction on each measurement day. This setup enabled the evaluation of measurement reproducibility over time and ensured the robustness of the ddPCR quantification.

Figure 30 shows the mean results of three independent DNA extractions from the VYB12 virus preparations. Four replicate measurements were performed for each extraction, the mean of these replicate measurements is shown (blue dots) with error bars representing the standard deviation of each set. The average DNA copy number determined across all extractions was 4.3×10^7 copies/µL (blue line). The solid red line shows the combined standard uncertainty of all extractions (9.0×10^6 copies/µl), which corresponds to a relative uncertainty of 21.1%. The red dashed lines show the combined expanded uncertainty (1.9×10^7 copies/µL).

All three extractions fall within the expanded uncertainty range, reflecting overall consistency and acceptable variability. However, extraction No. 3 shows a notably higher concentration than the other two. Its low replicate variability suggests that this difference is not due to random measurement error but may be caused by factors such as improved extraction efficiency or variation in the input material. While this outlier does not invalidate the results, since it lies within the uncertainty range, it highlights the importance of ongoing monitoring for extraction variability.

https://doi.org/10.7795/110.20260518

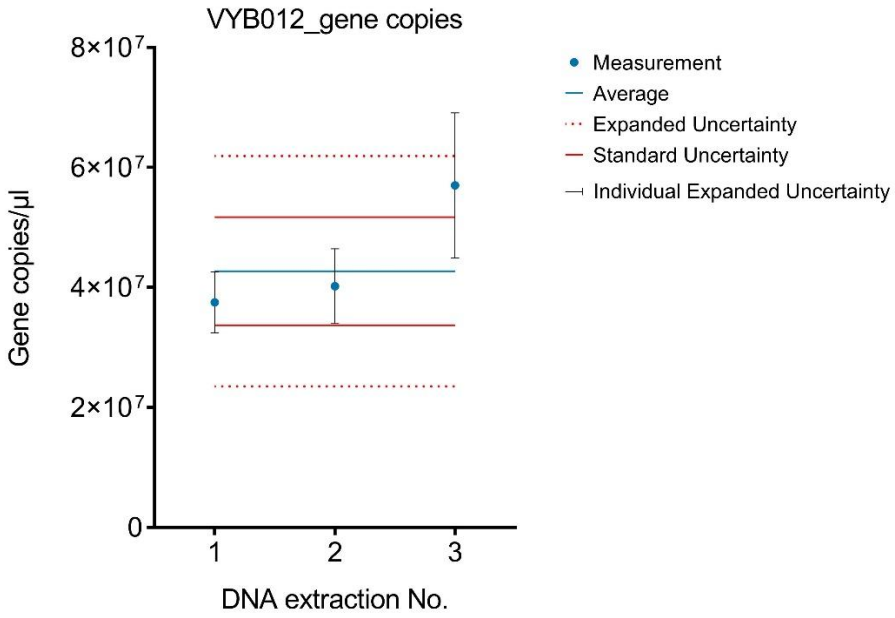

Figure 30: Summary of gene copies for VYB12

3.4.2 Capsid protein quantification of VYB12

To quantify the capsid protein, the VYB12 virus preparation was digested with trypsin, after which IDMS was performed on the chosen peptides. Isotopically labelled peptides served as internal standards, and natural synthetic peptides with values assigned by amino acid analysis were used as references to assign peptide quantities. The IDMS method developed was applied to quantify viral capsid proteins. According Table 29 (Chapter 3.3), Pep02 was used to quantify Tri1, Pep03 to quantify Tri2, and Pep06 to quantify MCP. Pep07 was not used because it was not possible to measure Pep07 within the complex matrices of the virus preparation. The concentration of for each peptide was determined using the double IDMS equation (see chapter 1.2.3, equation 1). The amount of substance content calculation for each peptide was done separately for each transition. The results for each peptide were averaged to determine the final peptide content. Due to instability and bad reinjection reproducibility (see Chapter 3.3), only one peptide was measured per protein. Complete digestion of the protein has been assumed, and therefore 1 mole of peptide is assumed to be formed from 1 mole of the original protein.

The values measured for each protein are given in Table 32 with a summary plot in Figure 31. For Tri1, the individual protein content from transitions T1-T3 ranged from 39.3 to 40.8 fmol/mg, with uncertainties between 1.6 and 2.4 fmol/mg. The combined result was 39.6 ± 1.5 fmol/mg, with a relative expanded uncertainty of 3.5%. All transitions were fully consistent with the combined result within

https://doi.org/10.7795/110.20260518

their reported uncertainties, indicating high agreement. The Tri2 data showed a slightly broader spread, with transition values ranging from 81.8 to 87.6 fmol/mg and individual uncertainties of up to 7.6 fmol/mg. Nevertheless, the combined value of 91.5 ± 6.4 fmol/mg remained representative of all transition-level results. For the MCP protein, only two transitions were measured (112.8 and 96.7 fmol/mg), with large corresponding uncertainties in (up to 26.7 fmol/mg). This led to a combined value of 104.7 ± 18.9 fmol/mg and a relative expanded uncertainty of 18.2%.

Table 32: Results of measured capsid proteins via LC-MS/MS

Peptide/ protein	transition	Amount of content (fmol/mg)				
		Protein content	u(Protein)	u in %	U(Protein)	U in %
Pep02/ Tri1	T1	39.3	1.6	4.1		
	T2	38.6	3.6	9.3		
	T3	40.8	2.4	5.9		
	average	**39.6**	**0.7**	**1.6**	**1.5**	**3.5**
Pep03/ Tri2	T1	91.2	7.6	8.3		
	T2	81.8	6.0	7.3		
	T3	89.9	3.5	3.9		
	average	**87.6**	**2.9**	**3.6**	**6.4**	**7.9**
MCP/ Pep06	T1	112.8	15.8	14.0		
	T2	96.7	26.7	27.6		
	average	**104.7**	**8.0**	**7.7**	**18.9**	**18.2**

The expansion factor k was obtained from the two-sided Student's T distribution within 95% confidence interval with n=12 for Tri1 and Tri2 and n=8 for MCP. This resulted in k=2.20 for Tri1 and Tri2 and k= 2.36 for MCP.

https://doi.org/10.7795/110.20260518

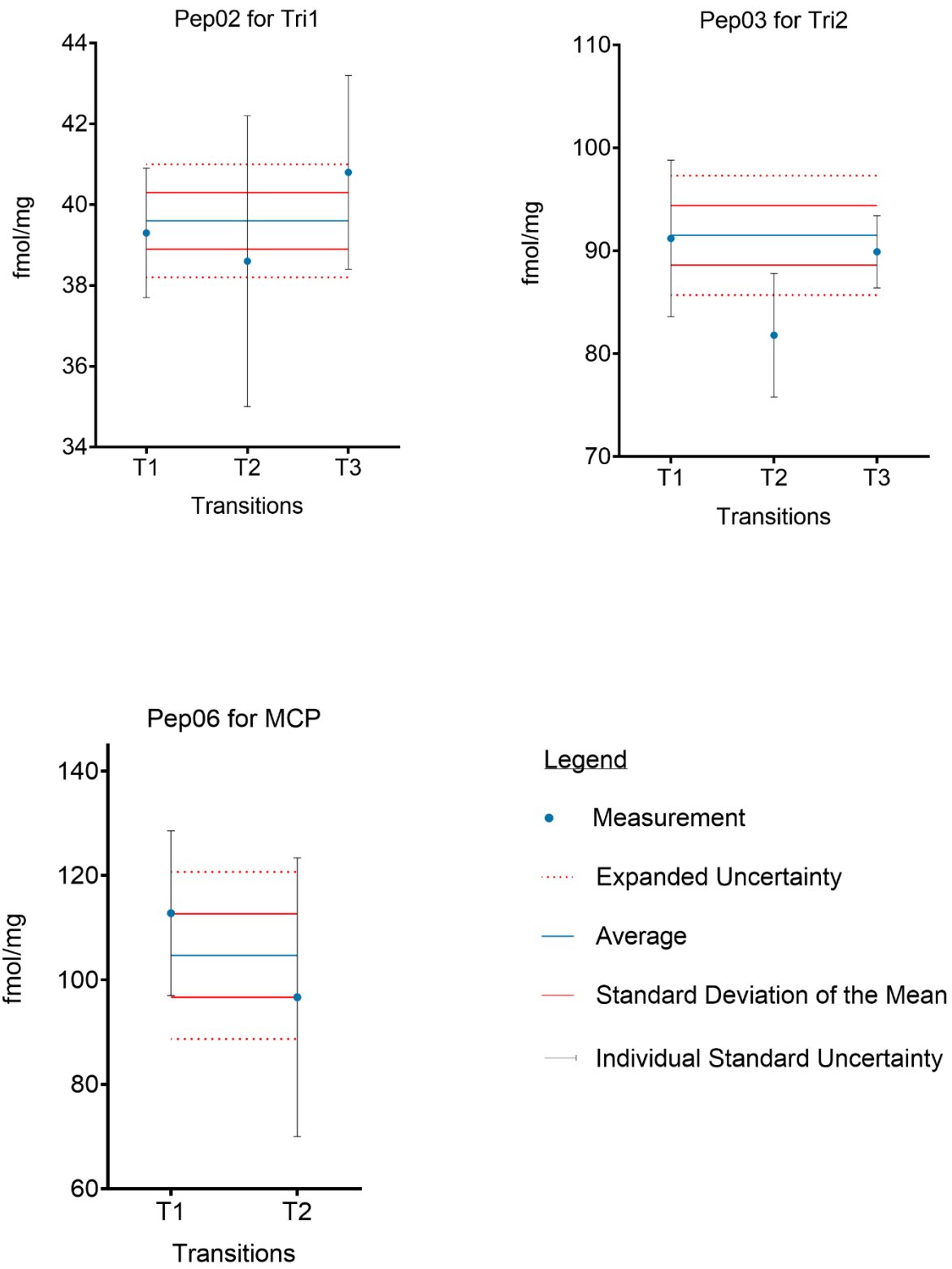

Figure 31: Transition-specific peptide quantification for Tri1, Tri2, and MCP.
Each peptide (Pep02 for Tri1, Pep03 for Tri2, and Pep06 for MCP) was measured in four replicates. The plots show the quantification results for individual transitions (T1–T3) with the mean value (blue line), standard deviation (black line), standard uncertainty (red line), and expanded uncertainty (red dotted line).

https://doi.org/10.7795/110.20260518

3.4.3 Viral load estimation of VYB12

To estimate the number of HCMV capsids in the VYB12 sample based on protein concentration, the established stoichiometry of capsids reported by Yu et al. 2017 was utilised. The HCMV capsid comprises 960 copies of the major capsid protein (MCP), 300 copies of the Tri1 triplex subunit and 600 copies of the Tri2 subunit. These values reflect the structural organisation of mature virions and were used to infer the number of capsids from measured protein amounts. The Avogardo constant was used to convert from protein numbers/capsid to mol/capsid. The respective number of protein/capsids was as conversion factor (CF) to convert from measured amount of protein to number of capsids.

Table 33: Capsid stoichiometry according Yu et al. 2017 (119)

Protein	Numbers/virions	CF (fmol/capsid)
Tri1	300	4.98×10^{-7}
Tri2	600	9.96×10^{-7}
MCP	960	1.59×10^{-6}

The number of complete capsids was estimated by dividing the measured amount of substance content of capsid proteins by the number of copies per capsid.

$$number\ of capsids = \frac{\kappa_x}{CF_x}$$

Equation17: Calculation of capsid numbers based on amount of substance content of capsid proteins

where CF_x *is the conversion factor,* the number of proteins (fmol) per capsid, and κ_x the measured amount of protein content (pmol/mg). Several studies have shown that cryo-electron microscopy (cryo-EM) data may be subject to uncertainty arising from factors such as map resolution, structural heterogeneity and refinement variability (142, 168-172). Consequently, any quantitative interpretation based on cryo-EM data, such as the application of a conversion factor (CF), must also incorporate an uncertainty estimate. A study by Herzik et al. (2019) analysed the variation between multiple cryo-EM models built into the same density maps (142). This variation (22%) was adopted as uncertainty and was applied directly to the CF to reflect uncertainty in the cryo-EM data in subsequent calculations.

https://doi.org/10.7795/110.20260518

Table 34: Capsid numbers based on protein measurements

Protein	Peptide	Capsid number/mg		
		Capsids	u	u in %
Tri1	Pep02	7.9×10^7	2.8×10^7	22.1
Tri2	Pep03	8.8×10^7	2.5×10^7	22.2
MCP	Pep06	6.6×10^7	3.5×10^7	23.3
Capsid	combined	7.8×10^7	6.5×10^7	8.3

The number of capsids were estimated based on measurements of the specific proteins of three capsid components: Tri1, Tri2 and MCP. For Tri1, which is represented by the Pep02 peptide, the capsid concentration of 7.9×10^7 capsids per mg was determined, with a standard uncertainty of 2.8×10^6, corresponding to a relative standard uncertainty of 22.1%. For Tri2 (peptide Pep03), the capsid concentration was estimated at 8.8×10^7 capsids per mg, with a standard uncertainty of 2.5×10^6 and a relative standard uncertainty of 22.2%. In case of MCP (peptide Pep06), the capsid concentration reached 6.6×10^7 capsids per mg, accompanied by a higher standard uncertainty of 3.5×10^7 and a relative standard uncertainty of 23.3%. When the three measurements were combined, the average capsid concentration was calculated to be 7.9×10^7 capsids per mg. The combined standard uncertainty was 1.1×10^6 (relative standard uncertainty 14%).

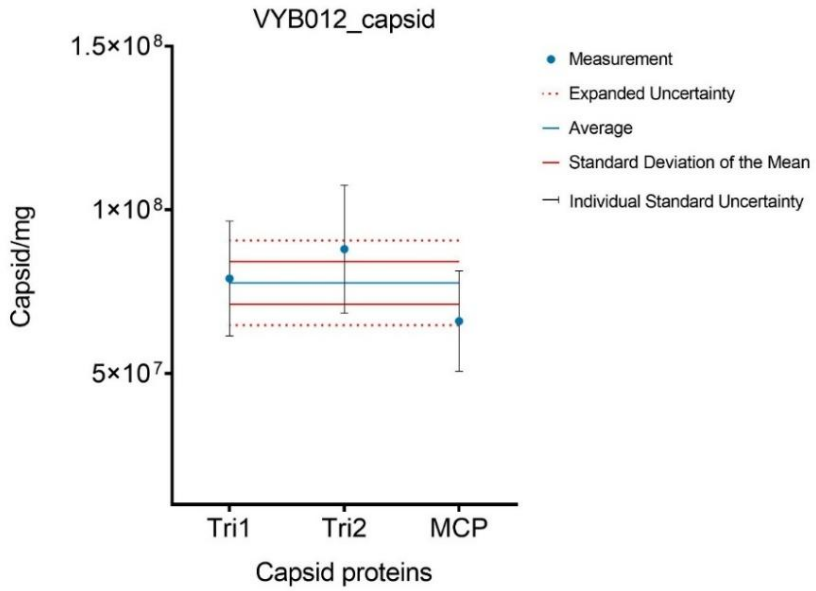

Figure 32: Quantification of capsid proteins in the VYB12 virus sample.
The amounts of the Tri1, Tri2 and MCP capsid proteins were determined from four replicate measurements. The blue line indicates the mean, while the blue data points represent the measured values. The red solid and dotted lines show the combined standard and expanded uncertainties, respectively, and the black bars represent the total expanded uncertainty.

https://doi.org/10.7795/110.20260518

The number of virions per milligram of sample was estimated using two independent quantification approaches: IDMS-based capsid protein measurements and ddPCR-based genome copy quantification. In the IDMS-based approach, the number of capsids was inferred from the absolute abundance of three capsid proteins: Tri1, Tri2 and MCP. Assuming that each complete capsid corresponds to one virion, the resulting capsid counts were taken as equivalent to virion counts. To refine the estimate, ddPCR-derived genome numbers were also incorporated. These gene copy counts were assumed to equal the number of genome copies being equivalent to number of virions. For the final calculation, the virion numbers derived from the two approaches were averaged to provide an estimate.

As shown in Figure 33, the combined virion concentration was estimated to 6.0 $x10^7$ virions per milligram of sample. This value was obtained by combining results from IDMS and ddPCR.

The standard uncertainty associated with the ddPCR method was 9.0 x 10^6 virions/mg, while the IDMS-based estimate a standard uncertainty of 6.48$x10^7$ virions/mg. The combined standard uncertainty was 1.8×10^7 virions/mg. The expanded uncertainty within a 95% confidence interval was 3.55 x 10^7 virions/mg. However, the results showed that the number of particles determined by IDMS was higher than that obtained by ddPCR. Several factors could explain this difference. One possible reason is the partial loss of viral DNA during the extraction process, which leads to an underestimation of genome copy numbers in the ddPCR analysis. Additionally, despite the virus sample being gradient purified, it cannot be ruled out that the preparation contained a small proportion of viral particles with capsids lacking DNA in addition to complete virions. Furthermore, the IDMS method quantifies structural capsid proteins on the assumption that only these proteins are present in the capsid, but single capsid proteins may also be present within the tegument. These proteins do not correlate with the viral genome yet still contribute to the measured protein amount. This might result in apparently higher particle numbers compared to the ddPCR-derived values. Finally, uncertainties in the conversion factor used to relate the measured amount of capsid protein to the number of capsids could also contribute to the observed difference. This factor is based on cryo-EM studies of virion structure, small deviations from the assumed stoichiometry could therefore influence the calculated particle numbers.

https://doi.org/10.7795/110.20260518

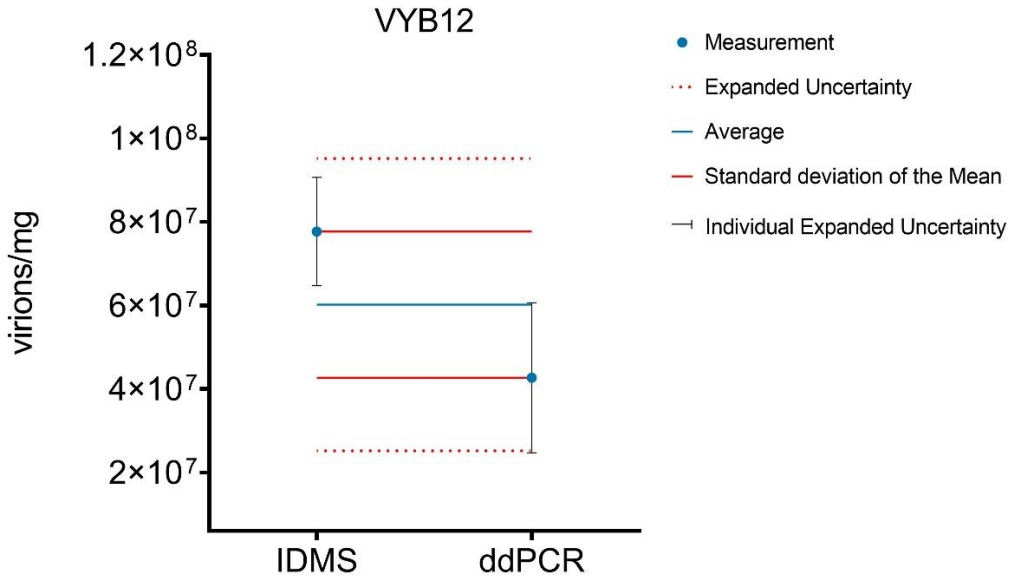

Figure 33: Estimation of the concentration of virions in the VYB12 sample by combining IDMS and ddPCR measurements. The ddPCR result is the mean of 12 independent measurements (three DNA extractions, each measured in four replicates), while the IDMS value is the average of 12 individual determinations derived from three signature peptides (MCP, Tri1 and Tri2; each measured in four replicates). The blue points show the measured values, the blue line shows the overall mean and the red solid and dotted lines show the combined standard and expanded uncertainties, respectively. Black bars denote the individual expanded uncertainties. While results of both approaches are close, the estimators for copy number via DNA and Proteins do not agree.

3.4.4 Uncertainty budget

The uncertainty budget was estimated using GUM workbench (version 2.4.1.392, Metrodata GmbH, Germany). To visualise the main contributors to measurement uncertainty in viral particle quantification, a fishbone diagram was constructed (Figure 34). This summarises the sources of uncertainty associated with each part of the analytical workflow, including the ddPCR and IDMS measurements and their subsequent combination. For ddPCR, the key contributors are pipetting variability, DNA extraction efficiency and replicate measurement precision. For IDMS, sources of uncertainty include peptide quantification, calibration and gravimetric preparation and the biological conversion factor derived from cryo-EM data. Combining both methods introduces an additional level of uncertainty relating to model integration and error propagation. Together, these elements provide a comprehensive overview of how different sources contribute to total uncertainty in viral particle estimation measurements.

https://doi.org/10.7795/110.20260518

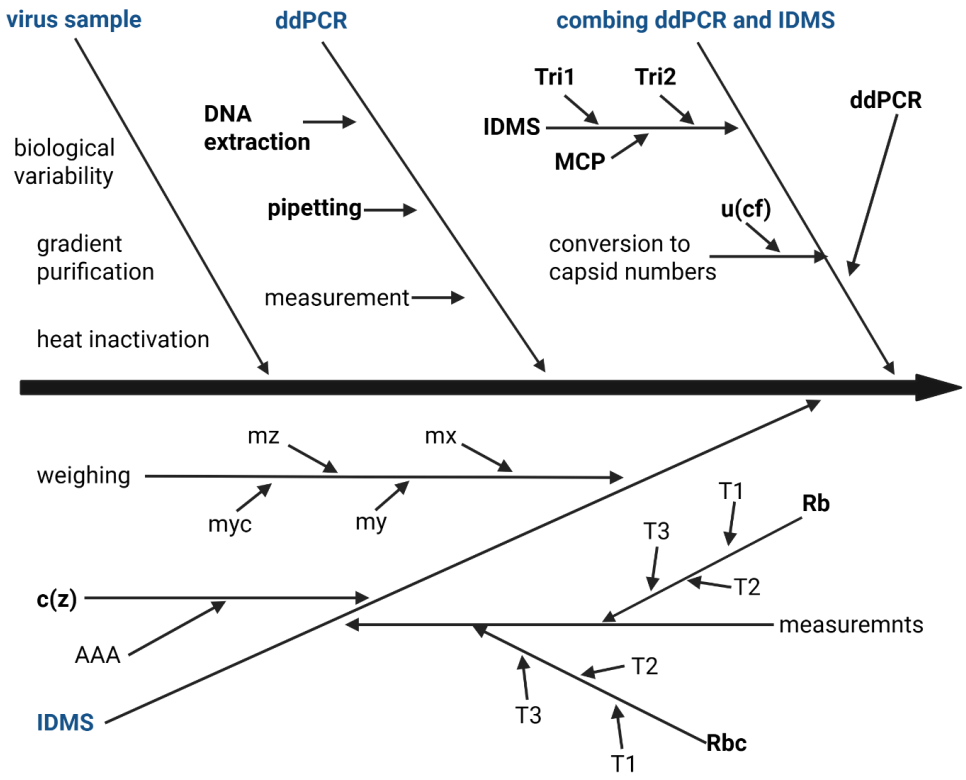

Figure 34: Overview of uncertainty contributors in viral particle quantification.
This fishbone diagram illustrates the main sources of uncertainty that contribute to the estimation of viral particle numbers when combining ddPCR and IDMS measurements. The diagram is organised according to the measurement workflow, starting with the virus sample and branching out into ddPCR, IDMS and their combination. For ddPCR, sources of uncertainty include pipetting variability, DNA extraction efficiency and measurement repeatability. For IDMS, contributions arise from peptide quantification, calibration model fitting, isotopic purity, and the gravimetric preparation of standards, as well as the biological factor (stoichiometry from cryo-EM data). The final step of combining the two measurement systems involves propagating uncertainty to account for independent and shared components, yielding the total uncertainty of viral particle quantification.

For gene copy quantification by ddPCR (Figure 35B), the main source of uncertainty is the measurement process itself (92.9%), whereas pipetting error contributes minimally (7.1%). A further breakdown of the measurement replicates (Figure 35C) shows that almost all of the uncertainty is associated with DNA extraction (99.4%), while technical replicates contribute only 0.6%. The estimation of viral capsid quantity via IDMS (Figure 35D) shows that stoichiometric uncertainty contributes 87.7% of the total uncertainty, while the measurement process accounts for 12.3%. The inset in Figure 35D shows the relative contributions of the different capsid proteins to the total uncertainty. MCP is the dominant source (46.5%), compared to Tri1 (29.8%) and Tri2 (23.7%). A detailed analysis of each capsid protein is shown in Figure 35E–G. For MCP (Figure 35E), the main sources of uncertainty are the measured ratio of the sample blend R_b at 90.1%, and the measured ratio of the calibration blend R_{bc} at 7.4%. Contributions from purity (P) and reference concentration κ_z are minimal at 3.7% and 1.2% respectively. In the case of Tri1 (Figure 35F), the sources of uncertainty are more evenly distributed: R_{bc} accounts for 52.7%, R_b for 36.1%, and there are minor contributions from P (5.8%) and κ_z (5.5%). A similar

https://doi.org/10.7795/110.20260518

pattern is observed for Tri2 (Figure 35G): R_{bc} and R_b contribute 59.9% and 30.3% respectively, while P and κ_z account for 5.9% and 3.8% respectively.

Taken together, these results indicate that the dominant sources of uncertainty in viral load quantification stem from the conversion from in protein to capsids quantification and sample preparation processes in ddPCR, particularly DNA extraction. Optimising DNA extraction and conducting further research into determination of capsid number could significantly reduce overall uncertainty in viral load measurements and improve confidence in viral load estimation.

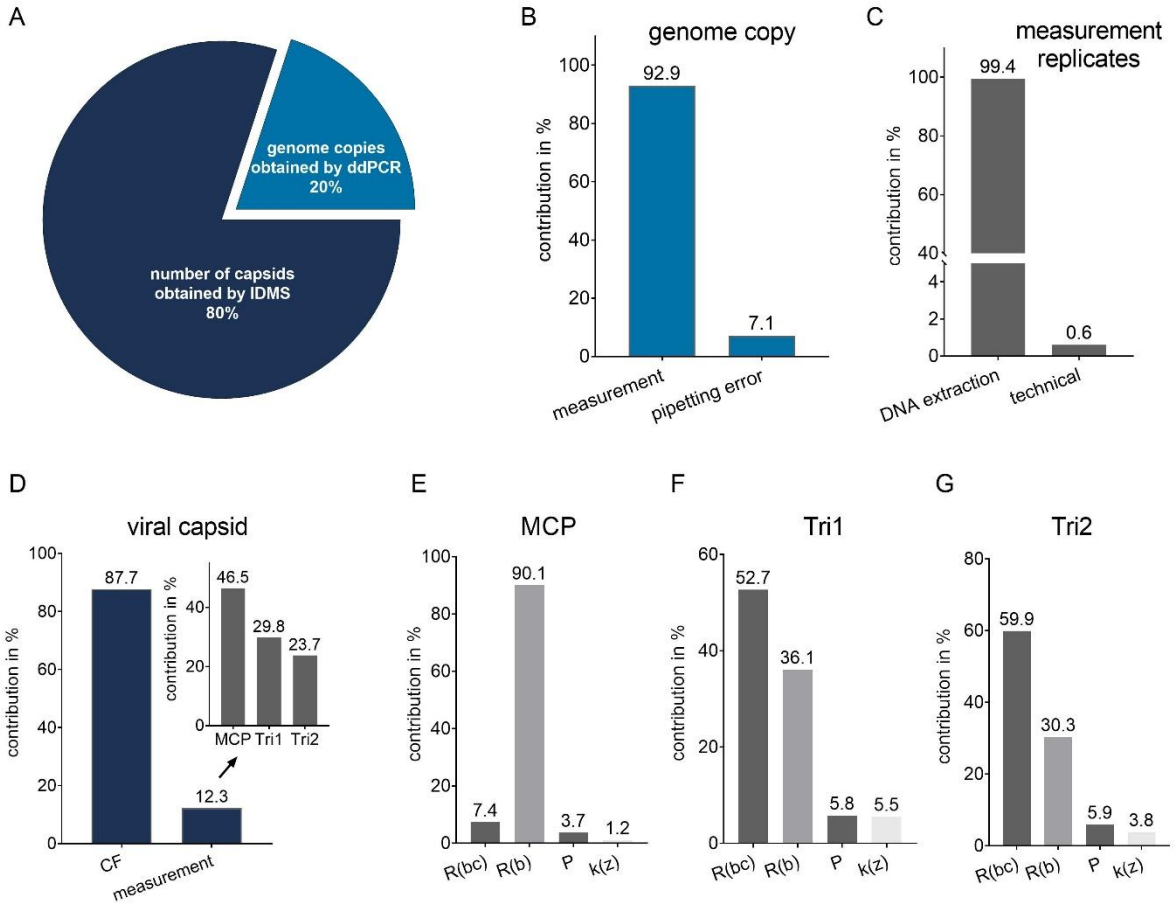

Figure 35: Uncertainty budget of viral load calculation based on IDMS and ddPCR measurements.
A Pie chart showing the overall contribution of each analytical method to total measurement uncertainty. B Breakdown of uncertainty sources in ddPCR-based gene copy quantification, with measurement contributing and pipetting error. C Uncertainty distribution among measurement replicates, dominated by DNA extraction versus technical replicates. D Uncertainty sources in viral capsid quantification by IDMS, with biological variation f_{bio} and measurement. Inset: relative contributions of individual capsid. E–G Uncertainty breakdown for individual capsid proteins MCP (E), Tri1 (F), and Tri2 (G). Contributions include measured ratio of calibration blend R_{bc}, measured ratio of sample blend R_b, peptide purity (P) and reference concentration κ_z

ddPCR enabled absolute determination of viral genome copy numbers by leveraging statistical partitioning of DNA molecules into thousands of droplets, followed by amplification and counting of

https://doi.org/10.7795/110.20260518

positive droplets. In this study, genome quantification was consistent across independent DNA extractions, with an average of 4.27 x 10^7 copies/µL and acceptable uncertainty, despite some variability in extraction efficiency.

Parallel to genome quantification, capsid protein measurement via IDMS provided an independent and complementary means to estimate virion concentration. Using well-characterized synthetic peptides and isotopically labelled internal standards, the absolute content of three major capsid proteins Tri1, Tri2, and MCP were quantified. These measurements were then translated into capsid numbers based on established stoichiometries of HCMV structural proteins. While the IDMS method showed good internal consistency, particularly for Tri1 and Tri2, MCP measurements exhibited higher uncertainty, likely due to signal variability or ion suppression. When compared to ddPCR-derived genome counts, the protein-based estimates aligned well, with overlapping uncertainty intervals. This convergence of results from two independent, primary methods supports the validity of the integrated approach. The final combined virion concentration was determined to be 6.0 x 10^7 particles per milligram, with well-characterized measurement uncertainty. Importantly, this methodology offers several advantages over conventional viral load assessments. Standard qPCR techniques, that needs external calibration, while widely used, depend on external standards and are subject to variable amplification efficiencies, therefore, results are not comparable between when measurements are performed in different labs. Infectivity-based assays such as plaque assays, on the other hand, provide information only on replication-competent particles and are influenced by cell type, assay conditions, and subjective interpretation. In contrast, the strategy used in this chapter delivers absolute, reproducible, and biologically relevant quantification that captures both genome-containing and structurally complete (but potentially non-infectious) virions. However, no statement can be made regarding infectivity. Further research into the link between viral particles and infectivity would be beneficial. From a metrological perspective, this work demonstrates the feasibility and value of integrating multiple primary measurement procedures for biological quantification. The ddPCR and IDMS methods each bring unique strengths, genome-level precision and structural specificity, respectively, and their combined use enhances confidence in the resulting data. Moreover, this approach facilitates traceable, comparable, and standardized virus quantification, which is essential for developing certified reference materials and harmonizing measurements across laboratories.

https://doi.org/10.7795/110.20260518

4 Final discussion and conclusion

Two independent primary measurement methods were applied to indirectly estimate the viral load. Each method quantifies a specific component of the virus directly, nucleic acids by ddPCR and proteins by IDMS. However, neither method directly measures the number of complete or infectious viral particles. Instead, these approaches provide complementary and accurate quantifications of viral genome and protein content, which can be used to infer particle numbers and assess consistency between the two measurement principles.

Quantifying viral load is one of the central challenges in modern virology. Although viral load is typically defined as the number of virions in a given sample, there is currently no method to directly measure virions. Instead, clinical and research practice relies on surrogate measurements, most often nucleic acid quantification using PCR-based techniques (135-137) or protein detection via immunological assays (132). While these approaches provide valuable information, they are not directly comparable across laboratories, lack SI traceability and do not capture the intended biological measurand: the number of virions. This thesis presents a method for viral load estimation using Human Cytomegalovirus (HCMV) as a model system, which addresses this gap. Two independent primary reference measurement procedures — droplet digital PCR (ddPCR) for genome quantification and isotope dilution mass spectrometry (IDMS) for capsid protein quantification, were combined and their results were integrated through the known stoichiometry of viral genome copies and structural proteins. By doing so, this thesis demonstrates the feasibility of producing SI-traceable viral load estimates and establishes a model for future developments in viral metrology.

From a metrological perspective, this work is significant because it systematically applies the principles of traceability, uncertainty evaluation and comparability. Both ddPCR and IDMS are primary measurement methods: ddPCR provides absolute quantification of nucleic acid molecules independent of external calibrators, and IDMS links protein quantification to the International System of Units (SI) via the gravimetric preparation of an SI-traceable calibrator for calibration blends and the use of isotopically labelled internal standards. By employing both methods in parallel and integrating them, the thesis provides a robust estimation of viral particle number that does not rely on external biological reference materials. This approach contrasts with poorly comparable conventional qPCR methods (173), which depend on Ct values, amplification efficiencies and relative comparisons to standards. The metrological advantage is clear: by establishing an unbroken traceability chain from SI units to viral particle concentration, this thesis establishes a foundation upon which results can be both accurate and comparable across laboratories and over time.

https://doi.org/10.7795/110.20260518

The experimental work involved the controlled production and purification of HCMV. The preparation of the virus was critical as it enabled the separation of distinct types of viral particle: virions, dense bodies and non-infectious enveloped particles. These were separated using density gradient ultracentrifugation and inactivated to enable them to be handled safely outside S2 facilities. Such preparations were essential for developing proteomics and nucleic acid quantification workflows. The availability of well-purified virus samples formed the basis of robust experimental quantification strategies.

Proteomic analysis played a pivotal role in identifying the most suitable viral proteins for quantification. While HCMV encodes over 200 proteins (116), only a subset is present in every particle at fixed stoichiometry. Capsid proteins, the major capsid protein (MCP) and the triplex subunits Tri1 and Tri2, were chosen as targets for quantification because of their invariant structural stoichiometry, a feature confirmed by cryo-electron microscopy studies (119). Using LC-MS/MS, signature peptides from these proteins were identified and carefully selected based on detectability, uniqueness, and stability. Synthetic versions of these peptides were purchased and value-assigned using amino acid analysis with exact matching IDMS, ensuring traceability to the SI. This step was critical, as the quality of the peptide standards directly affects the reliability of protein quantification, and therefore the integrity of the entire traceability chain.

The method development focused on optimising LC-MS/MS in multiple reaction monitoring (MRM) mode to enable sensitive and reproducible quantification of the selected peptides. The establishment of highly selective and sensitive assays was enabled by careful optimisation of precursor/product ion transitions, collision energies, and chromatographic conditions. The limits of detection were found to be below 2 fmol on column for most peptides, with limits of quantification below 8 fmol. Time-course experiments verified that complete tryptic digestion was achieved after 12 hours, ensuring peptide abundances reflected true protein amount of substance content. Together, these developments formed the basis of the methodology for SI-traceable, peptide-based quantification of viral capsid proteins.

ddPCR was employed to measure viral genome copy numbers. By partitioning DNA molecules into thousands of droplets and applying Poisson statistics, ddPCR enables absolute quantification independently of calibration curves. In the HCMV VYB12 preparation, ddPCR yielded consistent genome copy numbers across multiple extractions. Although variability was observed between extractions, this was reflected in the uncertainty budget and was primarily attributed to DNA extraction efficiency rather than random technical error. The dominance of extraction-related uncertainty highlights a key area for improvement in future work.

Protein-based quantification of capsid content was performed to provide an alternative estimate of viral particle concentration. The absolute contents of Tri1, Tri2 and MCP were determined by applying

https://doi.org/10.7795/110.20260518

IDMS with isotopically labelled peptides, and these values were translated into capsid numbers using established stoichiometries. Cryo-EM studies, have provided highly detailed structural data on capsid architecture (119). These analyses established the widely accepted stoichiometry of 960 copies of MCP, 600 copies of Tri2 and 300 copies of Tri1 in mature HCMV capsids. More recent proteome-wide analyses of HCMV virions, such as those reported by Bogdanow et al. (2023), have used this cryo-EM stoichiometry as a structural reference. In that study, the known copy numbers of capsid proteins per virion were used as fixed anchors to calculate the number of additional viral proteins per particle. Thus, cryo-EM data were employed not only as a structural benchmark, but also as a quantitative scaffold for extending proteomic analyses. However, it is important to note that the stoichiometry obtained by cryo-EM has never been independently confirmed by proteomic datasets, which have consistently reported different relative protein abundances. Proteomic analyses frequently produce protein abundance ratios that deviate from this idealised stoichiometry. For example, lower relative amounts of Tri1 or Tri2 compared to MCP have been reported (116, 174). Such discrepancies may be accounted for by several factors: systematic biases introduced during sample preparation, such as incomplete digestion or variable ionisation efficiencies of peptides, different quantification strategies, the presence of heterogeneous particle populations, including dense bodies and non-infectious enveloped particles, or averaging effects across large particle populations, which obscure the exact stoichiometry of intact virions. In contrast to these findings, the stoichiometric ratios obtained in this thesis through peptide-based IDMS were consistent with the cryo-EM stoichiometry reported by Yu et al. 2017. This suggests that careful selection of structurally invariant capsid proteins, use of isotopically labelled internal standards and reliance on SI-traceable calibrators reduced biases typically affecting proteomics workflows. At the same time, the concordance of the present results with cryo-EM stoichiometry reinforces the conclusion that cryo-EM provides the most reliable structural 'ground truth', whereas proteomics reflects the biochemical and biological variability inherent in bulk virus preparations. By reconciling these two perspectives through a metrological approach, a more realistic and SI-traceable estimate of viral particle numbers has been achieved. Further research is needed to determine the true biological facts about the number of proteins present in each virion. Fully labelled virus particles produced by propagation in isotopically enriched cell culture media, for example, would serve as the ultimate internal standards. These materials could account for the entire analytical workflow, from extraction and digestion to amplification, and could drastically reduce measurement uncertainty by providing an 'exact matching' standard at the whole-virion level. This represents a logical next step in the evolution of viral metrology.

When compared, the estimates of viral particle numbers obtained using ddPCR and IDMS showed agreement within their respective uncertainty estimations. This convergence validates the dual-

https://doi.org/10.7795/110.20260518

method approach and demonstrates the feasibility of establishing viral load as an SI-traceable quantity. Combining the two methods provided an integrated estimate of 6.0×10^7 virions per milligram of sample. Notably, the uncertainty budget revealed the primary sources of measurement variability: stoichiometric uncertainty for capsid counts based on IDMS measurements and DNA extraction for genome copy measurements though ddPCR. This clarity not only underscores the transparency of the measurement process but also indicates potential areas for future improvement.

Despite the advantage of combing DNA and protein measurements to be more confident in the viral load estimate, several limitations remain. Firstly, virions are not yet being measured directly; currently, only viral components such as genome copies and capsid proteins are being quantified, which makes the true number of virions unclear. Secondly, infectivity, arguably the most biologically relevant property, is not captured by genome- or protein-based quantification. Thirdly, using literature-derived correction factors for protein stoichiometry introduces additional uncertainty, given that different studies have reported divergent ratios for the same proteins. This highlights the need for more detailed structural proteomic analyses of well-characterised virus preparations, so that these factors can be refined. Fourthly, variability in ddPCR caused by DNA extraction efficiency continues to present a practical challenge. Finally, peptides such as those derived from MCP were found to be less reproducible, reflecting the inherent difficulty of peptide-based quantification for certain proteins.

Looking to the future, several promising avenues are emerging. One key area is integrating infectivity testing into the metrological framework. Although plaque and $TCID_{50}$ assays are traditional methods of assessing infectivity, neither are standardised or SI-traceable. Developing primary methods or reference systems that can be linked to SI units would bridge the current gap between viral load and biological activity. Another promising area is applying metrological concepts to monitoring viral treatment progression. Absolute, traceable measurements of viral load could provide more reliable indicators of therapeutic response. Additionally, establishing SI-traceable virus quantification standards is expected to play a pivotal role in preventing and preparing for future pandemics by enabling consistent surveillance, diagnostics and international comparability during global health crises.

Beyond these methodological refinements, the approach developed in this thesis has broad clinical and scientific implications. SI-traceable viral load measurements would allow for comparability across laboratories and over time, thus facilitating multicentre clinical trials and standardised patient monitoring. The reliability of diagnostic thresholds, which are currently assay- and laboratory-specific, would also improve. Furthermore, the development of plasmid-based laboratory standards for qPCR, offers a cost-effective and accessible way to implement absolute quantification in laboratories worldwide, including those without access to ddPCR or advanced proteomics.

https://doi.org/10.7795/110.20260518

In summary, this thesis shows that combining two independent primary reference methods can elevate viral load quantification from relative, poorly comparable measurements to robust, SI-traceable estimations. Applying ddPCR for DNA quantification and IDMS for capsid protein quantification, and integrating these results through biological stoichiometry, produced a transparent and reproducible estimate of viral particle concentration. Although infectivity and biological variability remain challenges, the methodological foundation established here paves the way for future developments, including the use of isotopically labelled viruses and the integration of infectivity testing. This work advances the metrological basis of virology and sets the foundation for standardised viral load measurement to become a key component of clinical diagnostics, epidemiology and public health.

Future work should focus on reducing the discrepancy between ddPCR- and IDMS-derived particle numbers in order to improve the accuracy of viral load estimation. Further optimisation of DNA extraction and the inclusion of process controls could help quantify and reduce DNA losses in ddPCR. In the IDMS workflow, using multiple peptides and full-length labelled protein standards would provide a more accurate representation of digestion efficiency and improve traceability.

Although gradient purification was employed, further steps to separate complete virions from empty or incomplete particles could refine both measurement approaches. Furthermore, independently verifying the protein-to-capsid conversion factor through cryo-EM analysis would reduce structural uncertainties.

Integrating ddPCR and IDMS data within a common uncertainty model that accounts for extraction, digestion and stoichiometric variability may ultimately provide a more robust, metrologically consistent estimate of viral particle numbers. These efforts would strengthen the quantitative link between genome- and protein-based measurements, contributing to more reliable viral load determination standards.

https://doi.org/10.7795/110.20260518

5 Appendix

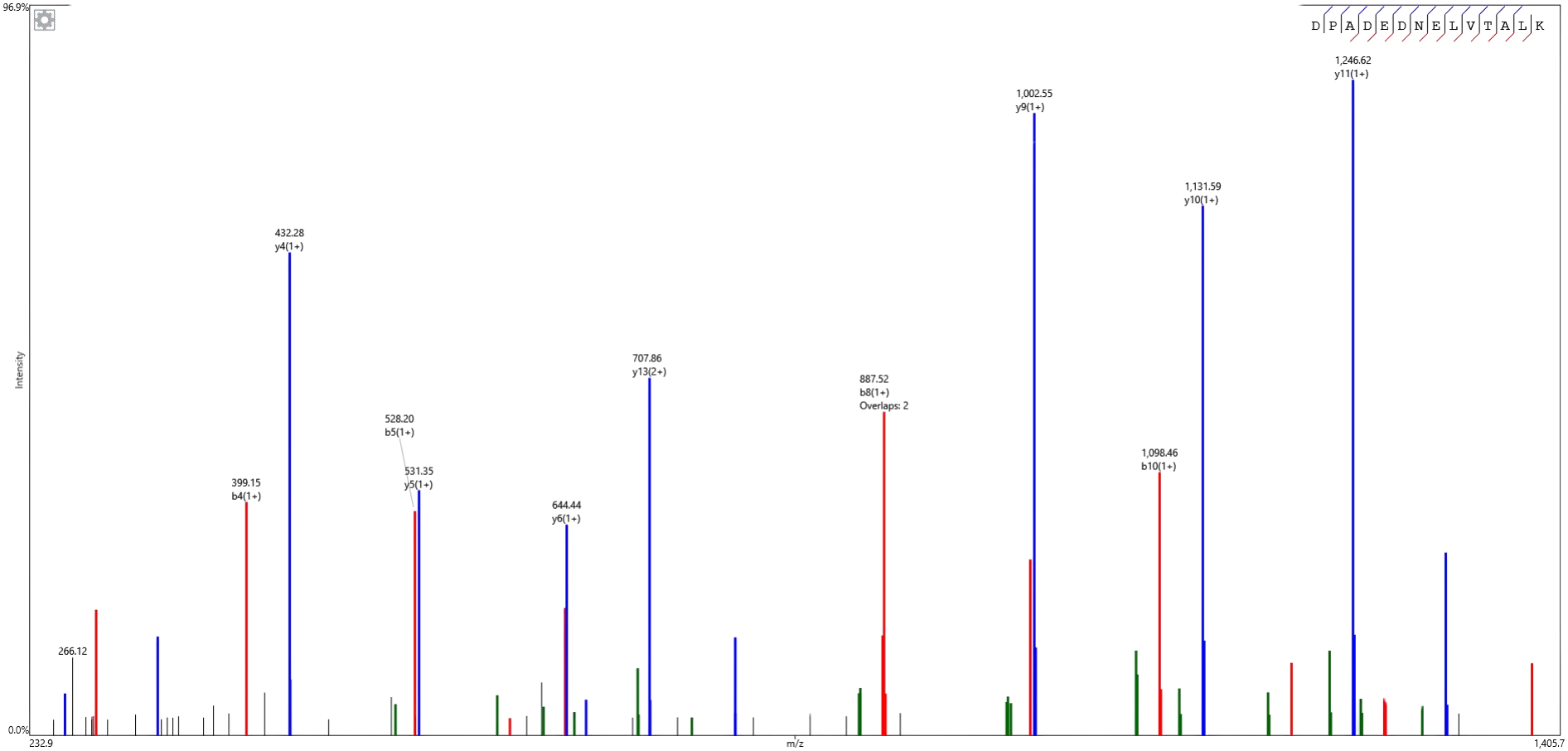

Figure A1: Fragmentation spectrum of the Pep01.
For the proteomics analysis, 10 µL of the digested virus sample was injected into the LC-MS/MS system. The figure shows the product ion spectrum of a selected peptide Pep01 derived from the Tri1 capsid protein. Annotated b- and y-type fragment ions confirm the peptide's sequence identity. Together, the y-ion series (blue) and b-ion series (red) provide high sequence coverage. The observed fragmentation pattern verifies the correct sequence assignment and demonstrates efficient peptide fragmentation during proteomic analysis.

https://doi.org/10.7795/110.20260518

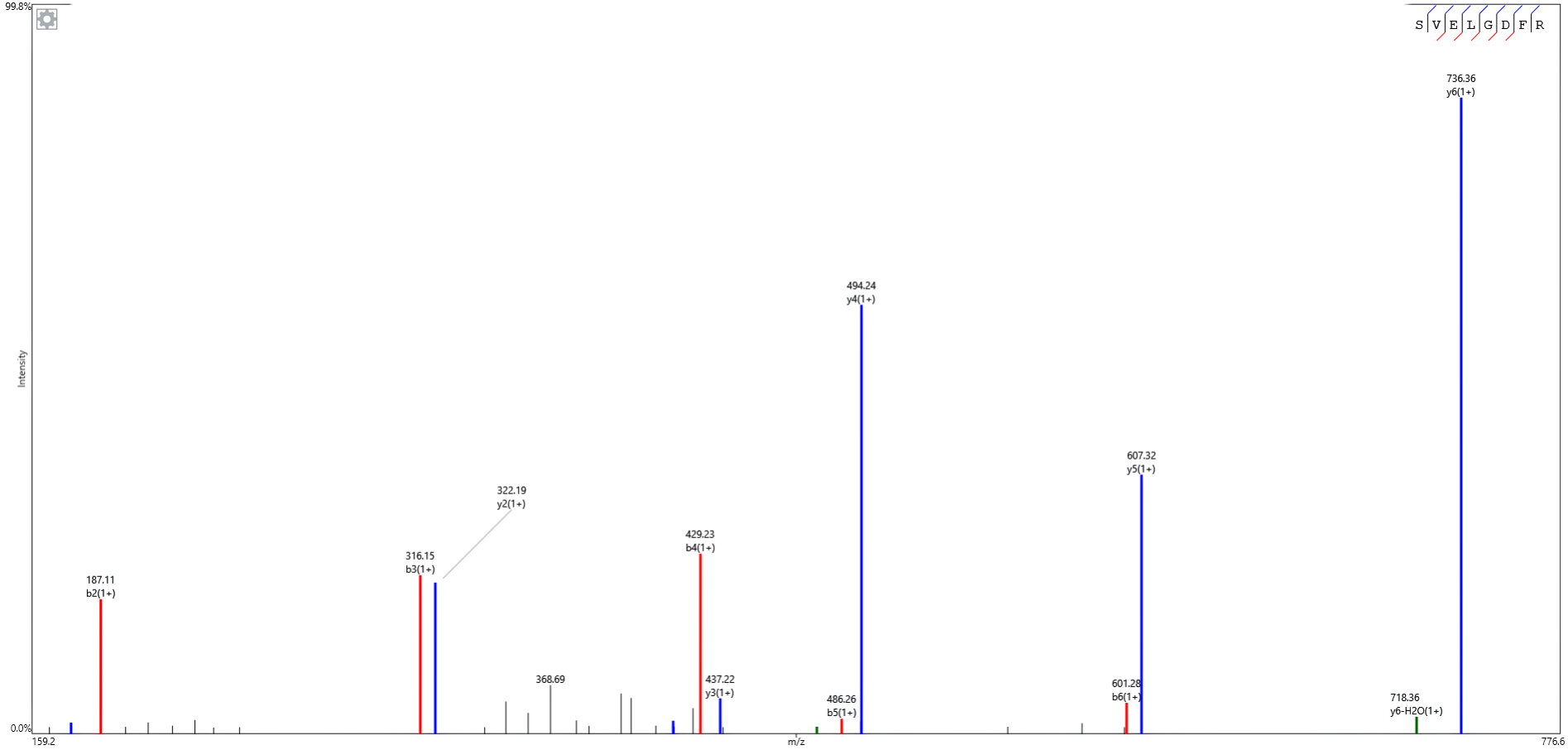

Figure A2: Fragmentation spectrum of the Pep02.
For the proteomics analysis, 10 µL of the digested virus sample was injected into the LC-MS/MS system. The figure shows the product ion spectrum of a selected peptide Pep02 derived from the Tri1 capsid protein. Annotated b- and y-type fragment ions confirm the peptide's sequence identity. Together, the y-ion series (blue) and b-ion series (red) provide high sequence coverage. The observed fragmentation pattern verifies the correct sequence assignment and demonstrates efficient peptide fragmentation during proteomic analysis.

https://doi.org/10.7795/110.20260518

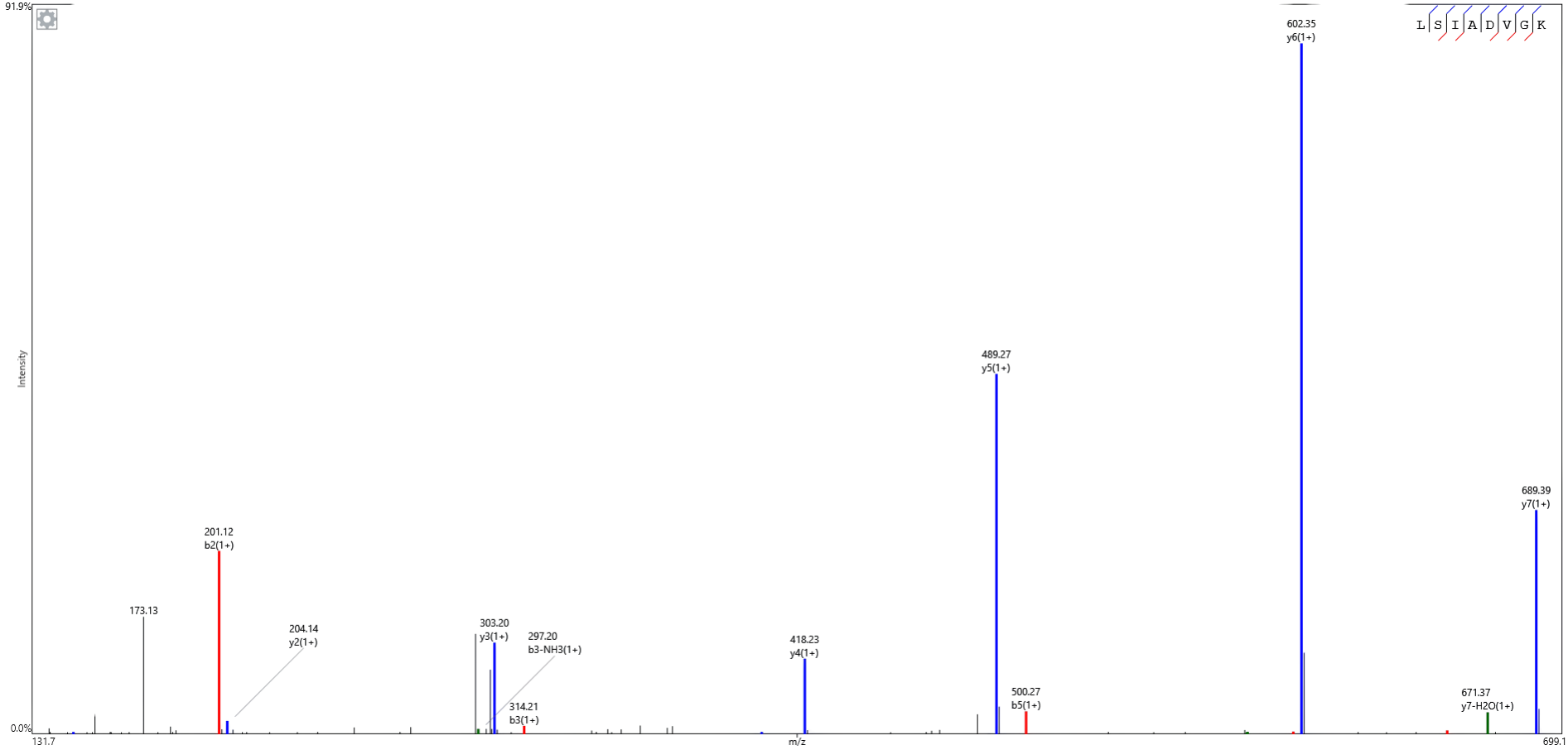

Figure A3: Fragmentation spectrum of the Pep03.
For the proteomics analysis, 10 µL of the digested virus sample was injected into the LC-MS/MS system. The figure shows the product ion spectrum of a selected peptide Pep03 derived from the Tri2 capsid protein. Annotated b- and y-type fragment ions confirm the peptide's sequence identity. Together, the y-ion series (blue) and b-ion series (red) provide high sequence coverage. The observed fragmentation pattern verifies the correct sequence assignment and demonstrates efficient peptide fragmentation during proteomic analysis.

https://doi.org/10.7795/110.20260518

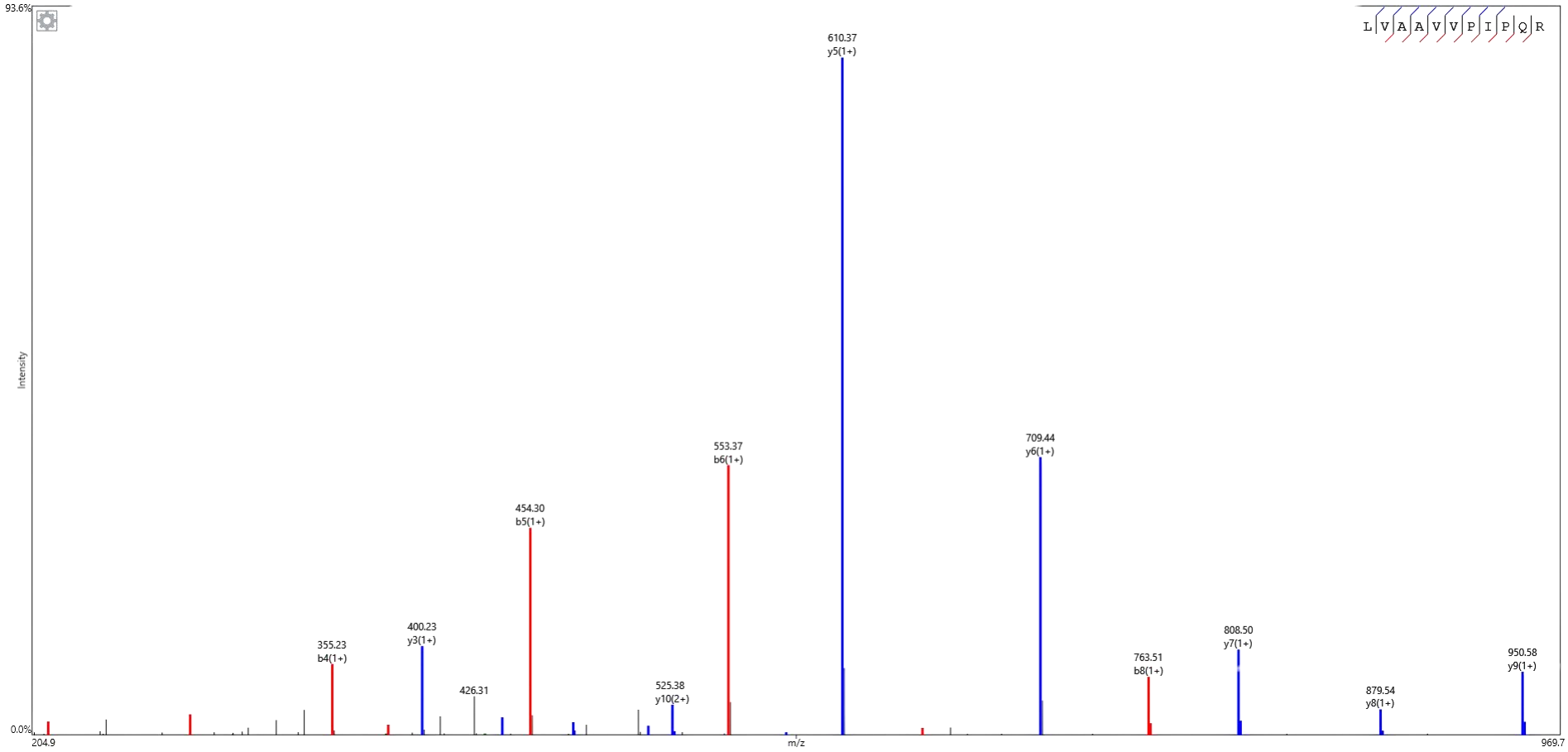

Figure A4 Fragmentation spectrum of the Pep04.
For the proteomics analysis, 10 µL of the digested virus sample was injected into the LC-MS/MS system. The figure shows the product ion spectrum of a selected peptide Pep04 derived from the Tri2 capsid protein. Annotated b- and y-type fragment ions confirm the peptide's sequence identity. Together, the y-ion series (blue) and b-ion series (red) provide high sequence coverage. The observed fragmentation pattern verifies the correct sequence assignment and demonstrates efficient peptide fragmentation during proteomic analysis.

https://doi.org/10.7795/110.20260518

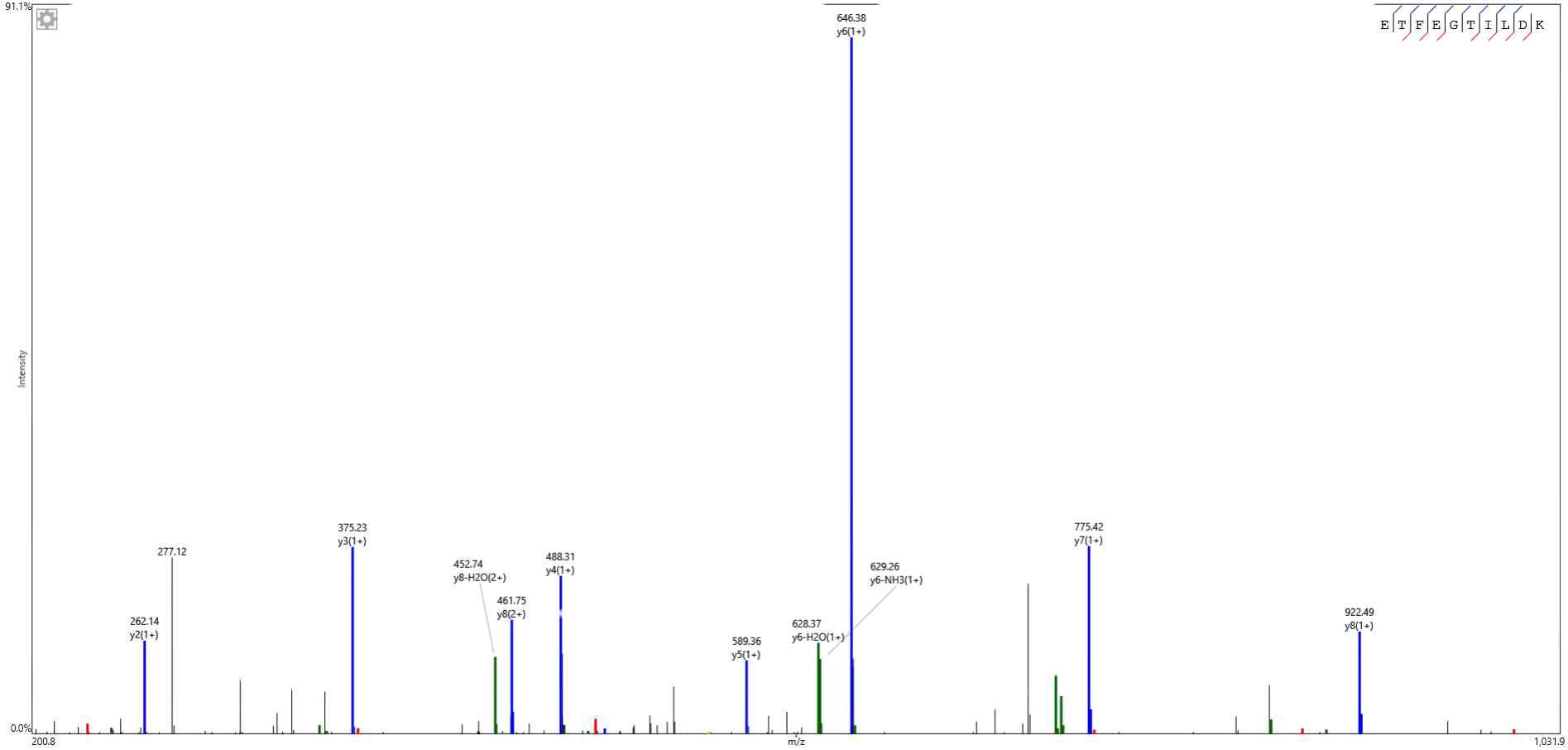

Figure A5: Fragmentation spectrum of the Pep05.
For the proteomics analysis, 10 µL of the digested virus sample was injected into the LC-MS/MS system. The figure shows the product ion spectrum of a selected peptide Pep05 derived from the MCP capsid protein. Annotated b- and y-type fragment ions confirm the peptide's sequence identity. Together, the y-ion series (blue) and b-ion series (red) provide high sequence coverage. The observed fragmentation pattern verifies the correct sequence assignment and demonstrates efficient peptide fragmentation during proteomic analysis.

https://doi.org/10.7795/110.20260518

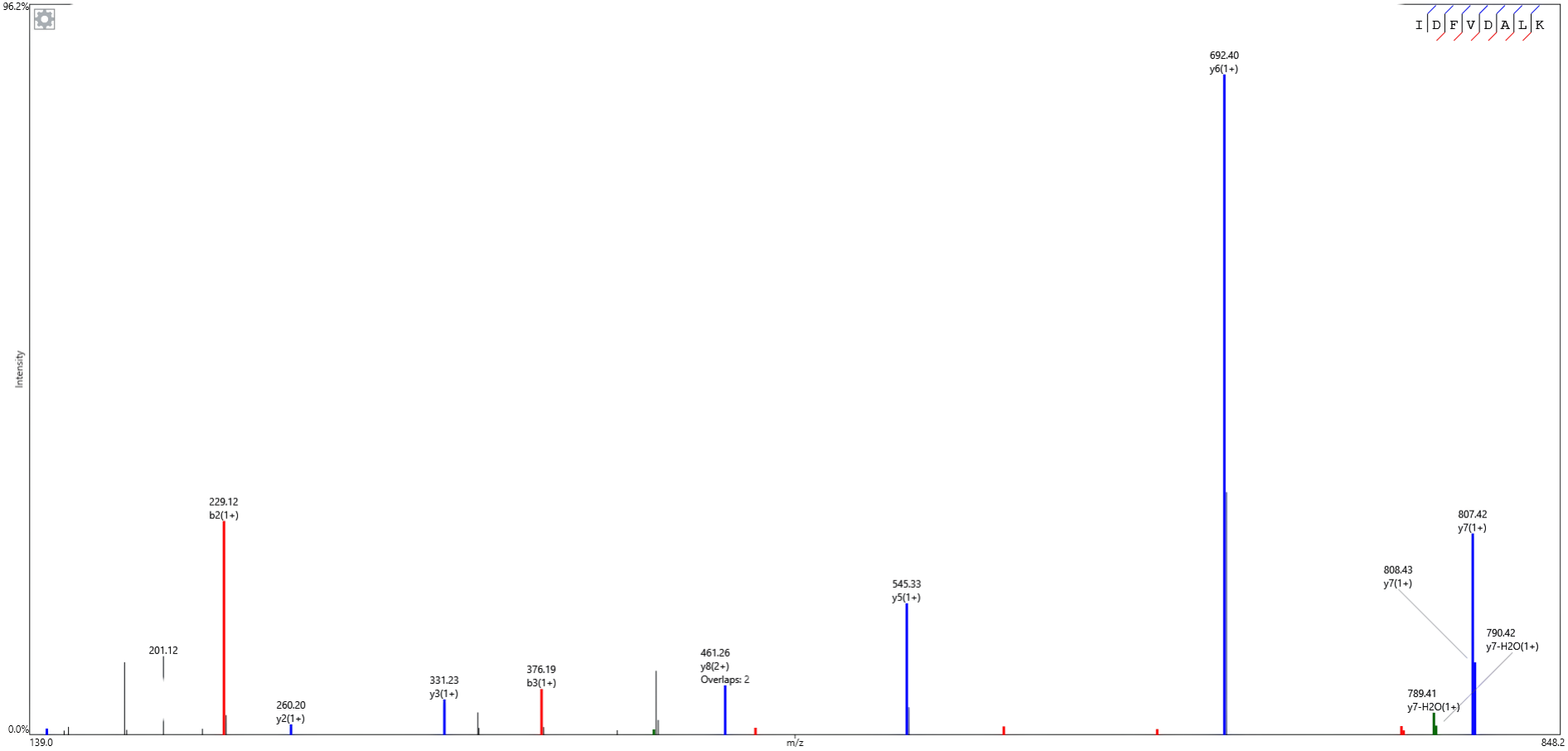

Figure A6: Fragmentation spectrum of the Pep06.
For the proteomics analysis, 10 µL of the digested virus sample was injected into the LC-MS/MS system. The figure shows the product ion spectrum of a selected peptide Pep06 derived from the MCP capsid protein. Annotated b- and y-type fragment ions confirm the peptide's sequence identity. Together, the y-ion series (blue) and b-ion series (red) provide high sequence coverage. The observed fragmentation pattern verifies the correct sequence assignment and demonstrates efficient peptide fragmentation during proteomic analysis.

https://doi.org/10.7795/110.20260518

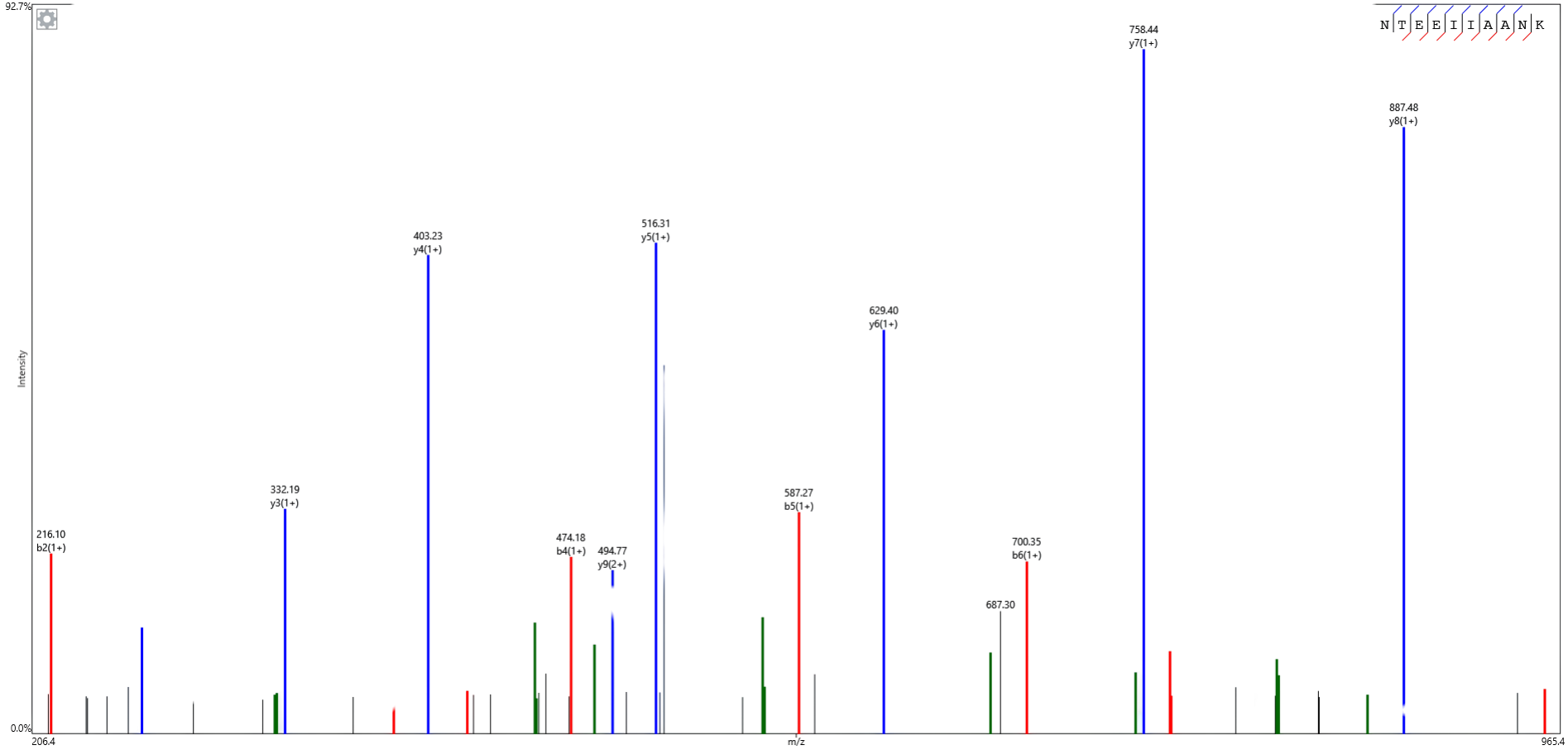

Figure A7: Fragmentation spectrum of the Pep07.
For the proteomics analysis, 10 µL of the digested virus sample was injected into the LC-MS/MS system. The figure shows the product ion spectrum of a selected peptide Pep07 derived from the MCP capsid protein. Annotated b- and y-type fragment ions confirm the peptide's sequence identity. Together, the y-ion series (blue) and b-ion series (red) provide high sequence coverage. The observed fragmentation pattern verifies the correct sequence assignment and demonstrates efficient peptide fragmentation during proteomic analysis.

https://doi.org/10.7795/110.20260518

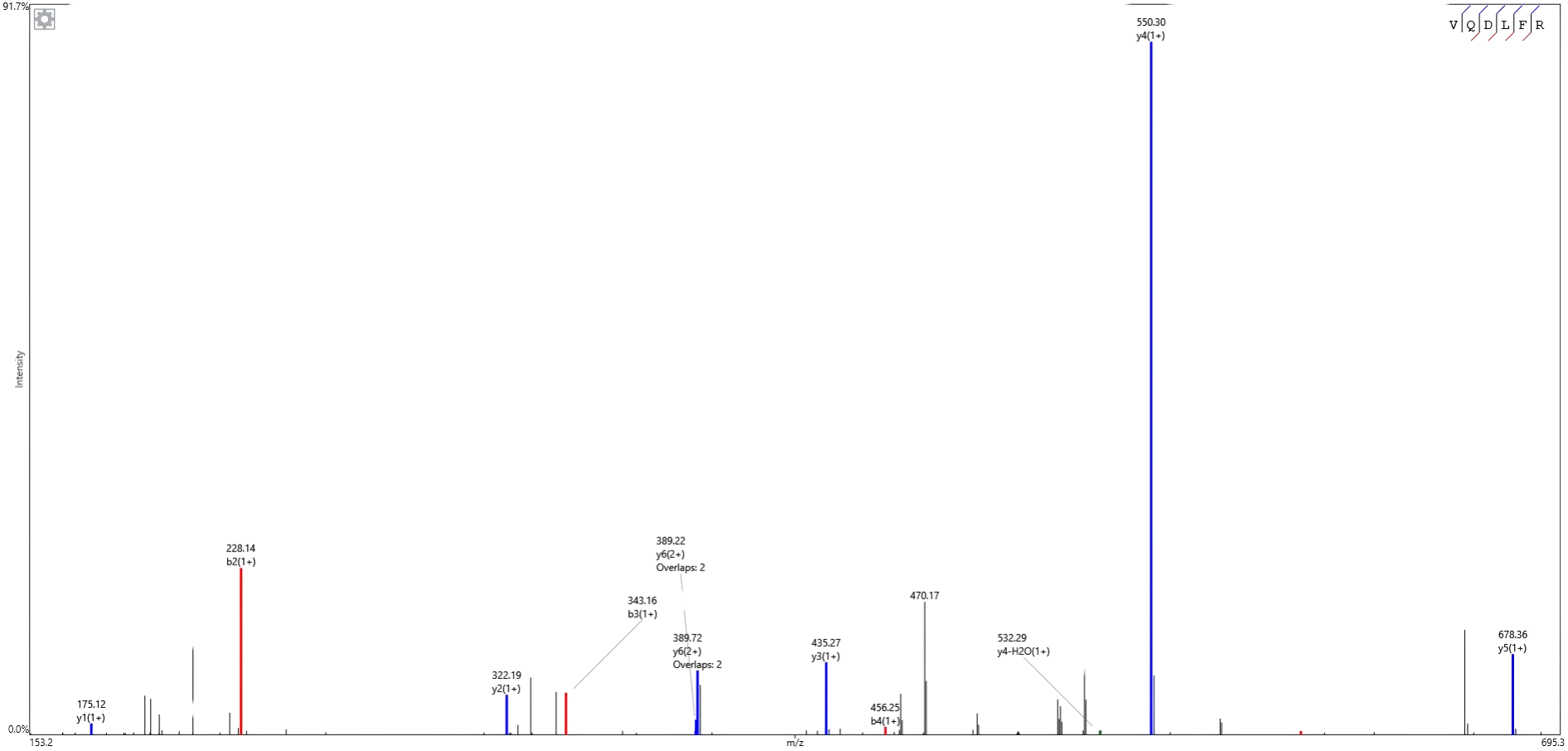

Figure A8: Fragmentation spectrum of the Pep08.
For the proteomics analysis, 10 µL of the digested virus sample was injected into the LC-MS/MS system. The figure shows the product ion spectrum of a selected peptide Pep08 derived from the MCP capsid protein. Annotated b- and y-type fragment ions confirm the peptide's sequence identity. Together, the y-ion series (blue) and b-ion series (red) provide high sequence coverage. The observed fragmentation pattern verifies the correct sequence assignment and demonstrates efficient peptide fragmentation during proteomic analysis.

https://doi.org/10.7795/110.20260518

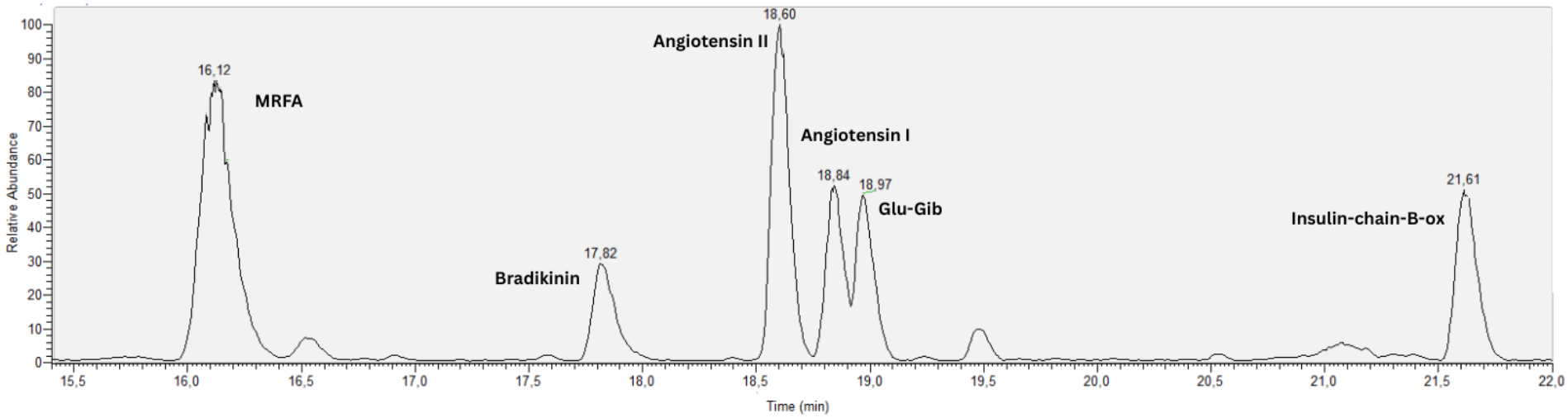

Figure A9: Example of a total ion chromatogram (TIC) of the PepMix measured on the LTQ Orbitrap Elite.
An aliquot of 5 µL of the PepMix (see Table A1 for the concentration) was analysed using LC-MS method. The y-axis shows the relative abundance and the x-axis shows the retention time in minutes

https://doi.org/10.7795/110.20260518

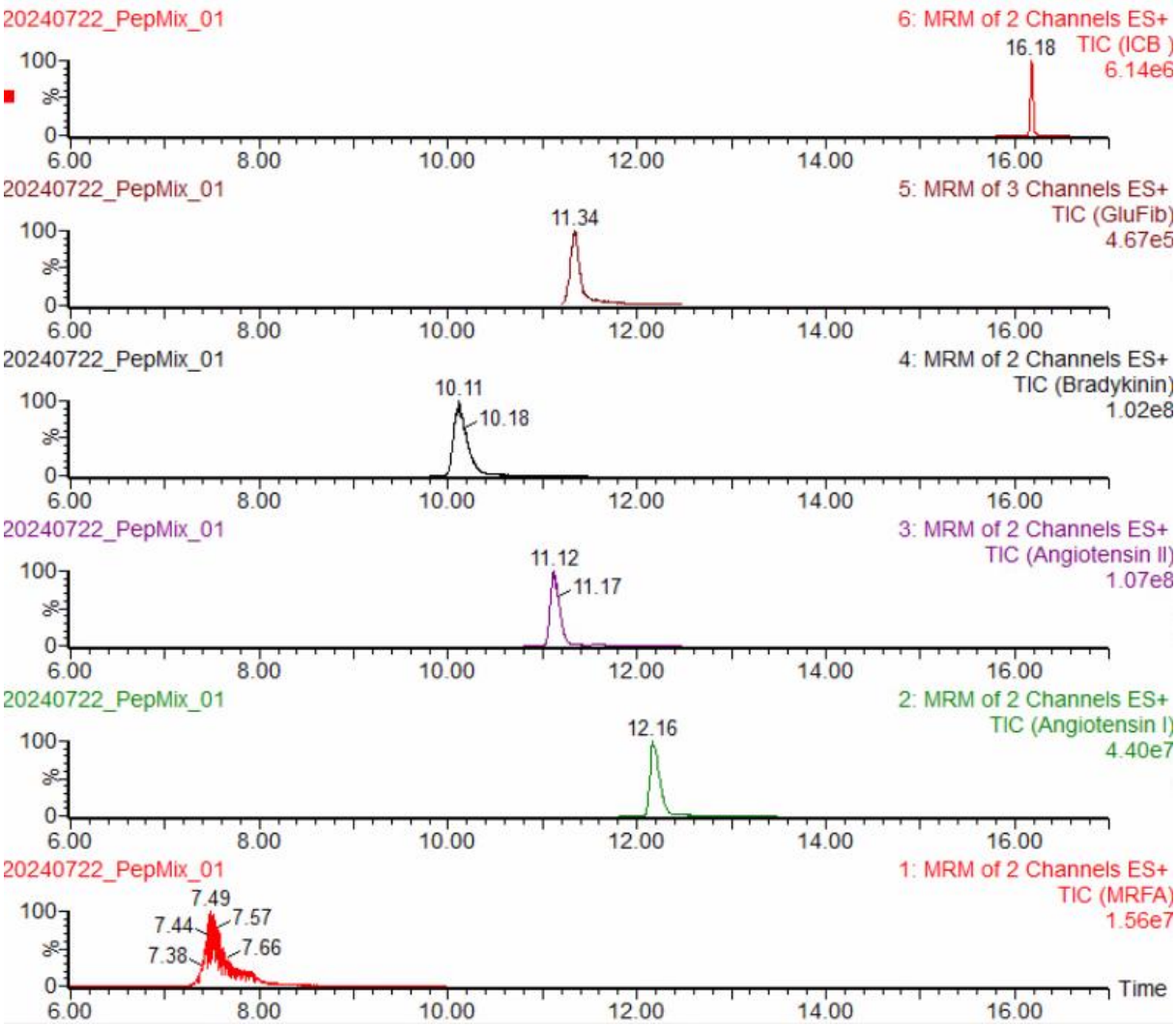

Figure A10: Example of a total ion chromatogram (TIC) of the PepMix measured on Waters Xevo TQ-XS instrument. An aliquot of 2 µL of the PepMix (see Table A1 for the concentration) was analysed using LC-MS/MS method. The y-axis shows the relative abundance and the x-axis shows the retention time in minutes

https://doi.org/10.7795/110.20260518

Table A1: Composition and concentration of the peptide mixture (PepMix) used for LC-MS/MS instrument control.

	Amino acid sequence	**Concentration of ready-to-use solution**	
		Orbitrap	Waters Xevo TQ-XS
Insulin-Cain-B-Ox	FVNQHLCGSHLVEALYLVCGERGFFYTPKA	0.4 pmol/µL	100 fmol/µL
Glu-Fibrinopeptide B	EGVNDNEEGFFSAR	4.8 pmol/µL	200 fmol/µL
Bradykinin	RPPGFSPFR	2.9 pmol/µL	10 fmol/µL
Angiotensin I	DRVYIHPFHL	1.0 pmol/µL	10 fmol/µL
Angiotensin II	DRVYIHPF	1.2 pmol/µL	1 fmol/µL
MRFA	MRFA	4.7 pmol/µL	1 fmol/µL

https://doi.org/10.7795/110.20260518

A1: Quantification of HCMV UL54 Gene Copies by qPCR – Method Protocol

Objective

Quantification of HCMV genome copies is achieved by measuring UL54 gene numbers using GoTag® qPCR Master Mix (Promega) and a calibration curve of HCMV lab standard pYB01.

Materials

- Light Cycler (Roche)
- optical-grade qPCR plate (e.g. LightCycler® 480 Multiwell plate 96, white from Roche)
- sterile, aerosol-resistant pipette tips
- autoclaved eppendorf tubes (1.5 mL)
- GoTag® qPCR Master Mix (Promega)
- Nuclease-free water
- HCMV lab standard pYB01 (10^9 copies/µL)
- HCMV DNA Samples: 3 independent DNA samples (extractions per virus prep or experiment)
- qPCR primers, 15 µM working solution
    - OLYB001 (UL54_For), sequence: 5'GGCCGTTACTGTCTGCAGGA3'
    - OLYB002 (UL54_Rev), sequence: 5'GGCCTCGTAGTGAAAATTAATGGT3'

Method

<u>Preparation of calibration curve</u>

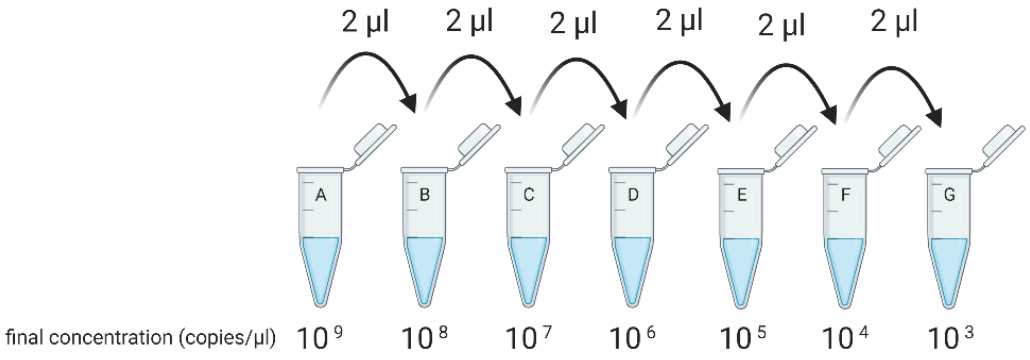

Figure A1.1: Preparation of the pYB01 calibration curve.
A plasmid DNA stock solution of pYB01 at 10^9 copies/µL was serially diluted 1:10 in nuclease-free water to generate a seven-point calibration curve ranging from 10^9 to 10^3 copies/µl. For each dilution step, 2 µl of the preceding dilution was transferred into 18 µl of water and gently mixed using a pipette.

1. Work on ice
2. Label 7 tubes A–G. Add 18 µL of MQ (molecular-grade water) to tubes B through G.
3. Add 2 µL of 10^9 copies/µL plasmid stock (pYB01) to tube A.
4. Prepare a 1:10 serial dilution from tube A to tube G:
    - Transfer 2 µL from tube A to B, mix gently by pipetting.
    - Continue serial dilution by transferring 2 µL from each previous tube to the next.

https://doi.org/10.7795/110.20260518

- Avoid vortexing to prevent DNA shearing

Reaction Mix Assembly

1. Thaw GoTaq qPCR Master Mix and nuclease-free water on ice. Do not thaw GoTaq above room temperature.
2. Briefly vortex the Master Mix (3–5 seconds) at low speed.
3. Calculate total reactions (samples + standard curve + no template control (NTC)), all in triplicates. Add 1–2 extra wells for pipetting error.
4. Prepare the master mix (per reaction):

Table A1.1: Master Mix for qPCR

Component	**Volume**	**Final Concentration**
GoTaq qPCR Master Mix (2X)	10µl	1X
OLYB001 (15 µM)	1 µL	0,75 µM
OLYB002 (15 µM)	1 µL	0,75 µM
Nuclease-Free Water	6 µL	
Total (excluding DNA template)	**18 µL**	

5. Dispense 18 µL of master mix into each well.
6. Add 2 µL of DNA sample, standard dilution, or nuclease-free water (for NTCs) to each well.
7. Seal plate and briefly centrifuge (2 min, 2000 g).
8. Proceed to qPCR run. Avoid prolonged light or heat exposure.

https://doi.org/10.7795/110.20260518

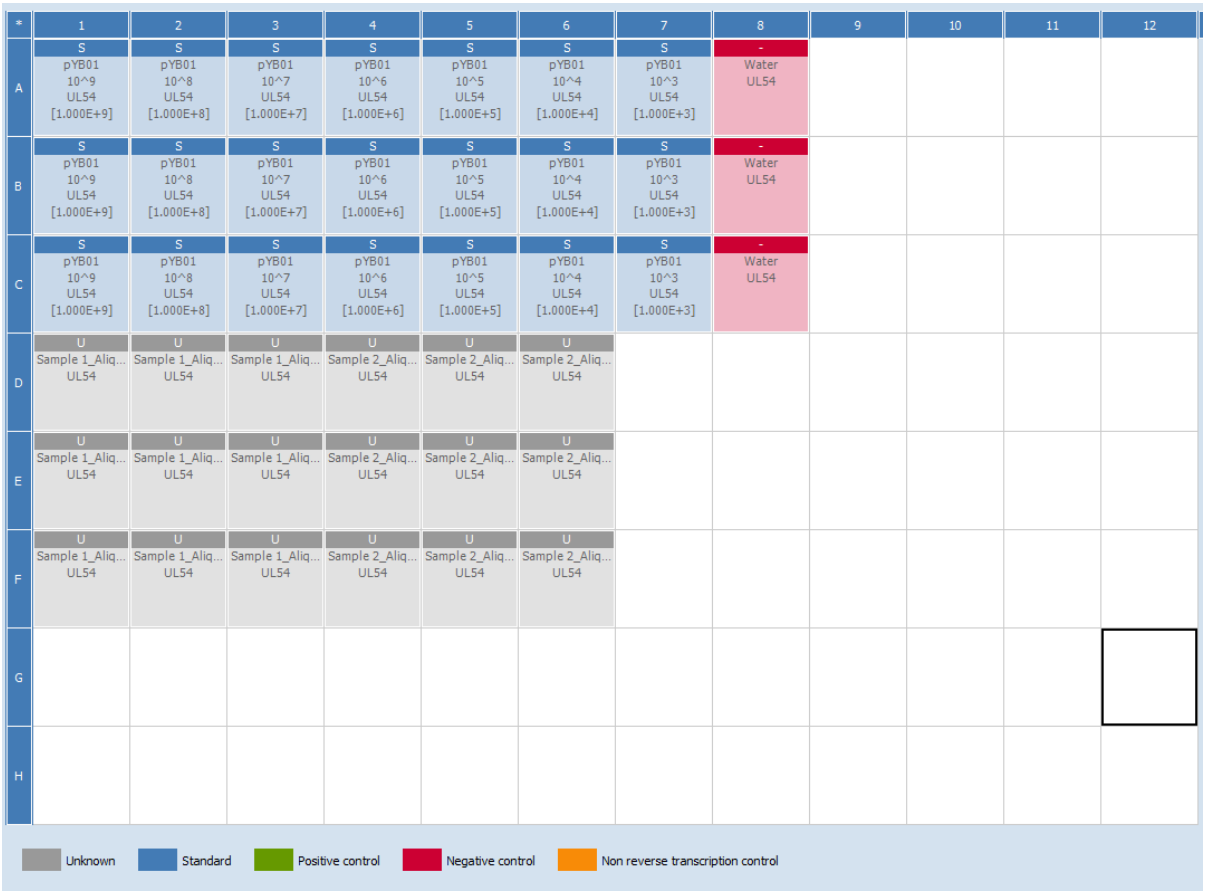

Figure A1.2: LightCycler qPCR plate layout for quantification of the HCMV UL54 gene.
The 96-well plate is organised to include a seven-point standard curve (blue wells, A1–G7), which is prepared using serial 10-fold dilutions of pYB01 plasmid DNA (10^9 to 10^3 copies/µL). Each dilution is run in triplicate. Negative controls containing nuclease-free water without template were included to monitor contamination (red wells, A8–C8). Triplicate experimental samples from two virus preparations (Sample_1 and Sample_2) were included in the grey wells (D1–F6). The colour coding indicates the following: standards (blue), unknown samples (grey) and negative controls (red).

qPCR cycling conditions on Light Cycler (Roche)

Run Definition

- No of Channels: 1
- Integration Time Mode: Dynamic
- Channel: 470/514
- Dye: SYBR Green I

https://doi.org/10.7795/110.20260518

Cycling Programs

Table 35: qPCR cycling set up for UL54 gene quantification on the Roche Light Cycler.

Program	Measurement	Duration	Ramp	Temperature	Cycles
Preincubation	none	600 s	4.4	95 °C	1
Amplification	none	10 s	4.4	95 °C	55
	none	10 s	2.2	60 °C	
	single	10 s	4.4	72 °C	
Melting	none	10 s	4.4	95 °C	1
	none	60 s	2.2	65 °C	
	continuous	1 s	0.2	97 °C	
Hold	none			4 °C	

Notes

- Ensure triplicate reactions for all samples and standards.
- Do not vortex DNA or standards; mix gently by pipetting.
- Always include NTCs to check for contamination.
- You might dilute your HCMV sample DNA to ensure the concentration is within the calibration curve.
- If you prepare the sample editor as shown in Figure A1.2, the software will give you automatically the gene copy numbers per sample.
- Do not freeze and thaw the lab standard pYB01
- Store pYB01 working aliquots (10^9 copies/µL) at -20 °C
- Store pYB01 stock aliquots ($1.2x10^{12}$ copies/µL) at -80 °C
- Preparing working aliquots:
    - Dilute 4.2 µL of pYB01 stock dilution into 5 mL nuclease-free water
    - Prepare 15 µL aliquots

https://doi.org/10.7795/110.20260518

I. List of abbreviations

AAA	Amino Acis Analysis
AGC	Automatic Gain Control
Arg	Arginine
b, y ions	Fragment ions produced in CID fragmentation
BAC	Bacterial Artificial Chromosome
BCA	Bicinchoninic Acid Assay
CCQM	Consultative Committee for Amount of Substance – Metrology in Chemistry and Biology
CID	Collision-Induced Dissociation
CRM	Certified Reference Material
cryo-EM	cryo-electron microscopy
CT	Cycle Thresholds
C-trap	Curved Linear trap
CV	Coefficient of variation
DB	Dense Body
ddPCR	Droplet Digital Polymerase Chain Reaction
DMEM	Dulbecco's modified Eagle's medium
DNA	Deoxyribonucleic Acid
DTT	Dithiothreitol
E.coli	Escherichia coli
EM-IDMS	Exact Matching Isotope Dilution Mass Spectrometry
EQA	External Quality Assessment
ESI	Electrospray Ionisation
FA	Formic Acid
FCS	Fetal Calf Serum
FDA	Food and Drug Administration
FWHM	Full Width at Half Maximum
GC–MS	Gas Chromatography–Mass Spectrometry
GFP	Green Fuorescence Protein
HCMV	Human Cytomegalovirus
HESI	Heated Electrospray Ionization
HPLC	High-Performance Liquid Chromatography
ID-LC-MS/MS	Isotope Dilution Liquid Chromatography–Tandem Mass Spectrometry
IDMS	Isotope Dilution Mass Spectrometry
JCTLM	Joint Committee for Traceability in Laboratory Medicine
lbld.	labelled
LC/ESI-Q MS	liquid chromatography-electrospray ionization quadrupole mass spectrometry
LC–MS/MS	Liquid Chromatography coupled to Tandem Mass Spectrometry
LOD	Limit of Detection
LOQ	Limit of Quantification
LTQ	Linear Trap Quadrupole
Lys	Lysine
m/z	mass-to-charge ratio
MCP	Major Capsid Protein

https://doi.org/10.7795/110.20260518

MQ	MilliQ
MRM	Multiple Reaction Monitoring
MS	Mass Spectrometry
Na	Sodium
NaCl	Sodium Chloride
nat.	natural
NIEPs	Non-infectious Enveloped Particles
NIST	National Institute of Standards and Technology
NMIJ	National Metrology Institute of Japan
NMR	Nuclear Magnetic Resonance
NTC	No Template Control
PCR	Polymerase Chain Reaction
Pep	Peptide Identifier
pGEM-T	cloning vector
ppm	parts per million
pYB01	Plasmid YB01 (HCMV vector construct)
qPCR	quantitative Polymerase Chain Reaction
QqQ	Triple Quadrupole Mass Spectrometer
RF	Radio Frequency
RT	Room Temperature
S2 laboratory	Saftey level 2 laboratory
SCP	Small Capsid Protein
SI	Système International d'Unités (International System of Units)
SIM	Selected Ion Monitoring
SPPS	Solid Phase Peptide Synthesis
SRM	Selected Reaction Monitoring
$TCID_{50}$	Tissue Culture Infectious Dose (50%)
TN buffer	Tris Sodium buffer
Tri1 / Tri2	Triplex Capsid Protein 1 / 2
UL54	HCMV DNA Polymerase Gene
UN	United Nations
UV	Ulraviolet
VYB	Virus Batch Identifier
WHO	World Health Organization
WT	Wildtype

https://doi.org/10.7795/110.20260518

II. List of tables

https://doi.org/10.7795/110.20260518

https://doi.org/10.7795/110.20260518

III. List of figures

https://doi.org/10.7795/110.20260518

IV. List of references

1. Nicholson E, F.I.C. Men and measures : a history of weights and measures, ancient and modern. In the digital collection Digital General Collection. 1912.
2. Desimoni E, Brunetti B. Uncertainty of measurement and conformity assessment: a review. Analytical and Bioanalytical Chemistry. 2011;400(6):1729-41.
3. Richter W. Recommendations on quantities, symbols and measurement units for publications in ACQUAL. Accreditation and Quality Assurance. 2007;12(9):497-8.
4. Thienpont LM, Van Uytfanghe K, De Leenheer AP. Reference measurement systems in clinical chemistry. Clin Chim Acta. 2002;323(1-2):73-87.
5. Siekmann L. Establishing measurement traceability in clinical chemistry. Accreditation and Quality Assurance. 2004;9(1-2):5-17.
6. Barwick V. Terminology in analytical measurement - Introduction to VIM 3. Eurachem. 2011.
7. Brown RJC. A metrological approach to quantities that are counted and the unit one. Metrologia. 2021;58(3):035014.
8. Brown RJC. Measuring measurement - What is metrology and why does it matter? Measurement (Lond). 2021;168:108408.
9. Brown RJC. The evolution of chemical metrology: distinguishing between amount of substance and counting quantities, now and in the future. Metrologia. 2018;55(3):L25-L33.
10. International B, Mesures dPe. The International System of Units (SI). 2019.
11. ISO. DIN EN ISO 80000-1:2023-08. Quantities and Units-Part 13: Information Science and Technology2023.
12. Asicioglu M, Swart C, Saban E, Yurek E, Karaguler NG, Oztug M. Comparative evaluation of peptide vs. protein-based calibration for quantification of cardiac troponin I using ID-LC-MS/MS. Clin Chem Lab Med. 2025;63(5):1016-30.
13. Nouri-Nigjeh E, Zhang M, Ji T, Yu H, An B, Duan X, et al. Effects of calibration approaches on the accuracy for LC-MS targeted quantification of therapeutic protein. Anal Chem. 2014;86(7):3575-84.
14. Scott KB, Turko IV, Phinney KW. Quantitative performance of internal standard platforms for absolute protein quantification using multiple reaction monitoring-mass spectrometry. Anal Chem. 2015;87(8):4429-35.
15. Barr JR, Maggio VL, Patterson DG, Jr., Cooper GR, Henderson LO, Turner WE, et al. Isotope dilution--mass spectrometric quantification of specific proteins: model application with apolipoprotein A-I. Clin Chem. 1996;42(10):1676-82.
16. Arsene CG, Ohlendorf R, Burkitt W, Pritchard C, Henrion A, Bunk DM, et al. Protein Quantification by Isotope Dilution Mass Spectrometry of Proteolytic Fragments: Cleavage Rate and Accuracy. Analytical Chemistry. 2008;80(11):4154-60.
17. Chaves Das Neves HJ, Vasconcelos AM. Capillary gas chromatography of amino acids, including asparagine and glutamine: sensitive gas chromatographic-mass spectrometric and selected ion monitoring gas chromatographic-mass spectrometric detection of the N,O(S)-tert.-butyldimethylsilyl derivatives. J Chromatogr. 1987;392:249-58.
18. Gehrke CW, Stalling DL. Quantitative Analysis of the Twenty Natural Protein Amino Acids by Gas-Liquid Chromatography. Separation Science. 1967;2(1):101-38.
19. Le Goff T, Champarnaud E, Fardus F. HPLC direct purity assay using ultra-purified materials as primary standards. Anal Bioanal Chem. 2010;398(7-8):3183-92.
20. Schoenberger T. Determination of standard sample purity using the high-precision 1H-NMR process. Anal Bioanal Chem. 2012;403(1):247-54.
21. Yamazaki T, Takatsu A. Quantitative NMR spectroscopy for accurate purity determination of amino acids, and uncertainty evaluation for different signals. Accreditation and Quality Assurance. 2014;19(4):275-82.

https://doi.org/10.7795/110.20260518

22. Burkitt WI, Pritchard C, Arsene C, Henrion A, Bunk D, O'Connor G. Toward Systeme International d'Unite-traceable protein quantification: from amino acids to proteins. Anal Biochem. 2008;376(2):242-51.
23. Fountoulakis M, Lahm HW. Hydrolysis and amino acid composition analysis of proteins. Journal of Chromatography A. 1998;826(2):109-34.
24. Pramanik BC, Moomaw CR, Evans CT, Cohen SA, Slaughter CA. Identification of phenylthiocarbamyl amino acids for compositional analysis by thermospray liquid chromatography/mass spectrometry. Anal Biochem. 1989;176(2):269-77.
25. Arsene CG, Henrion A, Diekmann N, Manolopoulou J, Bidlingmaier M. Quantification of growth hormone in serum by isotope dilution mass spectrometry. Anal Biochem. 2010;401(2):228-35.
26. Arsene CG, Kaiser P, Paleari R, Henrion A, Spannagl M, Mosca A, et al. Determination of HbA2 by quantitative bottom-up proteomics and isotope dilution mass spectrometry. Clin Chim Acta. 2018;487:318-24.
27. Josephs RD, Li M, Daireaux A, Choteau T, Martos G, Westwood S, et al. Pilot study on peptide purity—synthetic oxytocin. Metrologia. 2020;57(1A):08016.
28. Josephs RD, Li M, Song D, Daireaux A, Choteau T, Stoppacher N, et al. Pilot study on peptide purity—synthetic human C-peptide. Metrologia. 2017;54(1A):08011.
29. Josephs RD, Liu Q, Martos G, Bedu M, Daireaux A, Choteau T, et al. Pilot study on peptide purity - glycated hexapeptide of HbA1c. Metrologia. 2022;59(1A):08007.
30. Josephs RD, Li M, Daireaux A, Choteau T, Martos G, Westwood S, et al. Key comparison study on peptide purity - synthetic oxytocin. Metrologia. 2020;57(1A):08014.
31. Josephs RD, Li M, Song D, Westwood S, Stoppacher N, Daireaux A, et al. Key comparison study on peptide purity—synthetic human C-peptide. Metrologia. 2017;54(1A):08007.
32. Josephs RD, Liu Q, Martos G, Bedu M, Daireaux A, Choteau T, et al. Key comparison study on peptide purity - hexapeptide of HbA0. Metrologia. 2022;59(1A):08013.
33. JCGM. Evaluation of Measurement Data – Guide to the Expression of Uncertainty in Measurement. 2008.
34. Thomson JJ. Rays of Positive Electricity and their Application to Chemical Analysis. Nature. 1913;92(2307):549-50.
35. Aston FW. A positive ray spectrograph. The London, Edinburgh, and Dublin Philosophical Magazine and Journal of Science. 1919;38(228):707-14.
36. Aston FW. Mass-spectra and Isotopes. The Journal of Physical Chemistry. 1934;38(5):713-.
37. Jonsson AP. Mass spectrometry for protein and peptide characterisation. Cell Mol Life Sci. 2001;58(7):868-84.
38. Cravatt BF, Simon GM, Yates Iii JR. The biological impact of mass-spectrometry-based proteomics. Nature. 2007;450(7172):991-1000.
39. Aebersold R, Mann M. Mass spectrometry-based proteomics. Nature. 2003;422(6928):198-207.
40. McLafferty FW. Tandem mass spectrometry. Science. 1981;214(4518):280-7.
41. Rayleigh L. On the equilibrium of liquid conducting masses charged with electricity. The London, Edinburgh, and Dublin Philosophical Magazine and Journal of Science. 1882;14(87):184-6.
42. Dole M, Mack LL, Hines RL, Mobley RC, Ferguson LD, Alice MB. Molecular Beams of Macroions. Journal of Chemical Physics. 1968;49:2240-9.
43. Fenn JB, Mann M, Meng CK, Wong SF, Whitehouse CM. Electrospray Ionization for Mass-Spectrometry of Large Biomolecules. Science. 1989;246(4926):64-71.
44. Whitehouse CM, Dreyer RN, Yamashita M, Fenn JB. Electrospray interface for liquid chromatographs and mass spectrometers. Anal Chem. 1985;57(3):675-9.
45. Yang JZ, Bastian KC, Moore RD, Stobaugh JF, Borchardt RT. Quantitative analysis of a model opioid peptide and its cyclic prodrugs in rat plasma using high-performance liquid chromatography with fluorescence and tandem mass spectrometric detection. J Chromatogr B. 2002;780(2):269-81.

https://doi.org/10.7795/110.20260518

46. Banerjee S, Mazumdar S. Electrospray Ionization Mass Spectrometry: A Technique to Access the Information beyond the Molecular Weight of the Analyte. International Journal of Analytical Chemistry. 2012;2012:1-40.
47. Paul W, Steinwedel H. Ein neues Massenspektrometer ohne Magnetfeld. Zeitschrift für Naturforschung A. 1953;8(7):448-50.
48. Gallien S, Duriez E, Crone C, Kellmann M, Moehring T, Domon B. Targeted Proteomic Quantification on Quadrupole-Orbitrap Mass Spectrometer. Molecular & Cellular Proteomics. 2012;11(12):1709-23.
49. Lesur A, Domon B. Advances in high-resolution accurate mass spectrometry application to targeted proteomics. Proteomics. 2015;15(5-6):880-90.
50. Kingdon KH. A Method for the Neutralization of Electron Space Charge by Positive Ionization at Very Low Gas Pressures. Physical Review. 1923;21(4):408-18.
51. Makarov A, Denisov E, Kholomeev A, Balschun W, Lange O, Strupat K, et al. Performance Evaluation of a Hybrid Linear Ion Trap/Orbitrap Mass Spectrometer. Analytical Chemistry. 2006;78(7):2113-20.
52. Silva EMP, Varandas PAMM, Melo T, Barros C, Alencastre IS, Barreiros L, et al. Gas-phase structural characterization of neuropeptides Y Y1 receptor antagonists using mass spectrometry: Orbitrap vs triple quadrupole. J Pharmaceut Biomed. 2018;151:227-34.
53. Herrero P, Cortes-Francisco N, Borrull F, Caixach J, Pocurull E, Marce RM. Comparison of triple quadrupole mass spectrometry and Orbitrap high-resolution mass spectrometry in ultrahigh performance liquid chromatography for the determination of veterinary drugs in sewage: benefits and drawbacks. J Mass Spectrom. 2014;49(7):585-96.
54. Roepstorff P, Fohlman J. Proposal for a Common Nomenclature for Sequence Ions in Mass-Spectra of Peptides. Biomed Mass Spectrom. 1984;11(11):601-.
55. Syka JE, Coon JJ, Schroeder MJ, Shabanowitz J, Hunt DF. Peptide and protein sequence analysis by electron transfer dissociation mass spectrometry. Proc Natl Acad Sci U S A. 2004;101(26):9528-33.
56. Heumann KG. Isotope-Dilution Mass-Spectrometry of Inorganic and Organic-Substances. Fresen Z Anal Chem. 1986;325(8):661-6.
57. Henrion A. Reduction of systematic errors in quantitative analysis by isotope dilution mass spectrometry (IDMS): an iterative method. Fresenius' Journal of Analytical Chemistry. 1994;350(12):657-8.
58. Boyd RK. Quantitative Trace Analysis by Combined Chromatography and Mass-Spectrometry Using External and Internal Standards. Rapid Communications in Mass Spectrometry. 1993;7(4):257-71.
59. Lowenthal MS, Yen J, Bunk DM, Phinney KW. Certification of NIST standard reference material 2389a, amino acids in 0.1 mol/L HCl--quantification by ID LC-MS/MS. Anal Bioanal Chem. 2010;397(2):511-9.
60. Kinumi T, Goto M, Eyama S, Kato M, Kasama T, Takatsu A. Development of SI-traceable C-peptide certified reference material NMIJ CRM 6901-a using isotope-dilution mass spectrometry-based amino acid analyses. Anal Bioanal Chem. 2012;404(1):13-21.
61. Stoppacher N, Josephs RD, Daireaux A, Choteau T, Westwood S, Wielgosz RI. Accurate quantification of impurities in pure peptide material - angiotensin I: Comparison of calibration requirements and method performance characteristics of liquid chromatography coupled to hybrid tandem mass spectrometry and linear ion trap high-resolution mass spectrometry. Rapid Commun Mass Spectrom. 2015;29(18):1651-60.
62. Bedson P. Guidelines for Achieving High Accuracy in Isotope Dilution Mass Spectrometry (IDMS). In: Sargent M, Harte R, Harrington C, Sargent M, Harte R, Harrington C, editors. Guidelines for Achieving High Accuracy in Isotope Dilution Mass Spectrometry (IDMS): Royal Society of Chemistry; 2002. p. 0.

https://doi.org/10.7795/110.20260518

63. Hoofnagle AN, Whiteaker JR, Carr SA, Kuhn E, Liu T, Massoni SA, et al. Recommendations for the Generation, Quantification, Storage, and Handling of Peptides Used for Mass Spectrometry–Based Assays. Clinical Chemistry. 2016;62(1):48-69.
64. Mullis KB, Faloona FA. Specific synthesis of DNA in vitro via a polymerase-catalyzed chain reaction. Methods Enzymol. 1987;155:335-50.
65. Saiki RK, Gelfand DH, Stoffel S, Scharf SJ, Higuchi R, Horn GT, et al. Primer-directed enzymatic amplification of DNA with a thermostable DNA polymerase. Science. 1988;239(4839):487-91.
66. Erlich HA, Gelfand D, Sninsky JJ. Recent advances in the polymerase chain reaction. Science. 1991;252(5013):1643-51.
67. D'Amato RF, Wallman AA, Hochstein LH, Colaninno PM, Scardamaglia M, Ardila E, et al. Rapid diagnosis of pulmonary tuberculosis by using Roche AMPLICOR Mycobacterium tuberculosis PCR test. J Clin Microbiol. 1995;33(7):1832-4.
68. Pfyffer GE, Wittwer F. Incubation time of mycobacterial cultures: how long is long enough to issue a final negative report to the clinician? J Clin Microbiol. 2012;50(12):4188-9.
69. Taberlet P, Griffin S, Goossens B, Questiau S, Manceau V, Escaravage N, et al. Reliable genotyping of samples with very low DNA quantities using PCR. Nucleic Acids Res. 1996;24(16):3189-94.
70. Li P, Zhao Z, Wang Y, Xing H, Parker DM, Yang Z, et al. Nested PCR detection of malaria directly using blood filter paper samples from epidemiological surveys. Malar J. 2014;13:175.
71. Henegariu O, Heerema NA, Dlouhy SR, Vance GH, Vogt PH. Multiplex PCR: critical parameters and step-by-step protocol. Biotechniques. 1997;23(3):504-11.
72. Bartlett JM, Stirling D. A short history of the polymerase chain reaction. Methods Mol Biol. 2003;226:3-6.
73. Yang S, Rothman RE. PCR-based diagnostics for infectious diseases: uses, limitations, and future applications in acute-care settings. Lancet Infect Dis. 2004;4(6):337-48.
74. Kralik P, Ricchi M. A Basic Guide to Real Time PCR in Microbial Diagnostics: Definitions, Parameters, and Everything. Front Microbiol. 2017;8.
75. Huggett JF, Whale A. Digital PCR as a Novel Technology and Its Potential Implications for Molecular Diagnostics. Clinical Chemistry. 2013;59(12):1691-3.
76. Bustin SA, Benes V, Garson JA, Hellemans J, Huggett J, Kubista M, et al. The MIQE Guidelines: Minimum information for Publication of quantitative Real-Time PCR experiments. Clinical Chemistry. 2009;55(4):611-22.

77. Clementi M, Menzo S, Bagnarelli P, Manzin A, Valenza A, Varaldo PE. Quantitative PCR and RT-PCR in virology. PCR Methods Appl. 1993;2(3):191-6.
78. Berger A, Braner J, Doerr HW, Weber B. Quantification of viral load: clinical relevance for human immunodeficiency virus, hepatitis B virus and hepatitis C virus infection. Intervirology. 1998;41(1):24-34.
79. Gibellini D, Vitone F, Schiavone P, Ponti C, La Placa M, Re MC. Quantitative detection of human immunodeficiency virus type 1 (HIV-1) proviral DNA in peripheral blood mononuclear cells by SYBR green real-time PCR technique. J Clin Virol. 2004;29(4):282-9.
80. Ma H, Bell KN, Loker RN. qPCR and qRT-PCR analysis: Regulatory points to consider when conducting biodistribution and vector shedding studies. Molecular Therapy - Methods & Clinical Development. 2021;20:152-68.
81. Vonsky MS, Runov AL. Development of metrological support for nucleic acid measurements. Journal of Physics: Conference Series. 2022;2192(1):012011.
82. Falak S, O'Sullivan DM, Cleveland MH, Cowen S, Busby EJ, Devonshire AS, et al. The Application of Digital PCR as a Reference Measurement Procedure to Support the Accuracy of Quality Assurance for Infectious Disease Molecular Diagnostic Testing. Clinical Chemistry. 2024;71(3):378-86.
83. Tellinghuisen J, Spiess AN. Bias and imprecision in analysis of real-time quantitative polymerase chain reaction data. Anal Chem. 2015;87(17):8925-31.

https://doi.org/10.7795/110.20260518

84. Tellinghuisen J, Spiess AN. Statistical uncertainty and its propagation in the analysis of quantitative polymerase chain reaction data: comparison of methods. Anal Biochem. 2014;464:94-102.
85. Bilgrau AE, Falgreen S, Petersen A, Kjeldsen MK, Bødker JS, Johnsen HE, et al. Unaccounted uncertainty from qPCR efficiency estimates entails uncontrolled false positive rates. BMC Bioinformatics. 2016;17(1).
86. Vogelstein B, Kinzler KW. Digital PCR. Proceedings of the National Academy of Sciences. 1999;96(16):9236-41.
87. Hayden RT, Gu Z, Ingersoll J, Abdul-Ali D, Shi L, Pounds S, et al. Comparison of droplet digital PCR to real-time PCR for quantitative detection of cytomegalovirus. J Clin Microbiol. 2013;51(2):540-6.
88. Trypsteen W, Kiselinova M, Vandekerckhove L, De Spiegelaere W. Diagnostic utility of droplet digital PCR for HIV reservoir quantification. J Virus Erad. 2016;2(3):162-9.
89. Whale AS, Bushell CA, Grant PR, Cowen S, Gutierrez-Aguirre I, O'Sullivan DM, et al. Detection of Rare Drug Resistance Mutations by Digital PCR in a Human Influenza A Virus Model System and Clinical Samples. J Clin Microbiol. 2016;54(2):392-400.
90. Sedlak RH, Cook L, Huang ML, Magaret A, Zerr DM, Boeckh M, et al. Identification of chromosomally integrated human herpesvirus 6 by droplet digital PCR. Clin Chem. 2014;60(5):765-72.
91. Kelley K, Cosman A, Belgrader P, Chapman B, Sullivan DC. Detection of Methicillin-Resistant

by a Duplex Droplet Digital PCR Assay. Journal of Clinical Microbiology. 2013;51(7):2033-9.
92. Roberts CH, Last A, Molina-Gonzalez S, Cassama E, Butcher R, Nabicassa M, et al. Development and evaluation of a next-generation digital PCR diagnostic assay for ocular Chlamydia trachomatis infections. J Clin Microbiol. 2013;51(7):2195-203.
93. Weerakoon KG, Gordon CA, Williams GM, Cai P, Gobert GN, Olveda RM, et al. Droplet Digital PCR Diagnosis of Human Schistosomiasis: Parasite Cell-Free DNA Detection in Diverse Clinical Samples. J Infect Dis. 2017;216(12):1611-22.
94. Koepfli C, Nguitragool W, Hofmann NE, Robinson LJ, Ome-Kaius M, Sattabongkot J, et al. Sensitive and accurate quantification of human malaria parasites using droplet digital PCR (ddPCR). Sci Rep. 2016;6:39183.
95. Li HT, Lin BC, Huang ZF, Yang CZ, Huang WM. [Clinical value of droplet digital PCR in rapid diagnosis of invasive fungal infection in neonates]. Zhongguo Dang Dai Er Ke Za Zhi. 2019;21(1):45-51.
96. Rutsaert S, Bosman K, Trypsteen W, Nijhuis M, Vandekerckhove L. Digital PCR as a tool to measure HIV persistence. Retrovirology. 2018;15(1):16.
97. Kuypers J, Jerome KR. Applications of Digital PCR for Clinical Microbiology. J Clin Microbiol. 2017;55(6):1621-8.
98. Taylor SC, Laperriere G, Germain H. Droplet Digital PCR versus qPCR for gene expression analysis with low abundant targets: from variable nonsense to publication quality data. Scientific Reports. 2017;7(1).
99. Arvia R, Sollai M, Pierucci F, Urso C, Massi D, Zakrzewska K. Droplet digital PCR (ddPCR) vs quantitative real-time PCR (qPCR) approach for detection and quantification of Merkel cell polyomavirus (MCPyV) DNA in formalin fixed paraffin embedded (FFPE) cutaneous biopsies. J Virol Methods. 2017;246:15-20.
100. Dioverti MV, Razonable RR. Cytomegalovirus. Microbiol Spectr. 2016;4(4).
101. Staras SA, Dollard SC, Radford KW, Flanders WD, Pass RF, Cannon MJ. Seroprevalence of cytomegalovirus infection in the United States, 1988-1994. Clin Infect Dis. 2006;43(9):1143-51.
102. Cannon MJ, Schmid DS, Hyde TB. Review of cytomegalovirus seroprevalence and demographic characteristics associated with infection. Rev Med Virol. 2010;20(4):202-13.
103. Rafailidis PI, Mourtzoukou EG, Varbobitis IC, Falagas ME. Severe cytomegalovirus infection in apparently immunocompetent patients: a systematic review. Virol J. 2008;5:47.

https://doi.org/10.7795/110.20260518

104. Gugliesi F, Coscia A, Griffante G, Galitska G, Pasquero S, Albano C, et al. Where do we Stand after Decades of Studying Human Cytomegalovirus? Microorganisms. 2020;8(5):685.
105. Geder L, Sanford EJ, Rohner TJ, Rapp F. Cytomegalovirus and cancer of the prostate: in vitro transformation of human cells. Cancer Treat Rep. 1977;61(2):139-46.
106. Epstein SE, Speir E, Zhou YF, Guetta E, Leon M, Finkel T. The role of infection in restenosis and atherosclerosis: focus on cytomegalovirus. Lancet. 1996;348 Suppl 1:s13-7.
107. Harkins L, Volk AL, Samanta M, Mikolaenko I, Britt WJ, Bland KI, et al. Specific localisation of human cytomegalovirus nucleic acids and proteins in human colorectal cancer. Lancet. 2002;360(9345):1557-63.
108. Boppana SB, Ross SA, Fowler KB. Congenital cytomegalovirus infection: clinical outcome. Clin Infect Dis. 2013;57 Suppl 4(Suppl 4):S178-81.
109. Chee MS, Bankier AT, Beck S, Bohni R, Brown CM, Cerny R, et al. Analysis of the protein-coding content of the sequence of human cytomegalovirus strain AD169. Curr Top Microbiol Immunol. 1990;154:125-69.
110. Kanich RE, Craighead JE. Human cytomegalovirus infection of cultured fibroblasts. II. Viral replicative sequence of a wild and an adapted strain. Lab Invest. 1972;27(3):273-82.
111. Iwasaki Y, Furukawa T, Plotkin S, Koprowski H. Ultrastructural study on the sequence of human cytomegalovirus infection in human diploid cells. Arch Gesamte Virusforsch. 1973;40(3):311-24.
112. Irmiere AG, W. Isolation and Characterization of a Noninfectious Virion-like Particle Released from Cells Infected with Human Strains of Cytomegalovirus. Virology. 1983.
113. Dai W, Jia Q, Bortz E, Shah S, Liu J, Atanasov I, et al. Unique structures in a tumor herpesvirus revealed by cryo-electron tomography and microscopy. J Struct Biol. 2008;161(3):428-38.
114. Stinski MF. Human cytomegalovirus: glycoproteins associated with virions and dense bodies. J Virol. 1976;19(2):594-609.
115. Talbot P, Almeida JD. Human cytomegalovirus: purification of enveloped virions and dense bodies. J Gen Virol. 1977;36(2):345-9.
116. Varnum SM, Streblow DN, Monroe ME, Smith P, Auberry KJ, Pasa-Tolic L, et al. Identification of proteins in human cytomegalovirus (HCMV) particles: the HCMV proteome. J Virol. 2004;78(20):10960-6.
117. Bauer DW, Huffman JB, Homa FL, Evilevitch A. Herpes Virus Genome, The Pressure Is On. Journal of the American Chemical Society. 2013;135(30):11216-21.
118. Liashkovich I, Hafezi W, KüHn JE, Oberleithner H, Kramer A, Shahin V. Exceptional mechanical and structural stability of HSV-1 unveiled with fluid atomic force microscopy. Journal of Cell Science. 2008;121(14):2287-92.
119. Yu X, Jih J, Jiang J, Zhou ZH. Atomic structure of the human cytomegalovirus capsid with its securing tegument layer of pp150. Science. 2017;356(6345):eaam6892.
120. Pellett PER, B. Herpesviridae. In: D. M. Knipe PMH, editor. Fields virology: Wolters Kluwer Health/Lippincott Williams & Wilkins; 2013. p. 1802-22.
121. Cevenini A, De Antonellis P, Mazzarelli LL, Sarno L, D'Alessandro P, Pellicano M, et al. Lytic or Latent Phase in Human Cytomegalovirus Infection: An Epigenetic Trigger. International Journal of Molecular Sciences. 2025;26(23):11554.
122. Sathiyamoorthy K, Chen J, Longnecker R, Jardetzky TS. The COMPLEXity in herpesvirus entry. Curr Opin Virol. 2017;24:97-104.
123. Sodeik B. Mechanisms of viral transport in the cytoplasm. Trends Microbiol. 2000;8(10):465-72.
124. McVoy MA, Adler SP. Human cytomegalovirus DNA replicates after early circularization by concatemer formation, and inversion occurs within the concatemer. J Virol. 1994;68(2):1040-51.
125. Razonable RR, Inoue N, Pinninti SG, Boppana SB, Lazzarotto T, Gabrielli L, et al. Clinical Diagnostic Testing for Human Cytomegalovirus Infections. J Infect Dis. 2020;221(Suppl 1):S74-S85.
126. Yokoyama Y, Yamakawa T, Hirano T, Kazama T, Hirayama D, Wagatsuma K, et al. Current Diagnostic and Therapeutic Approaches to Cytomegalovirus Infections in Ulcerative Colitis Patients

https://doi.org/10.7795/110.20260518

Based on Clinical and Basic Research Data. International Journal of Molecular Sciences. 2020;21(7):2438.
127. Ho M. The history of cytomegalovirus and its diseases. Med Microbiol Immunol. 2008;197(2):65-73.
128. Rothbarth PH, Diepersloot RJ, Metselaar HJ, Nooyen Y, Velzing J, Weimar W. Rapid demonstration of cytomegalovirus in clinical specimens. Infection. 1987;15(4):228-31.
129. Romkens TE, Bulte GJ, Nissen LH, Drenth JP. Cytomegalovirus in inflammatory bowel disease: A systematic review. World J Gastroenterol. 2016;22(3):1321-30.
130. Pillet S, Pozzetto B, Roblin X. Cytomegalovirus and ulcerative colitis: Place of antiviral therapy. World J Gastroenterol. 2016;22(6):2030-45.
131. Chevillotte M, Landwehr S, Linta L, Frascaroli G, Luske A, Buser C, et al. Major tegument protein pp65 of human cytomegalovirus is required for the incorporation of pUL69 and pUL97 into the virus particle and for viral growth in macrophages. J Virol. 2009;83(6):2480-90.
132. Boeckh M, Boivin G. Quantitation of cytomegalovirus: methodologic aspects and clinical applications. Clin Microbiol Rev. 1998;11(3):533-54.
133. Gimeno C, Solano C, Latorre JC, Hernandez-Boluda JC, Clari MA, Remigia MJ, et al. Quantification of DNA in plasma by an automated real-time PCR assay (cytomegalovirus PCR kit) for surveillance of active cytomegalovirus infection and guidance of preemptive therapy for allogeneic hematopoietic stem cell transplant recipients. J Clin Microbiol. 2008;46(10):3311-8.
134. Haynes RJ, Kline MC, Toman B, Scott C, Wallace P, Butler JM, et al. Standard reference material 2366 for measurement of human cytomegalovirus DNA. J Mol Diagn. 2013;15(2):177-85.
135. Pavsic J, Devonshire A, Blejec A, Foy CA, Van Heuverswyn F, Jones GM, et al. Inter-laboratory assessment of different digital PCR platforms for quantification of human cytomegalovirus DNA. Anal Bioanal Chem. 2017;409(10):2601-14.
136. Bogozalec Kosir A, Cvelbar T, Kammel M, Grunert HP, Zeichhardt H, Milavec M. Digital PCR method for detection and quantification of specific antimicrobial drug-resistance mutations in human cytomegalovirus. J Virol Methods. 2020;281:113864.
137. Milavec M, Pavšič J, Bogožalec Košir A, Jones GM, O'Sullivan DM, Devonshire AS, et al. The performance of human cytomegalovirus digital PCR reference measurement procedure in seven external quality assessment schemes over four years. Methods. 2022;201:65-73.
138. Borst EM, Ständker L, Wagner K, Schulz TF, Forssmann W-G, Messerle M. A Peptide Inhibitor of Cytomegalovirus Infection from Human Hemofiltrate. Antimicrobial Agents and Chemotherapy. 2013;57(10):4751-60.
139. Santos MDM, Lima DB, Fischer JSG, Clasen MA, Kurt LU, Camillo-Andrade AC, et al. Simple, efficient and thorough shotgun proteomic analysis with PatternLab V. Nat Protoc. 2022.
140. Pavsic J, Zel J, Milavec M. Digital PCR for direct quantification of viruses without DNA extraction. Anal Bioanal Chem. 2016;408(1):67-75.
141. Sassenscheidt J, Rohayem J, Illmer T, Bandt D. Detection of beta-herpesviruses in allogenic stem cell recipients by quantitative real-time PCR. J Virol Methods. 2006;138(1-2):40-8.
142. Herzik MA, Jr., Fraser JS, Lander GC. A Multi-model Approach to Assessing Local and Global Cryo-EM Map Quality. Structure. 2019;27(2):344-58 e3.
143. Stern-Ginossar N, Weisburd B, Michalski A, Le VTK, Hein MY, Huang S-X, et al. Decoding Human Cytomegalovirus. Science. 2012;338(6110):1088-93.
144. Coute Y, Kraut A, Zimmermann C, Buscher N, Hesse AM, Bruley C, et al. Mass Spectrometry-Based Characterization of the Virion Proteome, Phosphoproteome, and Associated Kinase Activity of Human Cytomegalovirus. Microorganisms. 2020;8(6).
145. Hofstadter WA, Park JW, Lum KK, Chen S, Cristea IM. HCMV strain- and cell type-specific alterations in membrane contact sites point to the convergent regulation of organelle remodeling. J Virol. 2024;98(11):e0109924.
146. Merrifield RB. Solid Phase Peptide Synthesis. I. The Synthesis of a Tetrapeptide. Journal of the American Chemical Society. 1963;85(14):2149-54.

https://doi.org/10.7795/110.20260518

147. Munoz A, Kral R, Schimmel H. Quantification of protein calibrants by amino acid analysis using isotope dilution mass spectrometry. Anal Biochem. 2011;408(1):124-31.
148. Rutherfurd SM, Gilani GS. Amino Acid Analysis. Current Protocols in Protein Science. 2009;58(1).
149. Davidson I. Hydrolysis of samples for amino acid analysis. Methods Mol Biol. 1997;64:119-29.
150. Chen G, Pramanik BN. Application of LC/MS to proteomics studies: current status and future prospects. Drug Discov Today. 2009;14(9-10):465-71.
151. Vogeser M, Seger C. A decade of HPLC-MS/MS in the routine clinical laboratory - Goals for further developments. Clinical Biochemistry. 2008;41(9):649-62.
152. Kortz L, Helmschrodt C, Ceglarek U. Fast liquid chromatography combined with mass spectrometry for the analysis of metabolites and proteins in human body fluids. Anal Bioanal Chem. 2011;399(8):2635-44.
153. Dooley KC. Tandem mass spectrometry in the clinical chemistry laboratory. Clin Biochem. 2003;36(6):471-81.
154. Gregorich ZR, Chang Y-H, Ge Y. Proteomics in heart failure: top-down or bottom-up? Pflügers Archiv - European Journal of Physiology. 2014;466(6):1199-209.
155. Ong S-E, Mann M. Mass spectrometry–based proteomics turns quantitative. Nature Chemical Biology. 2005;1(5):252-62.
156. Bantscheff M, Schirle M, Sweetman G, Rick J, Kuster B. Quantitative mass spectrometry in proteomics: a critical review. Analytical and Bioanalytical Chemistry. 2007;389(4):1017-31.
157. Hortin GL. A New Era in Protein Quantification in Clinical Laboratories: Application of Liquid Chromatography-Tandem Mass Spectrometry. Clinical Chemistry. 2007;53(4):543-4.
158. Hortin GL, Carr SA, Anderson NL. Introduction: Advances in Protein Analysis for the Clinical Laboratory. Clinical Chemistry. 2010;56(2):149-51.
159. Lavagnini I, Magno F. A statistical overview on univariate calibration, inverse regression, and detection limits: Application to gas chromatography/mass spectrometry technique. Mass Spectrom Rev. 2007;26(1):1-18.
160. Rauh M. LC-MS/MS for protein and peptide quantification in clinical chemistry. J Chromatogr B Analyt Technol Biomed Life Sci. 2012;883-884:59-67.
161. ICH. VALIDATION OF ANALYTICAL PROCEDURES: TEXT AND METHODOLOGY Q2(R1). 2005.
162. Institute CaLS. CLSI guideline C62. Liquid Chromatography-Mass Spectrometry Methods. 2nd ed2022.
163. UNODC. Validation of Analytical Methodology and Calibration of Equipment used
or Testing of Illicit Drugs in Seized Materials and Biological Specimens. 2009.
164. COMMUNITIES TCOTE. Commission Decision 2002/657/EC. Official Journal of the European Communities. 2002.
165. USDA. Data and Instrumentation Revision 5. In: Service AM, editor. 2017.
166. FDA. Guidance for Industry 118 Confirmation of Identity of Animal Drug Residues, Food and Drug Administration. 2003.
167. Angeles LF, Aga DS. Establishing Analytical Performance Criteria for the Global Reconnaissance of Antibiotics and Other Pharmaceutical Residues in the Aquatic Environment Using Liquid Chromatography-Tandem Mass Spectrometry. Journal of Analytical Methods in Chemistry. 2018;2018:1-9.
168. Evans L, Dingeldein L, Gilles MA, Thiede EH, Cossio P. BPS2025 - Why counting particles can give wrong probabilities in cryo-EM. Biophysical Journal. 2025;124(3):488a.
169. Reggiano G, Lugmayr W, Farrell D, Marlovits TC, DiMaio F. Residue-level error detection in cryoelectron microscopy models. Structure. 2023;31(7):860-9 e4.
170. Lai TL, Wang S-H, Chung S-C, Chang W-h, Tu IP. Uncertainty Quantification in Dynamic Image Reconstruction with Applications to Cryo-EM. Statistica Sinica. 2023.

https://doi.org/10.7795/110.20260518

171. Bresch H, Hodoroaba VD, Schmidt A, Rasmussen K, Rauscher H. Counting Small Particles in Electron Microscopy Images-Proposal for Rules and Their Application in Practice. Nanomaterials (Basel). 2022;12(13).
172. Schneidman-Duhovny D, Pellarin R, Sali A. Uncertainty in integrative structural modeling. Curr Opin Struct Biol. 2014;28:96-104.
173. Buchta C, Gorzer I, Chiba P, Camp JV, Holzmann H, Puchhammer-Stockl E, et al. Variability of cycle threshold values in an external quality assessment scheme for detection of the SARS-CoV-2 virus genome by RT-PCR. Clin Chem Lab Med. 2021;59(5):987-94.
174. Reyda S, Tenzer S, Navarro P, Gebauer W, Saur M, Krauter S, et al. The tegument protein pp65 of human cytomegalovirus acts as an optional scaffold protein that optimizes protein uploading into viral particles. J Virol. 2014;88(17):9633-46.

https://doi.org/10.7795/110.20260518

Bundesministerium
für Wirtschaft
und Energie

Die Physikalisch-Technische Bundesanstalt, das nationale Metrologieinstitut, ist eine wissenschaftlich-technische Bundesoberbehörde im Geschäftsbereich des Bundesministeriums für Wirtschaft und Energie.

PTB

Physikalisch-Technische Bundesanstalt
Nationales Metrologieinstitut
ISNI: 0000 0001 2186 1887

Bundesallee 100
38116 Braunschweig

Presse- und Öffentlichkeitsarbeit

Telefon: (0531) 592-93 21
Fax: (0531) 592-30 08
E-Mail: presse@ptb.de
www.ptb.de